TECHNISCHE UNIVERSITÄT DRESDEN

Coherent state-based approaches to quantum dynamics: application to thermalization in finite systems

Dissertation
zur Erlangung des wissenschaftlichen Grades
Doctor rerum naturalium

vorgelegt von

Sreeja Loho Choudhury
geboren am 09.11.1994 in Patan, India

Institut für Theoretische Physik
Fachrichtung Physik
Fakultät für Mathematik und Naturwissenschaften
Technische Universität Dresden
2022

Eingereicht am 10.02.2022

1. Gutachter: Prof. Dr. Jan Carl Budich
2. Gutachter: Prof. Dr. Dmitry Shalashilin

Verteidigt am 14.04.2022

Abstract

We investigate thermalization in finite quantum systems using coherent state-based approaches to solve the time-dependent Schrödinger equation. Earlier, a lot of work has been done in the quantum realm, to study thermalization in spin systems, but not for the case of continuous systems. Here, we focus on continuous systems. We study the zero temperature thermalization i.e., we consider the ground states of the bath oscillators (environment).

In order to study the quantum dynamics of a system under investigation, we require numerical methods to solve the time-dependent Schrödinger equation. We describe different numerical methods like the split-operator fast fourier transform, coupled coherent states, static grid of coherent states, semiclassical Herman-Kluk propagator and the linearized semiclassical initial value representation to study the quantum dynamics. We also give a comprehensive comparison of the most widely used coherent state based methods. Starting from the fully variational coherent states method, after a first approximation, the coupled coherent states method can be derived, whereas an additional approximation leads to the semiclassical Herman-Kluk method. We numerically compare the different methods with another one, based on a static rectangular grid of coherent states, by applying all of them to the revival dynamics in a one-dimensional Morse oscillator, with a special focus on the number of basis states (for the coupled coherent states and Herman-Kluk methods the number of classical trajectories) needed for convergence.

We also extend the Husimi (coherent state) based version of linearized semiclassical theories for the calculation of correlation functions to the case of survival probabilities. This is a case that could be dealt with before only by use of the Wigner version of linearized semiclassical theory. Numerical comparisons of the Husimi and the Wigner case with full quantum results as well as with full semiclassical ones is given for the revival dynamics in a Morse oscillator with and without coupling to an additional harmonic degree of freedom. From this, we see the quantum to classical transition of the system dynamics due to the coupling to the environment (bath harmonic oscillator), which then can lead ultimately to our final goal of thermalization for long-time dynamics. In regard to thermalization in quantum systems, we address the following questions— is it enough to increase the interaction strength between the different degrees of freedom in order to fully develop chaos which is the classical prerequisite for thermalization, or if, in addition, the number of those degrees of freedom has to be increased (possibly all the way to the thermodynamic limit) in order to observe thermalization.

We study the "toppling pencil" model, i.e., an excited initial state on top of the barrier of a symmetric quartic double well to investigate thermalization. We apply the method of coupled coherent states to study the long-time dynamics of this system. We investigate if the coupling of the central quartic double well to a finite, environmental bath of harmonic oscillators in their ground states will let the central system evolve towards its uncoupled ground state. This amounts to thermalization i.e., a cooling down to the bath "temperature" (strictly only defined in the thermodynamic limit) of the central system. It is shown that thermalization can be achieved in finite quantum system with continuous variables using coherent state-based methods to solve the time-dependent Schrödinger equation. Also, here we witness thermalization by coupling the system to a bath of only few oscillators (less than ten), which until now has been seen for more than ten to twenty bath oscillators.

Acknowledgements

This thesis is the result of three years of research work during which several persons have contributed to ensure that the project reaches its completion. It brings me great pleasure now to express my gratitute to all of them.

First and foremost, with a profound sense of gratitude, I would like to express my heartfelt indebtedness to my respected supervisor and mentor, **Prof. Dr. Frank Grossmann**, for his immense support throughout. I learnt a lot from him about theoretical Physics research. I am thankful to him for being so patient with me and allowing me the time to learn and work in my own way, in order to explore the world of theoretical physics. I truly appreciate his kindness and generosity towards me, on every single occasion. I would also like to thank him for taking the time and effort to review my thesis.

I would like to thank **Prof. Dr. Jan Carl Budich**, Chair of Quantum Many-Body Theory group at our institute, for providing a scientifically rich environment to carry out the research work.

I am grateful to the International Max Planck Research School for Many Particle Systems in Structured Environments (IMPRS-MPSSE) for financial support and also for providing the opportunity for scientific exchanges through summer schools, retreats, seminars and talks. I would like to thank **Dr. Paul McClarty**, coordinator of IMPRS-MPSSE for his support, whenever needed during the course of my PhD years.

I am thankful to Prof. Dr. Dmitry Shalashilin for his valuable scientific input on our paper on thermalization. I would also like to thank Prof. Thomas Dittrich and Prof. Marcus Bonanca for the enlightening discussions about thermalization in finite quantum systems.

I would like to thank my Masters thesis advisor from India, **Dr. R. K. Paul**, for always believing in my abilities, sometimes more than I do. His conviction that I will do good research, has always boosted my confidence. He was in constant touch with me during the whole course of my PhD.

I am indebted to my colleague Max Buchholz for his immense help in learning about semiclassical mechanics during the initial phase of my doctoral study. In addition to that, he also helped me in settling down in the new city. Thank you Max, for being so helpful and cooperative.

I am thankful to my colleague Tobias Fiedlschuster for guiding and educating me about the regulations of doctoral studies at TU Dresden. I would also like to thank my colleagues Jan Handt and Michael Werther for their help and support, whenever it was needed. I thank my colleague Michael Werther for the valuable scientific discussions.

Working with others always helps to grow, as it gives the opportunity to learn good things from others. Through these years, I have incorporated a lot of good habits which I took from my colleagues and my supervisor. On this note, I thank my colleague Yulong Qiao for providing the motivation to work harder.

I would like to thank my supervisor and all my colleagues for the countless exchanges on variety of topics, ranging from politics, sports to spirituality, which we had everyday during the lunch time. I still remember the coffee breaks after lunch, when we used to solve crosswords. Max, Tobias and Jan always used to invite me for those coffee breaks. Max was quite good at solving crosswords. I am

thankful to all my friends and acquaintances in Dresden, with whom my time in Dresden has been quite enjoyable.
Last but not the least, I would like to thank my family for the constant motivation and moral support. I am grateful to my brother for his continuous motivation to work harder and also for all his help throughout. He always stood by me as a pillar.
I am blessed to have a father, who always believes in my dreams, sometimes more than I do. This provides me enough strength to work my way up to achieve my dreams. He is my greatest inspiration. My love for knowledge, comes from him. He taught me how to find positivity in everything and also how to remain calm and positive during situations of crisis. I am grateful to both my parents for inculcating good moral values and ethics in me, which always have helped me to come this far.
Finally, no words will ever be sufficient to thank my mother, who has been my constant source of motivation. Thank you Maa, for all your tireless efforts and silent sacrifices to make me what I am today.

List of abbreviations

FPUT	Fermi, Pasta, Ulam and Tsingou
ETH	Eigenstate Thermalization Hypothesis
TDSE	Time-dependent Schrödinger Equation
TDDFT	Time-dependent Density Functional Theory
MCTDH	Multi-configurational time-dependent Hartree(-Fock)
FFT	Fast Fourier Transformation
CCS	Coupled Coherent States
VCS	Variational Coherent States
SCS	Static Grid of Coherent States
SC-IVR	Semiclassical initial value representation
VVG	Van Vleck-Gutzwiller
IVR	Initial value representation
HK	Herman-Kluk
TGWD	Thawed Gaussian wavepacket dynamics
LSC-IVR	Linearized Semiclassical initial value representation
BCH	Baker-Campbell-Haussdorff
FFTW	Fastest Fourier transformation in the West
CS	Coherent State
HH	Henon-Heiles
RHS	Right-hand side
GWP	Gaussian wavepacket
vMCG	Variational multi-configurational Gaussian
TISE	Time-independent Schrödinger Equation

Contents

1. Introduction **1**

1.1. Motivation and Background . . . 1

1.2. Organization of Thesis . . . 4

2. Methods to solve the Time-Dependent Schrödinger Equation **7**

2.1. Quantum methods . . . 7

2.1.1. Split-Operator Method . . . 8

2.1.2. Coupled Coherent States Method . . . 10

2.1.3. Static grid of coherent states . . . 17

2.2. Semiclassical methods . . . 19

2.2.1. Herman-Kluk Propagator . . . 20

2.2.2. Thawed Gaussian Wavepacket Dynamics . . . 22

2.2.3. Linearized Semiclassical Initial Value Representation . . . 24

3. Comparison of different numerical methods **27**

3.1. Model potentials and observables . . . 27

3.1.1. The Morse oscillator and its Hamiltonian matrix . . . 28

3.1.2. Classical equations of motion for a single CS . . . 30

3.1.3. Potential parameters, time scales, initial state, and observables . . . 31

3.2. Numerical Case Study . . . 34

3.2.1. HK results and FFT benchmark . . . 34

3.2.2. SCS results . . . 37

3.2.3. CCS results . . . 39

3.3. Different potentials and their Hamiltonian matrix in the CS basis . . . 42

4. Staying Probability: Husimi Version **43**

4.1. Theory . . . 44

4.1.1. General Correlation Functions . . . 44

4.1.2. Comparison between Wigner LSC-IVR and Husimi LSC-IVR . . . 45

4.2. Quasiclassical Staying Probability Using the HK Propagator . . . 51

4.3. Numerical Results . . . 57

4.3.1. Uncoupled Case . . . 57

4.3.2. Coupling to a Harmonic Bath Degree of Freedom . . . 59

5. Thermalization **61**
5.1. Quartic Double Well coupled to a Finite Heat Bath . . . 62
5.1.1. Quartic Double Well . . . 63
5.1.2. Coupling to a Finite Heat Bath . . . 65
5.2. Long-time dynamics of the coupled system . . . 67
5.2.1. Different numerical measures . . . 68
5.2.2. Numerical results . . . 69

6. Summary and Outlook **75**

Appendix **81**
A. Proof by mathematical induction . . . 81
B. 1D Harmonic oscillator in SCS, CCS and VCS case . . . 82
C. SCS in the tight frame case . . . 85
D. Stability matrix and symplectic integration . . . 86
E. Eigenstates and eigenvalues of the Morse oscillator . . . 89
F. Calculation and Proof of Factorization of $\det \mathbf{A}$ . . . 91
F.1. Calculation of $\det \mathbf{A}$ . . . 91
F.2. Proof of Factorization of $\det \mathbf{A}$ . . . 93
G. Normally ordered Hamiltonian . . . 95
H. Analytical expression for the probability density . . . 99
I. Ground-state energy refers to the zero temperature . . . 102

Bibliography **105**

List of publications **121**

1. Introduction

In this introductory chapter, I would like to first lay out the motivation to study "thermalization" in quantum systems. I would also provide the foundation and background of the research to be presented in this thesis. Later on, the organization of the thesis will be presented.

1.1. Motivation and Background

Thermalization, a widely studied concept in Physics, is the process of physical bodies reaching thermal equilibrium through mutual interaction. In general, it is the natural tendency of a system towards a state of equipartition of energy and uniform temperature that maximizes the system's entropy. The system under investigation is assumed to be in thermal contact with a bath or reservoir. The concept of thermalization is used in almost all fields of Physics ranging from atomic to molecular, plasma physics and solid state system all the way to cosmology. Examples of thermalization include the achievement of equilibrium in plasma.

Thermalization can be studied in various realms like classical, semiclassical and quantum mechanical. In a conventional quantum Brownian motion setting, a system of interest with a relatively small number of degrees of freedom interacts with a much larger surrounding that gives rise to diffusive motion, decoherence and equilibration. Especially equilibration or thermalization, possibly towards a thermal state, has come in the focus of interest recently, due to some groundbreaking developments in the so-called canonical typicality [1–4]. In a nutshell, in a bipartite quantum system, consisting of a system proper and an environment with a high-dimensional Hilbert space, a description of thermalization on the wavefunction level is adequate, because almost every initial pure state will eventually yield for some observable a very similar outcome, e.g., will lead to a canonical density matrix for the system. It has been pointed out that entanglement between subsystems is responsible for the thermalization [4]. More recently these studies have been put to good use in a solid state context, where numerical methodology has been developed for spin dynamics of Hilbert spaces of dimensions almost 10^4 times larger than in existing exact diagonalization studies [5]. It should be mentioned that the typicality concept has also been established in purely classical context [2]. Furthermore, we stress that for typicality on the level of states (not only of some observables) the considered quantum system must be bipartite (e.g. of system bath type) [2].

In the classical realm, first groundbreaking studies of thermalization have been performed by Fermi, Pasta, Ulam and Tsingou (FPUT) for a chain of a few weakly coupled anharmonic oscillators [6]. Ever since then, the puzzle of energy exchange between subsystems, eventually leading to equlibration and thermalization in closed systems with a finite number of degrees of freedom has intrigued researchers

in the fields of classical [7–16], as well as semiclassical [17, 18] and quantum mechanics [2, 7, 19–27]. Most of the works on thermalization from the quantum mechanical realm, include spin systems whereas there hasn't been much work done on continuous systems except [24], where the authors study the quantum dynamics of vibrational energy flow in oscillator chains driven by anharmonic interactions. In this thesis, our focus will be on systems with *continuous* variables where every single degree of freedom has an infinitely large Hilbert space, in contrast to spin systems.

In the context of quantum thermalization, an important concept is the eigenstate thermalization hypothesis (ETH) [28, 29]. Thermalization in classical systems is closely related to the idea of chaos and ergodicity. The ETH can be regarded, very broadly, as the quantum manifestation of such ergodic behavior. The principal philosophy underlying the ETH is that instead of explaining the ergodicity of a thermodynamic system through the mechanism of dynamical chaos, as done in classical mechanics, one should instead examine the properties of matrix elements of observable quantities in individual energy eigenstates of the system. The eigenstate thermalization hypothesis states that for an arbitrary initial state of the system, the expectation value of any observable will ultimately evolve in time to its value predicted by a microcanonical ensemble, and thereafter will exhibit only small fluctuations around that value. However, there are also other alternative ways to investigate thermalization in quantum systems. Here, in contrast to the ETH, we look at the reduced dynamics of a system which is coupled to a finite heat bath, acting as the environment. The idea here is that the coupling between the system and bath acts as the mediator in the exchange of energy between the system and the bath which ultimately leads to thermalization by increasing the bath size up to few degrees of freedom. In this thesis, it will be shown that the system closely approaches a state of thermal equilibrium with a bath of only up to five degrees of freedom. Earlier it was claimed in [21] that as little as ten to twenty harmonic (bath) degrees of freedom are necessary to observe the energy loss to the bath without backflow on the observed time scales. The observables which we look at to investigate thermalization are energy expectation values, auto-correlation functions as well as reduced densities calculated using the quantum method, which is going to be discussed below and also in detail in Chapter 2.

In order to investigate thermalization in quantum systems, we need to study the quantum dynamics of the underlying system, which can be performed by solving time-dependent Schrödinger equation (TDSE). At the first sight, it seems to be quite an easy task – as to just take the almost century-old Schrödinger equation, plug in the potential and solve for Ψ, which is the wavefunction. But unfortunately analytic solutions exist only for a few simple model systems. As soon as there is nontrivial coupling between different degrees of freedom of the quantum system, one has to resort to numerical solutions. Again a full numerical solution of the TDSE is limited to systems with up to five or six degrees of freedom, because the number of basis states or grid points required for representing the wavefunction grows exponentially with the dimensionality of the system. Without having the possibility to find an analytical or numerically exact, full quantum solution to a general system, alternative descriptions and approximations of some kind have to be introduced in order to make its dynamics accessible. To date, there is no single method that is ideally suited to describe every conceivable quantum system; instead the approach has to be chosen according to the properties of the

particular atomic or molecular system and also according to the specific problem under investigation.

Therefore, over the last decades, a host of different numerical treatments for time-dependent quantum systems have been developed. One very popular approach is the time-dependent density functional theory (TDDFT). In TDDFT, one does not calculate the wavefunction but rather the single-particle density, from which in principle all time-evolved observables can be found. TDDFT has seen many successful applications in all areas of quantum dynamics, as exemplified by a recent review and extensive references therein [30]. Another approach, again with a wide range of applications, is known as the multi-configurational time-dependent Hartree(-Fock) (MCTDH) [31, 32]. It relies on a representation of the wavefunction in terms of a combination of single-particle wavefunctions. Using the Dirac-Frenkel variational principle, equations of motion can be derived for the coefficients as well as for the expansion functions. In order for the method to work efficiently and avoid exponential scaling, the Hamiltonian has to be represented in an appropriate product form, which is one of the main challenges of this methodology. Since its 25 years of introduction, MCTDH has seen several extensions such as multilayer MCTDH, which allows for the inclusion of hundreds of degrees of freedom. However, one of the most popular numerically exact method to solve the TDSE is the split-operator fast Fourier transformation (FFT) which is a grid based method and scales numerically as $N \log N$, where N is the number of grid points. But due to the exponential scaling of the method with the increase in the number of degrees of freedom, it can treat systems with no more than five degrees of freedom. In this thesis, however we have used split-operator FFT as the benchmark to compare our results from other numerical solutions as it is a numerically exact method in the limit of infinitely small time steps.

In this thesis, we have widely used the method of coupled coherent states (CCS), introduced by Shalashilin and Child [33] which is again based on the Dirac-Frenkel variational principle similar to the MCTDH. In the methods based on the variational principle, the wavefunction is expressed as an expansion in the coherent state basis, with time-dependent coefficients. The method of CCS is a first level of approximation to the full variational coherent states (VCS) method, where in the VCS method the coefficients as well as the coherent state parameters are propagated using the full variational equations of motion [34]. The approximation made to derive CCS from VCS is to refrain from the full variational solution of the coherent state parameters but to let those be determined by the classical equations of motion. One step higher level of approximation than CCS is the method of static grid of coherent states (SCS), which is not very well suited for treating large numbers of degrees of freedom.

Here we have also focused on semiclassical dynamics, and in particular semiclassical initial value representations (SC-IVRs) which is a different route towards describing the time evolution of a quantum system. While TDDFT, MCTDH and other variational methods take a top-down approach – starting from the full quantum problem and finding approximations such that analytical or numerical calculations become feasible, SC-IVRs go the opposite way, using classical trajectories as the backbone and adding a complex, action-dependent phase factor in order to allow for interference and thus incorporate quantum effects. Apart from the possible numerical savings, relying on classical

trajectories brings about the conceptual advantage of explaining and understanding quantum results intuitively in terms of classical mechanics. On the other hand, unlike in classical molecular dynamics, soft quantum effects such as zero-point energy and interference are an inherent part of semiclassical theories without having to resort to any ad-hoc additions to the equations of motion.

The semiclassical approximation for the time evolution of a quantum system can be derived from the (exact) path integral formulation of the position space matrix element of the time evolution operator or propagator, that has been introduced by R. Feynman [35]. The so-called semiclassical approximation makes a stationary phase approximation to the propagator, assuming that typical action differences between contributing trajectories of the system are much larger than the reduced Planck's constant $\hbar$. The resulting propagator is based on boundary value problem and is known as the Van Vleck-Gutzwiller (VVG) propagator. Alternatively, one can express the exact propagator in terms of coherent states and replace the resulting coherent state matrix element of the time evolution operator by its semiclassical approximation, which is found in the same way as before. Evaluating the integration over final positions in another stationary phase approximation [36] then yields an expression where only an integration over the initial phase space positions is left. This is referred to as the initial value representation (IVR). The IVR time evolution operator is widely used in the form suggested by M. Herman and E. Kluk [37] known as the Herman-Kluk (HK) propagator. Like any other SC-IVR, the HK propagator contains a phase space integration over initial conditions, and as before, each trajectory is weighted with a complex phase allowing for interference as well as a prefactor that depends on the stability of the given trajectory. Ten years after its first appearance, the HK propagator was shown to be an efficient special case of a more general IVR in a rederivation by K. Kay [38, 39].

Other semiclassical methods include thawed gaussian wavepacket dynamics (TGWD), semiclassical hybrid dynamics as well as the linearized semiclassical initial value representation (LSC-IVR). LSC-IVR, which is also known as classical Wigner dynamics ([40, 41]) and used for the calculation of correlation functions, serves as a classical comparison to semiclassical results. It was introduced by Sun, Wang and Miller [42–46]. Another LSC-IVR based on Husimi transforms was introduced by Antipov, Ye and Ananth [47], known as Husimi LSC-IVR. As an original contribution to the field of semiclassical mechanics, we extended the Husimi (coherent state) based version of linearized semiclassical theories for the calculation of correlation functions to the case of survival probabilities. This is the case that could be dealt with before only by use of the Wigner version of linearized semiclassical theory.

1.2. Organization of Thesis

In Chapter 2, different methods to solve the TDSE are given. The methods have been classified into full quantum solutions and semiclassical solutions. In the quantum methods, we discuss in detail the split-operator FFT, CCS and SCS. We describe the HK propagator, TGWD and LSC-IVR among the semiclassical methods. In Chapter 3, we provide a numerical comparison of different methods to

solve the TDSE. We choose a one dimensional Morse oscillator as the model potential to compare the different numerical methods. At the end of the Chapter 3, we also provide the Hamiltonian matrix elements of some of the very common potentials like Morse, harmonic, quartic, that are used in calculating CCS equations of motion in order to study the quantum dynamics.

In Chapter 4, we extend the Husimi (coherent state) based version of linearized semiclassical theories for the calculation of correlation functions to the case of survival probabilities. We develop a consistent approach to the linearized survival (or staying) probability, using the so-called HK propagator. The need to find the correct Husimi version for staying probability lies in the fact that Wigner-Weyl and Husimi transform version of linearized semiclassical theories lead to the same final formula for the case of dipole-dipole correlation function, whereas they are quite different in the case of survival probability, where strictly, the simple Husimi version is not applicable. The newly developed formalism is applied to the revival dynamics of a Morse oscillator coupled to a harmonic mode in order to see the quantum to classical transition of the system dynamics.

Finally, in Chapter 5, we investigate the longstanding problem of thermalization of quantum systems coupled to an environment by focusing on a bistable quartic oscillator interacting with a finite number of harmonic oscillators. In order to overcome the exponential wall that one usually encounters in grid based approaches to solve the TDSE of the extended system, methods based on time-dependent variational principle are best suited. We apply the method of CCS to study the quantum dynamics of the system under investigation. We investigate the dynamics of an initial wavefunction on the top of the barrier of the double well.

At the end, Chapter 6 provides the summary and conclusion of this thesis. It also throws light upon possible future work. The appendix complements this work by additional detailed calculations and numerical details.

2. Methods to solve the Time-Dependent Schrödinger Equation

In order to study the system dynamics quantum mechanically, we have two alternative approaches. One approach is using the density matrix known as the density matrix formulation. The other one is the wavefunction based method which is used to solve the time-dependent Schrödinger equation. Just as the Schrödinger equation describes how the pure states evolve in time, the von Neumann equation (also known as the Liouville-von Neumann equation) describes how a density operator evolves in time. Density matrices are, e.g., used to define a finite temperature state of the system [48]. However, the density matrix based approach is enormously costly in terms of memory as because even for a single degree of freedom, it requires a two-dimensional grid to represent the density matrix in position representation making it very memory demanding for higher degrees of freedom. In contrast wavefunction based methods require just a single grid per degree of freedom and if coupled to a bath, the system develops on short time scale into a "thermal state" [2]. Therefore, in this thesis our focus will be only on wavefunction based methods. In the following, different ways to solve the TDSE will be described like the split-operator fast Fourier transformation, which is a numerically exact method and then the coupled coherent states method based on a first level of approximation to the numerically exact full variational principle. Then at the end we will also discuss semiclassical propagators like the Herman-Kluk propagator. We have categorized the methods based on full quantum and semiclassical approaches.

2.1. Quantum methods

The equation we want to solve is the TDSE. In representation free form, the TDSE is given by

$$\mathrm{i}\hbar|\dot{\Psi}(\mathrm{t})\rangle = \hat{\mathrm{H}}|\Psi(\mathrm{t})\rangle. \tag{2.1}$$

Here in general, $\hat{H}$ is a many-body Hamiltonian, for f degrees of freedom, which in the remainder of this thesis is of the form

$$\hat{H} = \sum_{i=1}^{f} \hat{T}_i + \hat{V} \tag{2.2}$$

The explicit expression for the potential energy operator $\hat{V}$, which contains coupling terms between the different degrees of freedom will be detailed later. There are various full quantum mechanical

solutions of the TDSE. These can be distinguished by their treatment of discretization of time and space or the choice of finite basis. The time evolution can be treated in different ways as, e.g., finite differencing, the Crank-Nicolson method or polynomial methods [49]. Applying an expansion of the wavefunction in terms of eigenfunctions $|m\rangle$ of the Hamiltonian, according to

$$|\Psi\rangle = \sum_{m=1}^{M_f} c_m |m\rangle \tag{2.3}$$

the time-evolved wavefunction

$$|\Psi(t)\rangle = \sum_{m=1}^{M_f} c_m |m\rangle \mathrm{e}^{-\mathrm{i}\hat{\mathrm{E}}_\mathrm{m}\mathrm{t}/\hbar} \tag{2.4}$$

is determined by the eigenvalues E_m of the Hamiltonian. This expression would be exact if the summation would extend to infinity. The numerical effort of the solution of the eigenvalue problem of the $M_f \times M_f$ dimensional Hamiltonian matrix underlying the above approach, however, scales as M_f^3. If all the degrees of freedom are represented by a basis of identical dimension M, this amounts to M^{3f} and thus the eigenfunction approach is not viable, even for the moderate values of f and M.

If the wavefunction is represented on a position grid, however, with N being the number of grid points per degree of freedom and if the split-operator FFT method is used for the time evolution, the numerical effort just scales as $N^f f \log N$ [50]. That's why we have used split-operator FFT to compare some of our numerical results obtained using CCS method and also using HK propagator. A detailed comparison of different numerical propagation schemes for solving the TDSE in the position representation in one dimension for mixed quantum and molecular dynamics simulations is laid out in [51].

2.1.1. Split-Operator Method

Let us consider a particle moving in one spatial dimension under a Hamiltonian of usual form

$$\hat{H} = \hat{T}_k(\hat{p}) + \hat{V}(x) \tag{2.5}$$

In the split-operator method, we make use of the well-known Zassenhaus formula [52][1]

$$\mathrm{e}^{\hat{x}+\hat{y}} = \mathrm{e}^{\hat{x}}\mathrm{e}^{\hat{y}}\mathrm{e}^{-1/2[\hat{x},\hat{y}]}\mathrm{e}^{1/3[\hat{y},[\hat{x},\hat{y}]]+1/6[\hat{x},[\hat{x},\hat{y}]]}\ldots \tag{2.6}$$

in order to approximate the time-evolution operator. For very short but finite time steps Δt, one then finds from the Zassenhaus formula that

$$\mathrm{e}^{-\mathrm{i}\hat{\mathrm{H}}\Delta\mathrm{t}/\hbar} \approx \mathrm{e}^{-\mathrm{i}\hat{\mathrm{T}}_\mathrm{k}\Delta\mathrm{t}/\hbar}\mathrm{e}^{-\mathrm{i}\hat{\mathrm{V}}\Delta\mathrm{t}/\hbar}, \tag{2.7}$$

[1] The Baker-Campbell-Haussdorff (BCH) formula is the dual relation and reads $\exp\{\hat{x}\}\exp\{\hat{y}\} = \exp\{\hat{x}+\hat{y}+1/2[\hat{x},\hat{y}]+1/12([\hat{x},[\hat{x},\hat{y}]]+[\hat{y},[\hat{x},\hat{y}]])\}+\ldots$.

which is accurate up to the first order in Δt. This approximation is also referred to as the Trotter product [53]. A more "symmetric" splitting of the Hamiltonian also known as the Strang splitting according to

$$\mathrm{e}^{-\mathrm{i}\hat{\mathrm{H}}\Delta\mathrm{t}/\hbar} = \mathrm{e}^{-\mathrm{i}\hat{\mathrm{V}}\Delta\mathrm{t}/(2\hbar)}\mathrm{e}^{-\mathrm{i}\hat{\mathrm{T}}_\mathrm{k}\Delta\mathrm{t}/\hbar}\mathrm{e}^{-\mathrm{i}\hat{\mathrm{V}}\Delta\mathrm{t}/(2\hbar)} + O(\Delta t^3) \tag{2.8}$$

leads to an approximation of higher accuracy. In order to calculate the time-evolved wavefunction, we need to represent the initial wavefunction at time $t = 0$ on a position space grid $x_n \in [x_{min}, x_{max}], n = 1, 2, ..., N$. The wavefunction propagated for a small time step Δt at the grid point x_n is then given by

$$\begin{aligned}\psi(x_n, \Delta t) &= \langle x_n|\mathrm{e}^{-\mathrm{i}\hat{\mathrm{H}}\Delta\mathrm{t}/\hbar}|\psi(0)\rangle \\ &= \langle x_n|\mathrm{e}^{-\mathrm{i}\hat{\mathrm{V}}\Delta\mathrm{t}/(2\hbar)}\mathrm{e}^{-\mathrm{i}\hat{\mathrm{T}}_\mathrm{k}\Delta\mathrm{t}/\hbar}\mathrm{e}^{-\mathrm{i}\hat{\mathrm{V}}\Delta\mathrm{t}/(2\hbar)}|\psi(0)\rangle\end{aligned} \tag{2.9}$$

By inserting unity twice in terms of position states and once in terms of momentum states, the three-fold integral (for the numerics, the integrations are discretized due to the grid based representation of the wavefunction)

$$\begin{aligned}\psi(x_n, \Delta t) = &\int \mathrm{d}x' \int \mathrm{d}p' \int \mathrm{d}x'' \langle x_n|\mathrm{e}^{-\mathrm{i}\hat{\mathrm{V}}\Delta\mathrm{t}/(2\hbar)}|x''\rangle \\ &\langle x''|\mathrm{e}^{-\mathrm{i}\hat{\mathrm{T}}_\mathrm{k}\Delta\mathrm{t}/\hbar}|p'\rangle\langle p'|\mathrm{e}^{-\mathrm{i}\hat{\mathrm{V}}\Delta\mathrm{t}/(2\hbar)}|x'\rangle\langle x'|\psi(0)\rangle\end{aligned} \tag{2.10}$$

emerges. The integral over x'' can be performed immediately because of the diagonal nature of the potential in position space and the matrix element of the exponentiated potential operator between x_n and position state x'' can be written in terms of δ function as

$$\langle x_n|\mathrm{e}^{-\mathrm{i}\hat{\mathrm{V}}\Delta\mathrm{t}/(2\hbar)}|x''\rangle = \mathrm{e}^{-\mathrm{iV}(\mathrm{x_n})\Delta\mathrm{t}/(2\hbar)}\delta(x'' - x_n). \tag{2.11}$$

Also the second exponentiated potential term simplifies as

$$\begin{aligned}\langle p'|\mathrm{e}^{-\mathrm{i}\hat{\mathrm{V}}\Delta\mathrm{t}/(2\hbar)}|x'\rangle &= \langle p'|x'\rangle\mathrm{e}^{-\mathrm{iV}(\mathrm{x}')\Delta\mathrm{t}/(2\hbar)} \\ &= \frac{1}{\sqrt{2\pi\hbar}}\mathrm{e}^{-\mathrm{ip}'\mathrm{x}'/\hbar}\mathrm{e}^{-\mathrm{iV}(\mathrm{x}')\Delta\mathrm{t}/(2\hbar)}\end{aligned} \tag{2.12}$$

The x' integration is a Fourier transformation of the "intermediate wavefunction"

$$\tilde{\psi}(x', 0) = \mathrm{e}^{-\mathrm{iV}(\mathrm{x}')\Delta\mathrm{t}/(2\hbar)}\psi(x', 0) \tag{2.13}$$

into momentum space. This then leads to the fact that the exponentiated kinetic energy operator becomes a multiplicative factor and matrix element of that operator can be expressed as

$$\begin{aligned}\langle x''|\mathrm{e}^{-\mathrm{i}\hat{\mathrm{T}}_\mathrm{k}\Delta\mathrm{t}/\hbar}|p'\rangle &= \langle x''|p'\rangle \mathrm{e}^{-\mathrm{i}\mathrm{T}_\mathrm{k}(\mathrm{p}')\Delta\mathrm{t}/\hbar} \\ &= \frac{1}{\sqrt{2\pi\hbar}}\mathrm{e}^{\mathrm{i}\mathrm{p}'\mathrm{x}''/\hbar}\mathrm{e}^{-\mathrm{i}\mathrm{T}_\mathrm{k}(\mathrm{p}')\Delta\mathrm{t}/\hbar}\end{aligned} \tag{2.14}$$

The p' integration transforms the wavefunction back into position space. The algorithm for the implementation of the split-operator FFT method[2] is given below:

1. Use position space to represent the initial wavefunction.
2. Apply the diagonal operator $\mathrm{e}^{-\mathrm{i}\mathrm{V}(\mathrm{x}')\Delta\mathrm{t}/(2\hbar)}$.
3. Perform an FFT into momentum space.
4. Apply the diagonal operator $\mathrm{e}^{-\mathrm{i}\mathrm{T}_\mathrm{k}(\mathrm{p}')\Delta\mathrm{t}/\hbar}$.
5. Perform an inverse FFT back into position space.
6. Apply the diagonal operator $\mathrm{e}^{-\mathrm{i}\mathrm{V}(\mathrm{x}')\Delta\mathrm{t}/(2\hbar)}$.

The main numerical effort goes in performing two Fourier transforms during the propagation over single time step. However, these can be performed using FFT algorithm [55]. This procedure is applied for the propagation over a very small time step. For the propagation over a finite time it will be repeated frequently and if the intermediate values of the wavefunction are not needed the two half time steps of potential propagation can be combined (apart from the first and the last one). Furthermore, to propagate the wavefunction over the next time step, we will need its value not only at x_n but at all values of x. This reflects the *nonlocal* nature of quantum theory. To calculate the new wavefunction, the old one is needed everywhere. This is in contrast to classical mechanics. Classical mechanics is a local theory wherein a trajectory only depends on its initial conditions.

A nice review about the details of FFT and a corresponding subroutine is given in [55]. For implementation of the numerics it is important to note that the grid points N has to be a power of 2 i.e., $N = 2^j$. Also the grid points should be equidistant. In the case of split-operator FFT method, the numerical effort scales as $N \log N$ [55]. More details about the numerical implementation is given in [49]. There are more recent implementations of FFT which do not have the restriction to integer powers of 2 and which, through adaption to the platform that is used for the calculations can have considerable advantages in speed (FFTW: fastest Fourier transformation in the West [56]).

2.1.2. Coupled Coherent States Method

To tackle the quantum dynamics under the many-body Hamiltonian, grid based methods are running into an exponential wall and we will use a variational approach, based on coherent states, that has

[2] Originally this approach was proposed by Fleck, Morris and Feit for the solution of the Maxwell wave-equation [54].

been introduced by Shalashilin and Child [33, 57], and was recently reviewed in [34]. In the following we will introduce the so-called coupled coherent state Ansatz and its working equations, extending the notation of [34] towards many degrees of freedom.

We set the stage by considering a multidimensional system whose dynamics is governed by the Hamiltonian

$$\hat{H}(t) = \hat{T}(\hat{\mathbf{p}}) + \hat{V}(\hat{\mathbf{x}}, t), \tag{2.15}$$

consisting of a kinetic and a potential energy term, depending on momentum, respectively position (and possibly explicitly on time). For a system of f degrees of freedom, an Ansatz for the solution of the TDSE is given in terms of normalized coherent states (CSs) of multiplicity M by

$$|\Psi^{\mathrm{M}}_{\mathrm{CS}}(t)\rangle = \sum_{l=1}^{M} a_l(t)|\boldsymbol{z}_l(t)\rangle, \tag{2.16}$$

with time-dependent complex coefficients $a_l(t)$ and time-dependent f-dimensional complex displacement vectors

$$\boldsymbol{z}_l(t) = \frac{\boldsymbol{\gamma}^{1/2}\boldsymbol{q}_l(t) + \mathrm{i}\hbar^{-1}\boldsymbol{\gamma}^{-1/2}\boldsymbol{p}_l(t)}{\sqrt{2}}, \tag{2.17}$$

with the phase-space variables $\boldsymbol{q} = (q_1, \ldots, q_f)$ and $\boldsymbol{p} = (p_1, \ldots, p_f)$ and diagonal matrix $\boldsymbol{\gamma}$ with entries $\gamma_j = m_j\omega_j/\hbar, \quad j = 1, \ldots, f$, where the indices starting from 1 to f denote the different degrees of freedom. $\boldsymbol{\gamma}$ is known as the width parameter matrix. Here m_j and ω_j denote the mass and frequency of the j-th Harmonic oscillator (needed to create the coherent state basis) whose Hamiltonian reads

$$\hat{H}_{\mathrm{HO}_j} = \hbar\omega_j \left(\hat{a}_j^\dagger \hat{a}_j + \frac{1}{2}\right). \tag{2.18}$$

The f-mode CS is given by an f-fold tensor product

$$|\boldsymbol{z}_l\rangle = \bigotimes_{j=1}^{f} |z_{lj}\rangle \tag{2.19}$$

of normalized one-dimensional CSs

$$|z_{lj}\rangle = \exp\left[-\frac{1}{2}|z_{lj}|^2\right] \exp\left[z_{lj}\hat{a}_j^\dagger\right] |0_j\rangle, \tag{2.20}$$

where $\hat{a}_j^\dagger$ is the creation operator acting on the ground state of a suitably chosen j-th harmonic oscillator. In position representation the CSs are Gaussian wavefunctions, also known as "frozen

Gaussians". The multidimensional Gaussian wavepacket is given by

$$\begin{aligned}\langle \boldsymbol{x}|\boldsymbol{z}_l\rangle &= \left(\frac{\det\boldsymbol{\gamma}}{\pi^f}\right)^{\frac{1}{4}} \exp\left[-\left(\boldsymbol{x}-\boldsymbol{q}_l\right)^{\mathrm{T}}\frac{\boldsymbol{\gamma}}{2}\left(\boldsymbol{x}-\boldsymbol{q}_l\right)+\frac{\mathrm{i}}{\hbar}\boldsymbol{p}_l^{\mathrm{T}}\left(\boldsymbol{x}-\frac{\boldsymbol{q}_l}{2}\right)\right] \\ &= \prod_{j=1}^{f}\left(\frac{\gamma_j}{\pi}\right)^{\frac{1}{4}} \exp\left[-\frac{\gamma_j}{2}\left(x_j-q_{lj}\right)^2+\frac{\mathrm{i}}{\hbar}p_{lj}\left(x_j-\frac{q_{lj}}{2}\right)\right] \end{aligned} \tag{2.21}$$

with the Klauder phase convention [58]. The one-dimensional CS $|z_j\rangle$ is a (right) eigenfunction (eigenket) of the one-dimensional annihilation operator

$$\hat{a}_j = \frac{\gamma_j^{1/2}\hat{q}_j + \mathrm{i}\hbar^{-1}\gamma_j^{-1/2}\hat{p}_j}{\sqrt{2}}, \tag{2.22}$$

with eigenvalue z_j [59, 60]

$$\hat{a}_j|z_j\rangle = z_j|z_j\rangle. \tag{2.23}$$

Hence the eigenvalue of the multidimensional annihilation operator is given by

$$\hat{\boldsymbol{a}}|\boldsymbol{z}\rangle = \boldsymbol{z}|\boldsymbol{z}\rangle. \tag{2.24}$$

For notational simplicity, in the following, we set $\hbar = 1$. In representation free form, the CSs are given by the application of the displacement operator (see, e.g., the appendix of [61] for a collection of its properties) to the ground state, via

$$|\boldsymbol{z}_l\rangle = \hat{D}(\boldsymbol{z}_l)|0\rangle \equiv \exp\left[\boldsymbol{z}_l\hat{\boldsymbol{a}}^\dagger - \boldsymbol{z}_l^*\hat{\boldsymbol{a}}\right]|0\rangle = \exp\left[-\frac{1}{2}|\boldsymbol{z}_l|^2\right]\exp\left[\boldsymbol{z}_l\hat{\boldsymbol{a}}^\dagger\right]|0\rangle, \tag{2.25}$$

where $\hat{\boldsymbol{a}}^\dagger$ is the multidimensional creation operator and for the last equality it has been used that the application of the annihilation operator to the ground state gives zero.

Furthermore, a finitely spaced grid of CSs forms an over-complete and non-orthogonal basis set [62], allowing the representation of unity in terms of the double sum (for a heuristic proof, starting from Eq. (2.16) see, e.g., Exercise 8.81 in [63])

$$\hat{1} = \sum_{k,l}|\boldsymbol{z}_k\rangle(\boldsymbol{\Omega}^{-1})_{kl}\langle\boldsymbol{z}_l|, \tag{2.26}$$

with the overlap matrix $\boldsymbol{\Omega}$ with elements

$$\Omega_{kl} = \langle\boldsymbol{z}_k|\boldsymbol{z}_l\rangle, \tag{2.27}$$

if the requirement

$$z_{lj} = \beta(m_j + \mathrm{i}n_j), \tag{2.28}$$

with $k = (m_j, n_j)$ where m_j, n_j are integers and $0 < \beta \leq \sqrt{\pi}$, for the spacing of the grid points is met [62, 64], see also Chapter 10.5.1 in [63]. We call this criterion the Perelomov-Bargmann-Butera-Girardello-Klauder (PBBGK) criterion, whereas the special case $\beta = \sqrt{\pi}$ has the name of von Neumann attached to it [65, 66]. Physically, it means that the cells in (p, q) phase space that are spanned by the grid points must have an area less or equal to 2π in the present units (Planck cell). Thus completeness holds for a phase-space lattice of coherent states if and only if the density of states per Planck unit cell is equal to or greater than one. A corresponding graphical illustration is given in Fig. 2.1. The z-grid does not necessarily have to be square but may also be rectangular, as long as the Planck cell criterion is not surpassed [62]. This fact is corroborated by our numerical experience. The completeness relation (2.26) had been postulated by von Neumann [65], and a mathematical proof has been given independently by Perelomov [64] and Bargmann et al. [62].

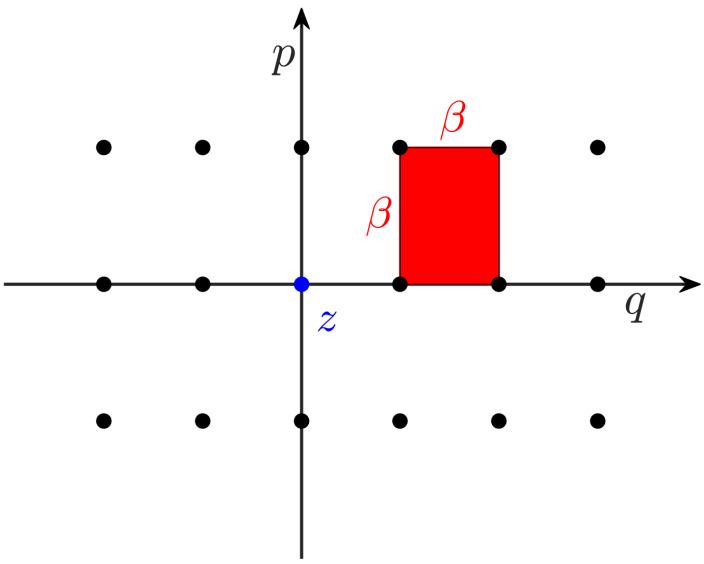

Figure 2.1.: Overcompleteness of CS: if the area of the phase-space region shaded in red is at most π (i.e. a Planck unit cell), the CS corresponding to the lattice form an overcomplete set.

The overlap of two f-dimensional CSs [59] is given by

$$\begin{aligned}
\langle \boldsymbol{z}_k | \boldsymbol{z}_l \rangle &= \exp\left[-\frac{1}{2}(|\boldsymbol{z}_k|^2 + |\boldsymbol{z}_l|^2) + \boldsymbol{z}_k^* \cdot \boldsymbol{z}_l\right] \\
&= \prod_{j=1}^{f} \langle z_{kj} | z_{lj} \rangle \\
&= \prod_{j=1}^{f} \exp\left[-\frac{1}{2}(|z_{kj}|^2 + |z_{lj}|^2) + z_{kj}^* z_{lj}\right] \\
&= \exp\left[-(\boldsymbol{q}_l - \boldsymbol{q}_k)^{\mathrm{T}} \frac{\boldsymbol{\gamma}}{4} (\boldsymbol{q}_l - \boldsymbol{q}_k) - (\boldsymbol{p}_l - \boldsymbol{p}_k)^{\mathrm{T}} \frac{\boldsymbol{\gamma}^{-1}}{4} (\boldsymbol{p}_l - \boldsymbol{p}_k) + \frac{\mathrm{i}}{2}(\boldsymbol{p}_l \cdot \boldsymbol{q}_k - \boldsymbol{q}_l \cdot \boldsymbol{p}_k)\right] \quad (2.29)
\end{aligned}$$

which has a different phase compared to the expression to be used below for the HK propagator [67] and is a product of the corresponding single-mode overlaps. The absolute value of the overlap of two one-dimensional CSs as a function of q_k and p_k is plotted in Fig. 2.2. It reveals that, although two arbitrary CSs have non-vanishing overlap, the overlap decreases exponentially with the distance between the CSs.

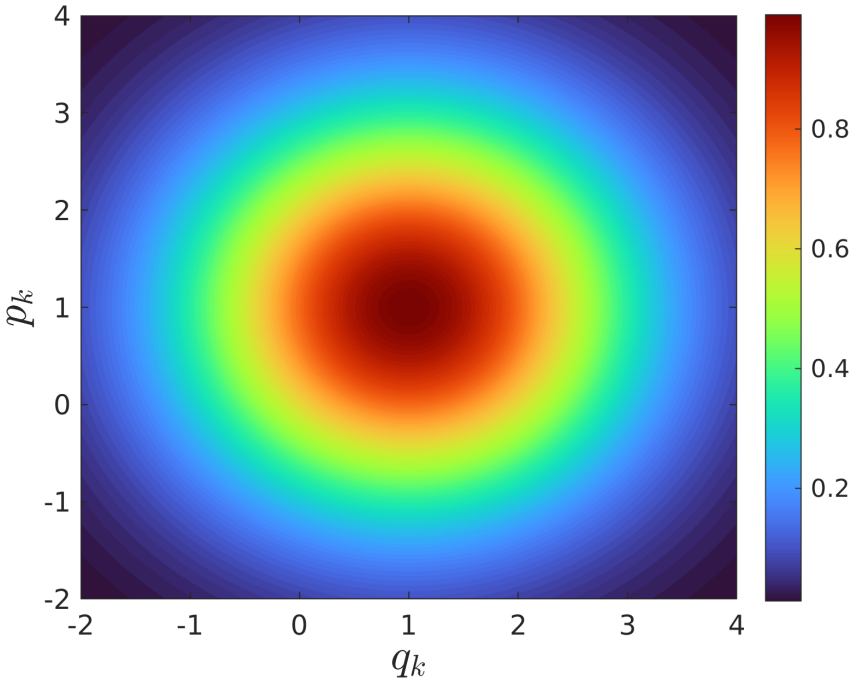

Figure 2.2.: Absolute value of the overlap $\langle z_k|z_l\rangle$ of two one-dimensional CSs for fixed $(q_l, p_l) = (1, 1)$ as a function of q_k and p_k with width parameter $\gamma = 1$.

In order to derive the CCS method from the numerically exact solution of the TDSE, we first discuss the numerically exact solution of the TDSE by varying, without any approximation, both $a_k(t)$ as well as $\boldsymbol{z}_k(t)$. This way, the partial differential TDSE is transformed into a set of coupled, nonlinear ordinary differential equations. The time-evolution of the coefficients and the displacements is governed by the Dirac-Frenkel variational principle [68–71]

$$\langle \delta\Psi^{\mathrm{M}}_{\mathrm{CS}}|\mathrm{i}\partial_t - \hat{H}|\Psi^{\mathrm{M}}_{\mathrm{CS}}\rangle = 0, \tag{2.30}$$

where the variation reads

$$\langle \delta\Psi^{\mathrm{M}}_{\mathrm{CS}}| \;=\; \sum_{k=1}^{M}\langle \boldsymbol{z}_k|\left\{\delta a_k^* + a_k^*\left[\left(-\frac{1}{2}\boldsymbol{z}_k + \hat{\boldsymbol{a}}\right)\cdot\delta\boldsymbol{z}_k^* \;-\; \frac{1}{2}\boldsymbol{z}_k^*\cdot\delta\boldsymbol{z}_k\right]\right\}. \tag{2.31}$$

The variation with respect to the displacements is most easily calculated from Eq. (2.20). All appear-

ing variations are mutually independent. Thus the equations of motion read

$$\langle \boldsymbol{z}_k | \mathrm{i}\partial_t - \hat{H} | \Psi_{\mathrm{CS}}^{\mathrm{M}} \rangle = 0, \tag{2.32}$$

$$a_k^* \langle \boldsymbol{z}_k | \hat{\boldsymbol{a}} \left(\mathrm{i}\partial_t - \hat{H} \right) | \Psi_{\mathrm{CS}}^{\mathrm{M}} \rangle = 0, \tag{2.33}$$

where Eq. (2.32) was obtained from the variations of the coefficients, Eq. (2.33) was obtained from the variations of the displacements, where the first equation was used to simplify the second one.

By insertion of the explicit expression for the time-derivative of the Ansatz wavefunction

$$\partial_t | \Psi_{\mathrm{CS}}^{\mathrm{M}} \rangle = \sum_{l=1}^{M} \left\{ \dot{a}_l + a_l \left[-\frac{1}{2} \left(\boldsymbol{z}_l \cdot \dot{\boldsymbol{z}}_l^* + \dot{\boldsymbol{z}}_l \cdot \boldsymbol{z}_l^* \right) + \dot{\boldsymbol{z}}_l \cdot \hat{\boldsymbol{a}}^\dagger \right] \right\} | \boldsymbol{z}_l \rangle, \tag{2.34}$$

the equations of motion (2.32, 2.33) then read

$$\mathrm{i} \sum_{l=1}^{M} \langle \boldsymbol{z}_k | \boldsymbol{z}_l \rangle \left[X_l + a_l \left(\boldsymbol{z}_k^* \cdot \dot{\boldsymbol{z}}_l \right) \right] = \langle \boldsymbol{z}_k | \hat{H} | \Psi_{\mathrm{CS}}^{\mathrm{M}} \rangle, \tag{2.35}$$

$$\mathrm{i} a_k^* \sum_{l=1}^{M} \langle \boldsymbol{z}_k | \boldsymbol{z}_l \rangle \left[\boldsymbol{z}_l \left\{ X_l + a_l \left(\boldsymbol{z}_k^* \cdot \dot{\boldsymbol{z}}_l \right) \right\} + a_l \dot{\boldsymbol{z}}_l \right] = a_k^* \langle \boldsymbol{z}_k | \hat{\boldsymbol{a}} \hat{H} | \Psi_{\mathrm{CS}}^{\mathrm{M}} \rangle, \tag{2.36}$$

where the definition

$$X_l := \dot{a}_l + a_l \left[-\frac{1}{2} \left(\boldsymbol{z}_l \cdot \dot{\boldsymbol{z}}_l^* + \dot{\boldsymbol{z}}_l \cdot \boldsymbol{z}_l^* \right) \right] \tag{2.37}$$

was used. The above differential equations (2.35, 2.36) are the full variational equations of motion. We call this method the Variational Coherent States (VCS) method. We note that the system of coupled, highly nonlinear differential equations (2.35, 2.36) is identical to the one given in (34) and (36) of [57]. The equivalence of Eq. (2.35) and Eq. (34) of [57] is obvious, whereas one needs the identity

$$\begin{aligned} \langle \boldsymbol{z}_k | \hat{\boldsymbol{a}} \hat{H} | \Psi_{\mathrm{CS}}^{\mathrm{M}} \rangle &= \sum_{l=1}^{M} a_l \langle \boldsymbol{z}_k | \hat{\boldsymbol{a}} \hat{H} | \boldsymbol{z}_l \rangle = \sum_{l=1}^{M} a_l \langle \boldsymbol{z}_k | \left\{ \hat{H} \hat{\boldsymbol{a}} + [\hat{\boldsymbol{a}}, \hat{H}] \right\} | \boldsymbol{z}_l \rangle \\ &= \sum_{l=1}^{M} a_l \langle \boldsymbol{z}_k | \left(\hat{H}_{\mathrm{ord}} \hat{\boldsymbol{a}} + \frac{\partial \hat{H}_{\mathrm{ord}}}{\partial \hat{\boldsymbol{a}}^\dagger} \right) | \boldsymbol{z}_l \rangle \\ &= \sum_{l=1}^{M} a_l \left(\boldsymbol{z}_l H_{\mathrm{ord}} + \frac{\partial H_{\mathrm{ord}}}{\partial \boldsymbol{z}_k^*} \right) \langle \boldsymbol{z}_k | \boldsymbol{z}_l \rangle, \end{aligned} \tag{2.38}$$

with the normally ordered Hamiltonian, where all powers of $\hat{\boldsymbol{a}}^\dagger$ precede those of $\hat{\boldsymbol{a}}$ [59], whose matrix elements are given by [57]

$$\langle \boldsymbol{z}_k | \hat{H}_{\mathrm{ord}} | \boldsymbol{z}_l \rangle = H_{\mathrm{ord}}(\boldsymbol{z}_k^*, \boldsymbol{z}_l) \langle \boldsymbol{z}_k | \boldsymbol{z}_l \rangle, \tag{2.39}$$

in order to see the second equivalence. In the second equality of Eq. (2.38), we have used the relation

for a normally ordered Hamiltonian (2.39),

$$\left[\hat{\boldsymbol{a}}, \hat{H}\right] = \frac{\partial \hat{H}_{\text{ord}}}{\partial \hat{\boldsymbol{a}}^\dagger} \tag{2.40}$$

where also the left-hand side is normally ordered. This can most easily be argued by principle of mathematical induction, by letting $\hat{H} = \left(\hat{\boldsymbol{a}}^\dagger\right)^n$ without loss of generality. The proof is given in Appendix A.

In Appendix B, we look at the dynamics under a 1D harmonic oscillator Hamiltonian. It turns out that if the frequencies of the harmonic oscillator whose dynamics is to be studied and of the one which is used for the construction of the basis are identical, uncoupled equations of motion

$$\mathrm{i}\dot{a}_l = \frac{\omega}{2} a_l \tag{2.41}$$

$$\mathrm{i}\dot{z}_l = \omega z_l \tag{2.42}$$

do hold.

In the case that the Ansatz (2.16) is restricted to a single term, i.e., $M = 1$, the equations of motion (2.35, 2.36) reduce to (see also [57])

$$\mathrm{i}\dot{a} = a\left[H_{\text{ord}}(\boldsymbol{z}^*, \boldsymbol{z}) - \frac{\mathrm{i}}{2}(\dot{\boldsymbol{z}} \cdot \boldsymbol{z}^* - \boldsymbol{z} \cdot \dot{\boldsymbol{z}}^*)\right], \tag{2.43}$$

$$\mathrm{i}\dot{\boldsymbol{z}} = \frac{\partial H_{\text{ord}}}{\partial \boldsymbol{z}^*}, \tag{2.44}$$

the second of which is the complexified Hamilton's equation and generically can only be solved numerically. The first one is easily solvable formally and we get

$$a(t) = a(0)\exp\{\mathrm{i}S(t)\}, \tag{2.45}$$

with the action-like expression

$$S(t) = \int_0^t \mathrm{d}t' \left[\frac{\mathrm{i}}{2}(\dot{\boldsymbol{z}} \cdot \boldsymbol{z}^* - \boldsymbol{z} \cdot \dot{\boldsymbol{z}}^*) - H_{\text{ord}}\right] = \int_0^t \mathrm{d}t' \left[\left(\frac{\boldsymbol{p} \cdot \dot{\boldsymbol{q}} - \boldsymbol{q} \cdot \dot{\boldsymbol{p}}}{2}\right) - H_{\text{ord}}\right]. \tag{2.46}$$

The single trajectory solution thus gained is the single frozen Gaussian method, in contrast to Heller's multiple frozen Gaussians [72], which we will discuss later in this chapter. The idea of the CCS method now is to propagate all the coherent state parameters $\boldsymbol{z}_l(t)$ in the Ansatz (2.16) according to the classical equation and to keep the fully variational equations of motion for the coefficients $a_l(t)$ [57]. By straightforward insertion of Eq. (2.44) equipped with index l into Eq. (2.35), we get the linear CCS differential equations for the coefficients

$$\mathrm{i}\sum_{l=1}^{M} \langle \boldsymbol{z}_k(t) | \boldsymbol{z}_l(t) \rangle \dot{a}_l(t) = \sum_{l=1}^{M} \tilde{H}_{kl}(t) a_l(t), \tag{2.47}$$

with the time-dependent matrix elements (even in the case of an autonomous Hamiltonian)

$$\tilde{H}_{kl}(t) = \langle \boldsymbol{z}_k(t)|\boldsymbol{z}_l(t)\rangle \Bigg[H_{\mathrm{ord}}(\boldsymbol{z}_k^*, \boldsymbol{z}_l) - \\ \frac{1}{2}\left(\boldsymbol{z}_l(t) \cdot \frac{\partial H_{\mathrm{ord}}(\boldsymbol{z}_l^*, \boldsymbol{z}_l)}{\partial \boldsymbol{z}_l} - \frac{\partial H_{\mathrm{ord}}(\boldsymbol{z}_l^*, \boldsymbol{z}_l)}{\partial \boldsymbol{z}_l^*} \cdot \boldsymbol{z}_l^*(t) \right) - \boldsymbol{z}_k^*(t) \cdot \frac{\partial H_{\mathrm{ord}}(\boldsymbol{z}_l^*, \boldsymbol{z}_l)}{\partial \boldsymbol{z}_l^*} \Bigg], \tag{2.48}$$

where we have used that $H^*_{\mathrm{ord}}(\boldsymbol{z}_l^*, \boldsymbol{z}_l) = H_{\mathrm{ord}}(\boldsymbol{z}_l, \boldsymbol{z}_l^*) = H_{\mathrm{ord}}(\boldsymbol{z}_l^*, \boldsymbol{z}_l)$. The above equations (2.44, 2.47) together with (2.48) are the CCS equations of motion. The special case of the harmonic oscillator is treated explicitely in Appendix B. In the general case, due to the fact that the numerical effort of matrix inversion scales cubically with the number of basis functions, we do not resolve the LHS of (2.47) for the vector of coefficients by using the inverse overlap matrix at every time-step but solve the equations with a non-trivial state-dependent mass matrix which is here given by the overlap matrix.

To minimize the coupling between the equations, usually, the coefficients are written as

$$a_l(t) = d_l(t) \exp\{\mathrm{i}S_l(t)\}, \tag{2.49}$$

with the action-like expression (2.46) and equation (2.47) is then rewritten for the slowly varying pre-exponential factor $d_l(t)$. We note that the matrix corresponding to $\tilde{\mathbf{H}}$ that emerges after the transformation (2.49) is traceless. Herein, however, we refrain from doing so and refer the interested reader to [57] and [73].

A few remarks concerning the usage of classical equations for the coherent state parameters seem in order. Because classical trajectories move independently and never cross in phase space, the problems encountered by coherent state parameters coalescing that had hampered their application for a long time [74] is relieved. This, however, comes at the price of leaving the full variational realm, because in numerical applications one has to start with a finite swarm of coherent states localized in a physically relevant region of phase space initially. Because their centers move classically, there may be situations (tunneling!) in which the CSs will not reach relevant regions at later stages, however. Furthermore, also runaway trajectories as in the Henon-Heiles (HH) potential may be an issue in CCS calculations [75]. A way to circumvent these issues would be to use quantum trajectories, calculated from Bohmian mechanics, as has been proposed in the Quantum Trajectories Gaussian Bases method [76].

2.1.3. Static grid of coherent states

For anharmonic systems, also a static grid of CSs can be used [33]. To make the connection between our present case and the one of Shalashilin and Child clear, we briefly review their approach.

The representation free form of the TDSE, i.e., Eq. (2.1) is used as the starting point. Projecting on a coherent state on both sides and inserting unity in the form

$$\hat{1} = \int \frac{\mathrm{d}^{2f} z'}{\pi} |\boldsymbol{z}'\rangle\langle \boldsymbol{z}'|, \tag{2.50}$$

on the right-hand side (RHS) leads to the integro-differential equation

$$\mathrm{i}\partial_t \Psi(\boldsymbol{z},t) = \int \frac{\mathrm{d}^{2f} z'}{\pi} \langle \boldsymbol{z}|\hat{H}|\boldsymbol{z}'\rangle \Psi(\boldsymbol{z}',t), \tag{2.51}$$

with $\Psi(\boldsymbol{z},t) = \langle \boldsymbol{z}|\Psi(t)\rangle$. In contrast to standard derivations of the TDSE in position or momentum space, where the Hamilton matrix element is proportional to a δ-function, here an integral remains.

This integral appearing on the RHS can now be discretized in principle but one has to be careful and use Eq. (2.26) for the representation of the unit operator from the start. Then one ends up with the system of coupled ordinary differential equations

$$\mathrm{i}\dot{\bar{a}}_k(t) = \sum_{l,j} \langle \boldsymbol{z}_k|\hat{H}|\boldsymbol{z}_l\rangle (\boldsymbol{\Omega}^{-1})_{lj} \bar{a}_j(t), \tag{2.52}$$

with the scalar products

$$\bar{a}_j(t) = \langle \boldsymbol{z}_j|\Psi(t)\rangle. \tag{2.53}$$

In a straightforward discretization of the integral in Eq. (2.51), without the use of (2.26), no inversion of the overlap matrix would be necessary. This is, however, only a good approximation for very dense grids of CSs (also termed tight frame [33, 77, 78]), something one wants to avoid in doing numerics (for a large number of degrees of freedom), however. In order not to disturb the flow of the presentation, we give the equations of motion for single degree of freedom for the tight frame case in Appendix C.

The equality of the reviewed approach with our Eq. (2.35) in the static case is now obvious. First of all, using our Ansatz (2.16), we get (sub- and superscripts of the wavefunction dropped)

$$\bar{a}_k(t) = \langle \boldsymbol{z}_k|\Psi(t)\rangle = \sum_{l=1}^{M} \langle \boldsymbol{z}_k|\boldsymbol{z}_l\rangle a_l(t) = \sum_{l=1}^{M} \Omega_{kl} a_l(t) \tag{2.54}$$

for the relation between the coefficients $\{a_l\}$ and the scalar products $\{\bar{a}_k\}$. The reverse relation is

$$a_l(t) = \sum_{j=1}^{M} (\boldsymbol{\Omega}^{-1})_{lj} \bar{a}_j(t), \tag{2.55}$$

which, together with the resolution of unity in Eq. (2.26) can be used to verify the Ansatz (2.16). The two sets would be identical in the case of an orthonormal basis. The distinction between them is of utmost importance in the later parts of this presentation.

Secondly, in the present case of static CSs, all time derivatives of the coherent state parameters are zero and therefore Eq. (2.35) (as well as Eq. (2.47)) simplify to

$$\mathrm{i}\sum_{l=1}^{M} \langle \boldsymbol{z}_k|\boldsymbol{z}_l\rangle \dot{a}_l(t) = \sum_{l=1}^{M} \langle \boldsymbol{z}_k|\hat{H}|\boldsymbol{z}_l\rangle a_l(t), \tag{2.56}$$

which is equivalent to Eq. (2.52). The case of the harmonic oscillator is again treated in Appendix B. Because the overlap matrix appearing above is time-independent in the present case, for numerical purposes it is appropriate to rewrite the present equation in explicit (matrix) form (vector $\mathbf{a}$ contains all M coefficients a_l) as

$$\mathrm{i}\,\dot{\mathbf{a}}(t) = \mathbf{\Omega}^{-1}\mathbf{H}\mathbf{a}(t). \tag{2.57}$$

If, in addition to the inverse overlap matrix, also the Hamilton matrix is time-independent, this linear system of differential equations can, e.g., be solved by matrix exponentiation. In passing, we note that the overlap matrix on the RHS of the equation above does not cancel out, because in the definition of the Hamilton matrix elements (2.39), the multiplication is to be performed element-wise!

Finally, it is worthwhile to mention that the SCS method seems to be especially suited for imaginary time propagation [79].

2.2. Semiclassical methods

Equation (2.1) can be solved exactly analytically only for a few very simple model systems [49]. The split-operator FFT method provides a straightforward numerical solution to the TDSE of high accuracy. Since the number of grid points that are needed to desribe the wavefunction $|\Psi(t)\rangle$ increases exponentially with the number of degrees of freedom of the system, a full numerical solution of the TDSE is limited up to five or six degrees of freedom i.e., no bigger than the hydrogen molecule [80].

In order to describe the time evolution of large many-body systems, there exists a huge variety of approximate methods like the MCTDH method [31, 32, 81] as well as the TDDFT [82]. Nevertheless, in both approaches approximations have to be made. In the former method, one has to make assumptions for the potential, while the latter method is based on an effective, so-called Kohn-Sham potential, which consists of some external, a Coulomb and an exchange-correlation potential. The exchange-correlation potential is unknown and thus has to be approximated. Here we will focus on methods that are based on semiclassical approximations to the full quantum propagator. Besides the capability of semiclassical methods to treat large quantum systems, they can also help to gain a better understanding of quantum dynamics in terms of classical mechanics, as the underlying physics is based on classically propagated trajectories. However, in contrast to purely classical methods, these classical trajectories carry phase information and thus can interfere with each other. Hence, semiclassical methods contain so-called soft quantum effects like interference. However, there are also attempts to approach hard quantum effects like tunneling via multiple-spawning of trajectories [83] or propagation in imaginary time [84]. However, we will focus on real time propagation without trajectory spawning since no tunneling problems are considered here. In this section, we will describe some well-established semiclassical initial value methods that are widely used for numerical computations. We will briefly touch the differences between boundary value problem based propagators such as the VVG and initial value representations like the HK propagator.

2.2.1. Herman-Kluk Propagator

The time-evolved wavefunction for an f-dimensional system subject to Hamiltonian $\hat{H}(t)$ in position representation can be expressed as:

$$\Psi(\mathbf{x},t) = \int \mathrm{d}^f x' K(\mathbf{x},t;\mathbf{x}',0)\Psi(\mathbf{x}',0) \tag{2.58}$$

where the propagator

$$K(\mathbf{x},t;\mathbf{x}',0) = \langle \mathbf{x}|\mathrm{e}^{-\frac{\mathrm{i}}{\hbar}\hat{H}(t)}|\mathbf{x}'\rangle \tag{2.59}$$

is the matrix element of the time-evolution operator in position representation. In order for $\Psi(\mathbf{x},t)$ to be the exact solution of the TDSE (2.1), the propagator has to take the form of a functional integral over all paths leading from initial position $\mathbf{x}(0) = (x_1(0),\cdots,x_f(0))^{\mathrm{T}}$ to final position $\mathbf{x}(t) = (x_1(t),\cdots,x_f(t))^{\mathrm{T}}$

$$K(\mathbf{x},t;\mathbf{x}',0) = \int_{\mathbf{x}(0)=\mathbf{x}'}^{\mathbf{x}(t)=\mathbf{x}} \mathrm{d}[\mathbf{x}] \exp\left\{\mathrm{i}\frac{\mathrm{S}[\mathbf{x}]}{\hbar}\right\} \tag{2.60}$$

as shown by Feynman [35]. Assuming that the action functional $S[\mathbf{x}]$ of the classical path is much larger than $\hbar$, the rapidly oscillating integrand in (2.60) can be evaluated in stationary phase approximation around this classical path. Van Vleck [85] first found a semiclassical approximation of the quantum mechanical propagator and later on it was generalized and modified by Gutzwiller [86]

$$K^{VVG}(\mathbf{x},t;\mathbf{x}',0) = \left(\frac{1}{2\pi\mathrm{i}\hbar}\right)^{-\frac{f}{2}} \sum_j \left[\det\left(\frac{\partial^2 S_j}{\partial\mathbf{x}\partial\mathbf{x}'}\right)\right]^{\frac{1}{2}} \exp\left\{\frac{\mathrm{i}}{\hbar}S_j[\mathbf{x},\mathbf{x}',t] - \mathrm{i}\pi\frac{\nu_\mathrm{j}}{2}\right\} \tag{2.61}$$

where the sum runs over all classical paths (trajectories) going from $\mathbf{x}'$ to $\mathbf{x}$ in time from 0 to t. $S_j[\mathbf{x},\mathbf{x}',t]$ is the classical action and ν_j is the so-called Maslov index which counts the number of caustics of every trajectory. A typical derivation of the Van Vleck-Gutzwiller propagator is based on the expansion of the action functional in the exponent of the Feynman path integral up to the second order in stationary phase approximation [87]. There are, however two things that make it difficult to evaluate this expression. First is the root search in order to solve the boundary value problem that is increasingly hard to solve as the number of degrees of freedom gets bigger. Second, since the action derivative fulfills

$$\frac{\partial^2 S_j}{\partial\mathbf{x}\partial\mathbf{x}'} = -\frac{\partial\mathbf{p}'}{\partial\mathbf{x}}, \tag{2.62}$$

this expression becomes singular at points where $\partial\mathbf{x}/\partial\mathbf{p}' = 0$. Fortunately, both issues can be resolved elegantly by expressing the original propagator from Eq. (2.58) in terms of coherent states by inserting unity twice. Then one can use the semiclassical expression for the coherent state propagator and finally evaluate the integration over final positions in another stationary phase approximation [36] to arrive

at the Herman-Kluk propagator [37]

$$K^{HK}(\mathbf{x},t;\mathbf{x}',0) = \int \frac{\mathrm{d}^f p \mathrm{d}^f q}{(2\pi\hbar)^f} \langle \mathbf{x}|\mathbf{z}\left(\mathbf{p}_t,\mathbf{q}_t\right)\rangle R\left(\mathbf{p},\mathbf{q},t\right) \mathrm{e}^{\frac{\mathrm{i}}{\hbar}S(\mathbf{p},\mathbf{q},t)} \langle \mathbf{z}\left(\mathbf{p},\mathbf{q}\right)|\mathbf{x}'\rangle. \tag{2.63}$$

This expression now only depends on initial phase space points making it an initial value representation of the propagator instead of the boundary value problem encountered earlier. Here the phase space integration is performed over initial conditions which serve as the starting points for trajectories that are propagated in time numerically via symplectic integration discussed in Appendix D. These classical trajectories are represented as Gaussian wavepackets (GWPs) which are coherent states in position representation given as

$$\langle \mathbf{x}|\mathbf{z}\left(\mathbf{p}_t,\mathbf{q}_t\right)\rangle = \left(\frac{\det\boldsymbol{\gamma}}{\pi^f}\right)^{\frac{1}{4}} \exp\left\{-\left(\mathbf{x}-\mathbf{q}_t\right)^{\mathrm{T}} \frac{\boldsymbol{\gamma}}{2}\left(\mathbf{x}-\mathbf{q}_t\right) + \frac{\mathrm{i}}{\hbar}\mathbf{p}_t^{\mathrm{T}}\left(\mathbf{x}-\mathbf{q}_t\right)\right\} \tag{2.64}$$

As the width parameters of the GWPs remain fixed throughout the propagation, it is also referred to as "Frozen Gaussians", originally discussed in the present context by Heller [72]. The classical action no longer depends on path from initial to final position, but only depends on the initial conditions and therefore becomes

$$S\left(\mathbf{p},\mathbf{q},t\right) = \int_0^t L\mathrm{d}t' = \int_0^t \left[\mathbf{p}_{t'}\cdot\dot{\mathbf{q}}_{t'} - H\right]\mathrm{d}t' \tag{2.65}$$

where L is the classical Lagrangian of the system. The HK determinantal prefactor, which ensures the appropriate normalization of the final expression for the HK propagator is given by

$$R\left(\mathbf{p},\mathbf{q},t\right) = \frac{1}{2^{f/2}}\left(\det\left\{\mathbf{m}_{11} + \boldsymbol{\gamma}\mathbf{m}_{22}\boldsymbol{\gamma}^{-1} - \mathrm{i}\hbar\boldsymbol{\gamma}\mathbf{m}_{21} - \frac{1}{\mathrm{i}\hbar}\mathbf{m}_{12}\boldsymbol{\gamma}^{-1}\right\}\right)^{\frac{1}{2}}, \tag{2.66}$$

where $\mathbf{m}_{11}, \mathbf{m}_{12}, \mathbf{m}_{21}$ and $\mathbf{m}_{22}$ are the elements of the so-called monodromy (or stability) matrix $\mathbf{M}$ [49],

$$\mathbf{M} = \begin{pmatrix} \mathbf{m}_{11} & \mathbf{m}_{12} \\ \mathbf{m}_{21} & \mathbf{m}_{22} \end{pmatrix} = \begin{pmatrix} \frac{\partial\mathbf{p}_t}{\partial\mathbf{p}^{\mathsf{T}}} & \frac{\partial\mathbf{p}_t}{\partial\mathbf{q}^{\mathsf{T}}} \\ \frac{\partial\mathbf{q}_t}{\partial\mathbf{p}^{\mathsf{T}}} & \frac{\partial\mathbf{q}_t}{\partial\mathbf{q}^{\mathsf{T}}} \end{pmatrix}. \tag{2.67}$$

This stability matrix $\mathbf{M}$ describes the time-evolution of the dependence of a classical trajectory on its initial conditions and can be obtained by solving linearized Hamilton equations as reviewed in Appendix D. A wavefunction propagated with the HK propagator can be regarded as a sum of Gaussians centered around the final points of classically propagated trajectories. Each of these Gaussians are weighted by the overlap of the initial wavefunction and Gaussians centered at the corresponding initial phase space points.

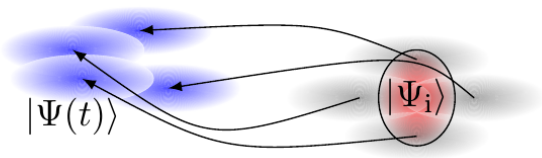

Figure 2.3.: Sketch of HK semiclassical propagation from [88]; Red: initial wavepacket $|\Psi_i\rangle$, Black: coherent states at initial phase space points, Blue: coherent states at final phase space points forming the final wavefunction $|\Psi(t)\rangle$.

The HK propagator is related to the original VVG propagator via stationary phase approxiamtion [89]. Moreover, the HK method is more accurate and a uniform semiclassical method [90] i.e., it becomes exact as $\hbar \to 0$ uniformly. This goes along with the advantage that HK method does not exhibit singularities at caustics as is the case for VVG propagator. The problem of counting these caustics in order to obtain the right Maslov index in the VVG propagator is replaced by ensuring the continuity of the determinantal prefactor $R(\mathbf{p}, \mathbf{q}, t)$ by switching between both Riemann surfaces of the square root function appropriately while propagating each trajectory [38]. The propagated wavefunction $\Psi(\mathbf{x}, t)$ can be expressed as

$$\Psi(\mathbf{x}, t) = \int \frac{\mathrm{d}^f p \mathrm{d}^f q}{(2\pi\hbar)^f} \langle \mathbf{x} | \mathbf{z}(\mathbf{p}_t, \mathbf{q}_t) \rangle R(\mathbf{p}, \mathbf{q}, t) \, \mathrm{e}^{\frac{\mathrm{i}}{\hbar} S(\mathbf{p}, \mathbf{q}, t)} \langle \mathbf{z}(\mathbf{p}, \mathbf{q}) | \Psi_\alpha(0) \rangle \tag{2.68}$$

where the initial wavefunction $|\Psi_\alpha(0)\rangle$ is centered at $(\mathbf{p}_\alpha, \mathbf{q}_\alpha)$ and has the same width parameters as the propagator wavepackets. The necessary numerical phase space integration can be done very efficiently using the Box Muller algorithm [55] in order to sample the initial phase space points weighted with the overlap $\langle \mathbf{z}(\mathbf{p}, \mathbf{q}) | \Psi_\alpha(0) \rangle$ which emerges after a Gaussian integration as

$$\begin{aligned} \langle \mathbf{z}(\mathbf{p}, \mathbf{q}) | \Psi_\alpha(0) \rangle = \exp\Bigg(& -\frac{1}{4} (\mathbf{q} - \mathbf{q}_\alpha)^\intercal \boldsymbol{\gamma} (\mathbf{q} - \mathbf{q}_\alpha) - \frac{1}{4\hbar^2} (\mathbf{p} - \mathbf{p}_\alpha)^\intercal \boldsymbol{\gamma}^{-1} (\mathbf{p} - \mathbf{p}_\alpha) \\ & + \frac{\mathrm{i}}{2\hbar} (\mathbf{q} - \mathbf{q}_\alpha)^\intercal (\mathbf{p} + \mathbf{p}_\alpha) \Bigg). \end{aligned} \tag{2.69}$$

Finally we would like to mention that the HK propagator conserves unitarity in the semiclassical limit [91].

2.2.2. Thawed Gaussian Wavepacket Dynamics

The multi-trajectory HK approach can become computationally enormously costly in situation where classical chaos prevails [92], and therefore there is another semiclassical method known as Thawed Gaussian Wavepacket Dynamics which is based on the propagation of only a single-trajectory and hence involving a smaller computational effort. This single-trajectory approach was introduced by

Heller [93, 94] and can be directly derived from the HK wavefunction. Recalling that the expression for a propagated wavefunction in Eq. (2.68) contains a phase space integration which can also be performed approximately analytically, one can derive Heller's TGWD from HK. Let the initial wavefunction $\Psi_\alpha(\mathbf{x},0)$ is centered around $(\mathbf{p}_\alpha,\mathbf{q}_\alpha)$ with width parameter matrix γ_α. The overlap of $\Psi_\alpha(\mathbf{x},0)$ with the coherent state centered around $(\mathbf{p},\mathbf{q})$ in Eq. (2.68) reads

$$\begin{aligned}\langle \mathbf{z}(\mathbf{p},\mathbf{q})|\Psi_\alpha(0)\rangle &= \int \mathrm{d}^f x' \langle \mathbf{z}(\mathbf{p},\mathbf{q})|\mathbf{x}'\rangle\langle \mathbf{x}'|\Psi_\alpha(0)\rangle \\ &= 4^{f/4}\frac{(\det(\boldsymbol{\gamma}\boldsymbol{\gamma}_\alpha))^{\frac{1}{4}}}{\sqrt{\det(\boldsymbol{\gamma}+\boldsymbol{\gamma}_\alpha)}}\exp\Bigg(-\frac{\boldsymbol{\gamma}\boldsymbol{\gamma}_\alpha}{2}(\boldsymbol{\gamma}+\boldsymbol{\gamma}_\alpha)^{-1}(\mathbf{q}-\mathbf{q}_\alpha)^2 \\ &\quad -\frac{1}{2\hbar^2}(\boldsymbol{\gamma}+\boldsymbol{\gamma}_\alpha)^{-1}(\mathbf{p}-\mathbf{p}_\alpha)^2+\frac{\mathrm{i}}{\hbar}(\boldsymbol{\gamma}+\boldsymbol{\gamma}_\alpha)^{-1}(\mathbf{q}-\mathbf{q}_\alpha)(\boldsymbol{\gamma}_\alpha\mathbf{p}+\boldsymbol{\gamma}\mathbf{p}_\alpha)\Bigg) \\ &= \exp\Bigg(-\frac{1}{4}(\mathbf{q}-\mathbf{q}_\alpha)^\intercal\boldsymbol{\gamma}(\mathbf{q}-\mathbf{q}_\alpha)-\frac{1}{4\hbar^2}(\mathbf{p}-\mathbf{p}_\alpha)^\intercal\boldsymbol{\gamma}^{-1}(\mathbf{p}-\mathbf{p}_\alpha) \\ &\quad +\frac{\mathrm{i}}{2\hbar}(\mathbf{q}-\mathbf{q}_\alpha)^\intercal(\mathbf{p}+\mathbf{p}_\alpha)\Bigg). \end{aligned} \tag{2.70}$$

In the last equality of the above equation we assume that both Gaussians have the same width parameter matrix i.e., $\boldsymbol{\gamma}=\boldsymbol{\gamma}_\alpha$. The more general case can also be dealt with analytically but leads to a less transparent final result. In order to derive TGWD from the HK propagator as applied to an initial Gaussian wavepacket, a second order expansion of the exponent together with a zeroth order expansion of the prefactor around the center $(\mathbf{p}_\alpha,\mathbf{q}_\alpha)$ is made. This is explicitly shown in appendix C of [67]. There in the Gaussian expansion approximation, the action is expanded up to a second order around the initial center $(\mathbf{p}_\alpha,\mathbf{q}_\alpha)$ of the wavepacket to be propagated while keeping first order expansions for the final momentum and position $(\mathbf{p}_t,\mathbf{q}_t)$. After performing the Gaussian integration analytically, one gets a wavefunction in terms of a single trajectory

$$\begin{aligned}\Psi_\alpha(\mathbf{x},t) &= \left(\frac{\det\boldsymbol{\gamma}}{\pi^f}\right)^{\frac{1}{4}}(\det(\mathbf{m}_{22}+\mathrm{i}\hbar\mathbf{m}_{21}\boldsymbol{\gamma}))^{-\frac{1}{2}}\exp\Bigg(-\left(\mathbf{x}-\mathbf{q}_{\alpha,t}\right)^{\mathrm{T}}\boldsymbol{\gamma}_t\left(\mathbf{x}-\mathbf{q}_{\alpha,t}\right) \\ &\quad +\frac{\mathrm{i}}{\hbar}\mathbf{p}_{\alpha,t}^{\mathrm{T}}\left(\mathbf{x}-\mathbf{q}_{\alpha,t}\right)+\frac{\mathrm{i}}{\hbar}S\left(\mathbf{p}_\alpha,\mathbf{q}_\alpha,t\right)\Bigg)\end{aligned} \tag{2.71}$$

where $\mathbf{p}_{\alpha,t}=\mathbf{p}(\mathbf{p}_\alpha,\mathbf{q}_\alpha,t)$ and $\mathbf{q}_{\alpha,t}=\mathbf{q}(\mathbf{p}_\alpha,\mathbf{q}_\alpha,t)$. $\boldsymbol{\gamma}_t$ is the time-dependent $f\times f$ inverse width parameter matrix given as

$$\boldsymbol{\gamma}_t=\boldsymbol{\gamma}\left(\mathbf{m}_{11}+\frac{1}{\mathrm{i}\hbar\boldsymbol{\gamma}}\mathbf{m}_{12}\right)(\mathbf{m}_{22}+\mathrm{i}\hbar\boldsymbol{\gamma}\mathbf{m}_{21}) \tag{2.72}$$

In contrast to the HK expression (2.68), this expression is given in terms of just one single trajectory with initial conditions according to the center of the initial Gaussian. The Gaussian form of the wavepacket is retained throughout the propagation, only the position and the width change in time. This is the reason why the more simple single Gaussian method is called the "thawed" Gaussian wavepacket dynamics, whereas the more complex, multiple Gaussian HK method is referred to as the

"frozen" Gaussian wavepacket dynamics of Heller [72]. TGWD is exact for potentials that are at most quadratic [93]. However, due to the additional approximation which was applied to obtain Eq. (2.71), TGWD is obviously less accurate than HK approximation applied to an initial Gaussian wavepacket.

2.2.3. Linearized Semiclassical Initial Value Representation

Before leaving the discussion of the different methods to solve the TDSE, it is worthwhile to mention recent progress on the calculation of correlation functions. In this final subsection on semiclassical methods, we will present one last HK-based method that will serve as a classical comparison to semiclassical results, the so-called Linearized Semiclassical Initial Value Representation introduced by Sun, Wang and Miller [42–46] (also known as classical Wigner dynamics [40, 41]). The general time correlation function of two arbitrary operators $\hat{A}$ and $\hat{B}$ is of the form

$$C_{AB}(t) = \mathrm{Tr}\left[\hat{A}\hat{B}(t)\right] = \mathrm{Tr}\left[\hat{A}\mathrm{e}^{\frac{\mathrm{i}}{\hbar}\hat{H}t}\hat{B}\mathrm{e}^{-\frac{\mathrm{i}}{\hbar}\hat{H}t}\right] \tag{2.73}$$

where the operator $\hat{A}$ represents the initial state, whereas the Heisenberg time-evolved operator

$$\hat{B}(t) := \mathrm{e}^{\frac{\mathrm{i}}{\hbar}\hat{H}t}\hat{B}\mathrm{e}^{-\frac{\mathrm{i}}{\hbar}\hat{H}t} \tag{2.74}$$

defines the measure of interest. By using a form of the semiclassical evolution operator different from the HK expression [45], expanding the exponent to second order and integrating over the difference variables of the forward and backward trajectories, one obtains an expression for the LSC-IVR of the time correlation function [42]

$$C_{AB}^{W}(t) = \int \frac{\mathrm{d}^f p \mathrm{d}^f q}{(2\pi\hbar)^f} A_W(\mathbf{p},\mathbf{q}) B_W(\mathbf{p}_t,\mathbf{q}_t), \tag{2.75}$$

where $A_W(\mathbf{p},\mathbf{q})$ and $B_W(\mathbf{p}_t,\mathbf{q}_t)$ are the Wigner-Weyl transforms of operators $\hat{A}$ and $\hat{B}$ and $(\mathbf{p}_t,\mathbf{q}_t)$ are classically time-evolved phase space points (trajectories). The Wigner-Weyl transform $A_W(\mathbf{p},\mathbf{q})$ is defined as

$$A_W(\mathbf{p},\mathbf{q}) = \int \mathrm{d}^f \Delta q \mathrm{e}^{-\mathrm{i}\frac{\mathbf{p}\Delta\mathbf{q}}{\hbar}} \left\langle \mathbf{q} + \frac{\Delta\mathbf{q}}{2}\middle|\hat{A}\middle|\mathbf{q} - \frac{\Delta\mathbf{q}}{2}\right\rangle. \tag{2.76}$$

Since the Wigner transforms are real functions, the expression for the time correlation function in Eq. (2.75) does not contain any phases and thus no interference terms. Hence, this method is known as the classical Wigner method.

There is another semiclassical work by Antipov, Ye and Ananth [47], which we will be discussed in detail in Chapter 4, based on Husimi transforms as

$$A_H(\mathbf{p},\mathbf{q}) = \langle \mathbf{z}(\mathbf{p},\mathbf{q})|\hat{A}|\mathbf{z}(\mathbf{p},\mathbf{q})\rangle. \tag{2.77}$$

The corresponding linearized version of the correlation function for a large class of relevant operators

is then given as

$$C_{AB}^{H}(t) = \int \frac{\mathrm{d}^f p \mathrm{d}^f q}{(2\pi\hbar)^f} A_H(\mathbf{p}, \mathbf{q}) B_H(\mathbf{p}_t, \mathbf{q}_t), \tag{2.78}$$

whereas in general, if to be determined semiclassically, a double phase space integral (double HK) has to be dealt with. In Chap. 4, we discuss a slightly corrected Husimi version of the linearized semiclassical initial value representation for the survival probability where

$$\hat{A} = \hat{B} = |\Psi_\alpha\rangle\langle\Psi_\alpha|, \tag{2.79}$$

are both projection operators. These linearized versions do not contain complex-valued exponentials any more. More quantum are so-called forward-backward semiclassical approximations to the correlation functions, developed by Makri, Miller and coworkers [95, 96].

3. Comparison of different numerical methods

In this chapter, we will numerically compare the different methods to solve the TDSE which we already discussed in the previous chapter. Here we take a pure one-dimensional Morse oscillator as our model potential to make the numerical case study. This is a nonlinear model system used frequently to describe the anharmonic oscillations in a diatomic molecule and has been investigated using CSs by Heather and Metiu [97, 98] as well as by Shalashilin and Child [33] and using HK methodology, among others, by Wang and Heller [99], who have focused on the interference nature of wavefunction revivals. But before that, we will discuss some of the model potentials that have been studied earlier using CSs. In the very last section of this chapter, we will provide discussion about some of the very common potentials and their hamiltonian matrix elements that is used in calculating CCS equations of motion in order to study the quantum dynamics.

3.1. Model potentials and observables

An analytically given potential that has been dealt with using CSs early on is the 1D Brickmann-Russegger potential [100, 101], which is a linear combination of a Morse and a harmonic potential. In this case, for the same number of trajectories, HK results are much better converged than the other four semiclassical results[1] considered in [38]. Early applications of the HK method to the nonlinear HH model [102] have been given by Walton and Manalopoulos [103] and to the Porter-Karplus potential for the hydrogen exchange reaction [104] by Frank Grossmann and his coworkers [105, 106]. Later on, the Secrest-Johnson scattering potential [107] has again been used by Grossmann in a HK application [67] and the HH-problem has been treated with CCS by Shalashilin and Child [108] and with variable multi-configurational gaussian (vMCG) method by Worth and Burghardt [109]. Also double-well tunneling has been studied with CCS [108]. For this and also other tunneling problems, a single bare HK propagation in general is not sufficient. As shown by Mandelshtam and Ovchinnikov, the calculation of a correlation function matrix is necessary to extract tunneling splittings from a HK calculation [110]. Tanaka has used a folding Hamiltonian to inspect the boundary between so-called deep and shallow tunneling [111] in a HK approach and Moix and Pollak have studied the dynamics in a modified corrugated Morse potential in 2D using different methods, among them the HK method [112].

Electronic motion has been successfully tackled using the HK propagator for the hydrogen problem [113, 114] and soft-core as well as short-range variants thereof [115, 116]. Furthermore, Helium [117]

[1] which are smoothed van Vleck, Fourier transform of the momentum space propagator, a combination of both, as well as the thawed Gaussian approximation propagator

and the Coulomb repulsion have been treated semiclassically using HK [118, 119] as well as frozen Gaussians [120]. For fermionic many-particle systems, also CCS calculations have been published [121, 122]. It turns out that the Coulomb singularity is smoothed naturally by considering a classical dynamics with the ordered Hamiltonian of Eq. (2.39).

In addition, the single site Bose-Hubbard model [123] and the chaotic dynamics in different coupled quartic oscillator systems [92, 124, 125], even with coupling to an external driving field [126] and, more recently, the coserf-map [127] have been studied with the HK propagator. Frozen Gaussians have been used to study pump-probe spectroscopy [128] and, furthermore, combined electron-nuclear (non-adiabatic) dynamics has been tackled with the HK propagator [95, 129, 130], as well as with ab initio multiple spawning [131, 132], CCS [133] and different variants of vMCG [134, 135], to list only a few examples. Also (standard) thawed Gaussians have shown their potential in a study of the decay of electronic coherences in polyatomic systems [136], whereas off-center thawed Gaussians showed unexpected long-time accuracy for the stadium billard [137, 138].

The number of more complex models and systems whose quantum dynamics have been investigated using CSs is so large that we refer to some original papers [89, 95, 133, 139, 140]. For a lot of degrees of freedom, as it is the case if a molecular vibration is coupled to phonons in a surrounding host, the combination of HK with more crude semiclassical methods seems to be promising [17, 141–143]. A closely related approach to VCS, the multi Davydov-Ansatz, is frequently employed in spin-boson type of problems [144, 145].

3.1.1. The Morse oscillator and its Hamiltonian matrix

The Hamilton function for the Morse potential, in case of unit mass, is given by

$$H = T + V_M = \frac{p^2}{2} + V_M. \tag{3.1}$$

In Figure 3.1 a pictorial representation of the Morse potential

$$V_M = D(1 - \mathrm{e}^{-\alpha \mathrm{x}})^2, \tag{3.2}$$

where

$$x = R - R_0 \tag{3.3}$$

is given. D is the dissociation energy, which depicts the binding energy of a diatomic molecule (with equilibrium distance R_0 and internuclear separation R). α is the range parameter which controls the width of the potential. The larger the constant α, the less harmonic is the potential.

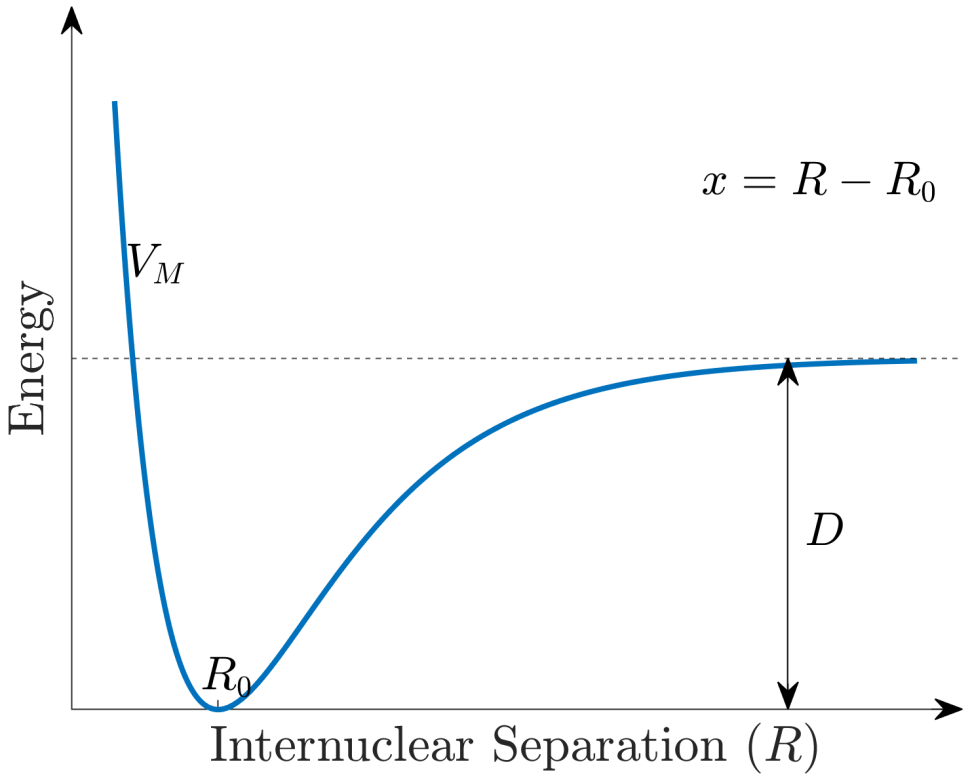

Figure 3.1.: Morse potential V_M with dissociation energy D, equilibrium distance R_0, internuclear separation R and range parameter α.

Using the correspondence principle, we then replace position as well as momentum by the corresponding operators and then the Hamiltonian looks like

$$\hat{H} = \frac{\hat{p}^2}{2} + D(1 - \mathrm{e}^{-\alpha\hat{\mathrm{x}}})^2 \tag{3.4}$$

To make progress, position and momentum operators are expressed via creation and annihilation operators of the harmonic oscillator in Eq. (2.18) ($\omega = \gamma$ in the present units and $\hbar = 1$), via

$$\hat{x} = \frac{1}{\sqrt{2\gamma}}(\hat{a}^\dagger + \hat{a}), \qquad \hat{p} = \mathrm{i}\sqrt{\frac{\gamma}{2}}(\hat{a}^\dagger - \hat{a}). \tag{3.5}$$

Using the fundamental commutation relation

$$[\hat{a}, \hat{a}^\dagger] = \hat{1}, \tag{3.6}$$

the normal ordered form of the kinetic energy operator is found to be

$$\hat{T}_{\mathrm{ord}}(\hat{a}^\dagger, \hat{a}) = \frac{1}{2}\hat{p}^2 = -\frac{\gamma}{4}(\hat{a}^\dagger - \hat{a})^2 = -\frac{\gamma}{4}\left[(\hat{a}^\dagger)^2 - 2\hat{a}^\dagger\hat{a} - 1 + \hat{a}^2\right] \tag{3.7}$$

and the normal ordered form of the potential energy is

$$\hat{V}_{\mathrm{ord}}(\hat{a}^\dagger, \hat{a}) = D\left(1 - 2\mathrm{e}^{\alpha_1^2/2}\mathrm{e}^{-\alpha_1\hat{a}^\dagger}\mathrm{e}^{-\alpha_1\hat{a}} + \mathrm{e}^{2\alpha_1^2}\mathrm{e}^{-2\alpha_1\hat{a}^\dagger}\mathrm{e}^{-2\alpha_1\hat{a}}\right), \tag{3.8}$$

where the abbreviation $\alpha_1 = \alpha/\sqrt{2\gamma}$ as well as the Zassenhaus formula [49] have been used. We note that the final expression cannot be written in terms of a single square any more.

Now the matrix elements of the Hamilton operator between CSs can be calculated from Eq. (2.39) with Eq. (2.29) for the overlap and with

$$\begin{aligned} H_{\mathrm{ord}}(z_k^*, z_l) &= -\frac{\gamma}{4}[(z_k^* - z_l)^2 - 1] \\ &+ D\left(1 - 2\mathrm{e}^{\alpha_1^2/2}\mathrm{e}^{-\alpha_1(z_k^*+z_l)} + \mathrm{e}^{2\alpha_1^2}\mathrm{e}^{-2\alpha_1(z_k^*+z_l)}\right). \end{aligned} \tag{3.9}$$

This expression is needed in the CCS and SCS approaches. It could also have been derived using the differential calculus employed in Theorem II on page 142 of [59]. There one replaces $\hat{a}$ by $z + \partial/\partial z^*$ and $\hat{a}^\dagger$ by z^* and applies the expression to the unit operator to arrive at the matrix elements of the normal form of an operator.

A collection of V_{ord} for the Morse case just discussed and the harmonic and quartic case is given in Section 3.3.

3.1.2. Classical equations of motion for a single CS

Also the derivatives appearing in Eq. (2.38) can now be evaluated explicitly, yielding

$$\frac{\partial \hat{T}_{\mathrm{ord}}}{\partial \hat{a}^\dagger} = -\frac{\gamma}{2}(\hat{a}^\dagger - \hat{a}), \tag{3.10}$$

$$\frac{\partial \hat{V}_{\mathrm{ord}}}{\partial \hat{a}^\dagger} = 2D\alpha_1\left[\mathrm{e}^{\alpha_1^2/2}\mathrm{e}^{-\alpha_1\hat{a}^\dagger}\mathrm{e}^{-\alpha_1\hat{a}} - \mathrm{e}^{2\alpha_1^2}\mathrm{e}^{-2\alpha_1\hat{a}^\dagger}\mathrm{e}^{-2\alpha_1\hat{a}}\right]. \tag{3.11}$$

The equation of motion that is following in the case of $M = 1$ is the one that is used in the CCS method (but again for many CSs) and reads

$$\begin{aligned} \mathrm{i}\dot{z} &= \frac{\partial H_{\mathrm{ord}}(z^*, z)}{\partial z^*} \\ &= -\frac{\gamma}{2}(z^* - z) + 2D\alpha_1\left[\mathrm{e}^{\alpha_1^2/2}\mathrm{e}^{-\alpha_1(z^*+z)} - \mathrm{e}^{2\alpha_1^2}\mathrm{e}^{-2\alpha_1(z^*+z)}\right]. \end{aligned} \tag{3.12}$$

Using the definition (2.17) of the complex displacement, the real and imaginary part can be disentangled and we get modified Hamilton's equations

$$\dot{q} = p, \tag{3.13}$$

$$\dot{p} = -2D\alpha\left(\mathrm{e}^{\alpha^2/4\gamma}\mathrm{e}^{-\alpha q} - \mathrm{e}^{\alpha^2/\gamma}\mathrm{e}^{-2\alpha q}\right), \tag{3.14}$$

where the last equation is slightly different from the purely classical equation of motion

$$\dot{p} = -2D\alpha\left(\mathrm{e}^{-\alpha q} - \mathrm{e}^{-2\alpha q}\right), \tag{3.15}$$

that one gets by evaluating the Hamilton matrix element in between position states instead of coherent states. That latter equation is used in the HK case.

3.1.3. Potential parameters, time scales, initial state, and observables

For the following numerical results we used the parameters also used by Wang and Heller in their revival study [99]. There the potential parameters were

$$D = 150, \qquad \alpha = 0.288, \tag{3.16}$$

leading to

$$\omega_{\mathrm{M}} = \sqrt{2D}\alpha \approx 5 \tag{3.17}$$

for the frequency of (harmonic) oscillations around the minimum of the potential (to be distinguished from the harmonic oscillator frequency $\omega = \gamma$ that appears in the coherent state basis!). The corresponding classical period is given by

$$T_{\mathrm{cl}} = 2\pi/\omega_{\mathrm{M}} = 2\pi/(\sqrt{2D}\alpha) \approx 2\pi/5. \tag{3.18}$$

In most calculations using one of the methods discussed so far, Gaussian wavepackets with the same width parameter as the coherent state are used as initial states. This is due to the fact that molecular ground states are very close to Gaussian, but it is not a principle restriction of the methods. Other initial states (e.g., also Gaussians with different width parameters than the coherent states) can be expanded in terms of the CSs, resulting in the fact that more than a single a-coefficient is nonzero initially for the CCS and SCS cases. The initial wavepacket used in the following 1D study is given by

$$\Psi(x,0) = \left(\frac{\gamma}{\pi}\right)^{1/4} \exp\left\{-\frac{\gamma}{2}(x-q_\alpha)^2 + \mathrm{i}p_\alpha(x-q_\alpha)\right\} \tag{3.19}$$

and is localized on the soft side of the potential around $q_\alpha = 3.5$, with zero initial momentum and with initial width parameter $\gamma = 4$, that we choose to be identical to the harmonic oscillator's frequency, that defines the coherent states. The phase convention for the Gaussian is irrelevant in the present case of $p_\alpha = 0$. Furthermore, the classical energy at the phase space center of the wavepacket is $E_\alpha = H(p_\alpha, q_\alpha) \approx 60.5$. For the oscillation period of a particle with this specific energy, one finds the local period $T_{\mathrm{loc}} = 2\pi/\omega_{\mathrm{loc}} \approx 1.63$, where the local frequency $\omega_{\mathrm{loc}} = \omega_{\mathrm{M}}\sqrt{1 - E_\alpha/D}$ was used [146].

Quantities to be monitored during the dynamics can be expectation values of position and momentum and their respective variances or the kinetic or potential energy. It is most appropriate to use Eq. (2.16) for the wavefunction to express expectation values in the form

$$\langle\hat{A}\rangle(t) = \langle\Psi(t)|\hat{A}|\Psi(t)\rangle = \sum_{k,l} a_k^*(t)\langle z_k(t)|z_l(t)\rangle A_{\mathrm{ord}}(z_k^*, z_l)a_l(t), \tag{3.20}$$

with the ordered form of the operator written in terms of creation and annihilation operators (see, e.g., Eq. (2.39) for the Hamiltonian).

Especially in the HK case, which needs a sizeable number of trajectories for convergence, the double sum appearing in the expectation values makes these objects hard to calculate. Therefore, the quantity of interest in the following section is the autocorrelation function

$$c(t) = \langle \Psi(0)|\Psi(t)\rangle = \sum_l a_l(t)\langle \Psi(0)|z_l(t)\rangle = \sum_{k,l=1}^{M} a_k^*(0)\langle z_k(0)|z_l(t)\rangle a_l(t) \tag{3.21}$$

that will be followed up to the first full revival time,

$$T_{\mathrm{rev}} = 2\pi/\alpha^2 \tag{3.22}$$

which, in the present case, is close to 60 times the classical period of the Morse oscillator. The absolute value squared of $c(t)$ is the survival probability.

Before turning to the numerical calculation of the autocorrelation, we briefly review the solution of the dynamical problem by using the solution of the time-independent Schrödinger equation (TISE) for the Morse oscillator given in Appendix E. For the time-evolution of the autocorrelation of the initial state from above one can then write

$$\langle \Psi(0)|\Psi(t)\rangle = \sum_n |d_n|^2 \mathrm{e}^{-\mathrm{i}E_n t}, \tag{3.23}$$

with the energies E_n and overlaps d_n given by equation (E.6), respectively (E.7) in Appendix E. We now compare the results for the analytical autocorrelation gained in such a way with another calculation that uses a purely Gaussian overlap centered around $n_0 = 14$ (see the red curve in Fig. E.1) and "artificial" energies that are also centered around the same value, according to

$$E_n = \omega_{\mathrm{M}}\,(n-14) - \frac{\alpha^2}{2}\,(n-14)^2\,, \tag{3.24}$$

similar to the procedure in [147]. We stress that these energies are different from the Morse ones given in Appendix E. The results are displayed in Fig. 3.2. We can see that the two results both display fractional and full revivals at similar times but for the "artificial" solution based on energies centered around $n_0 = 14$, the overlap shows a faster initial oscillation with the classical period, whereas the Morse solution oscillates with the local period, as expected from the motion of a classical particle starting with a large initial excitation.

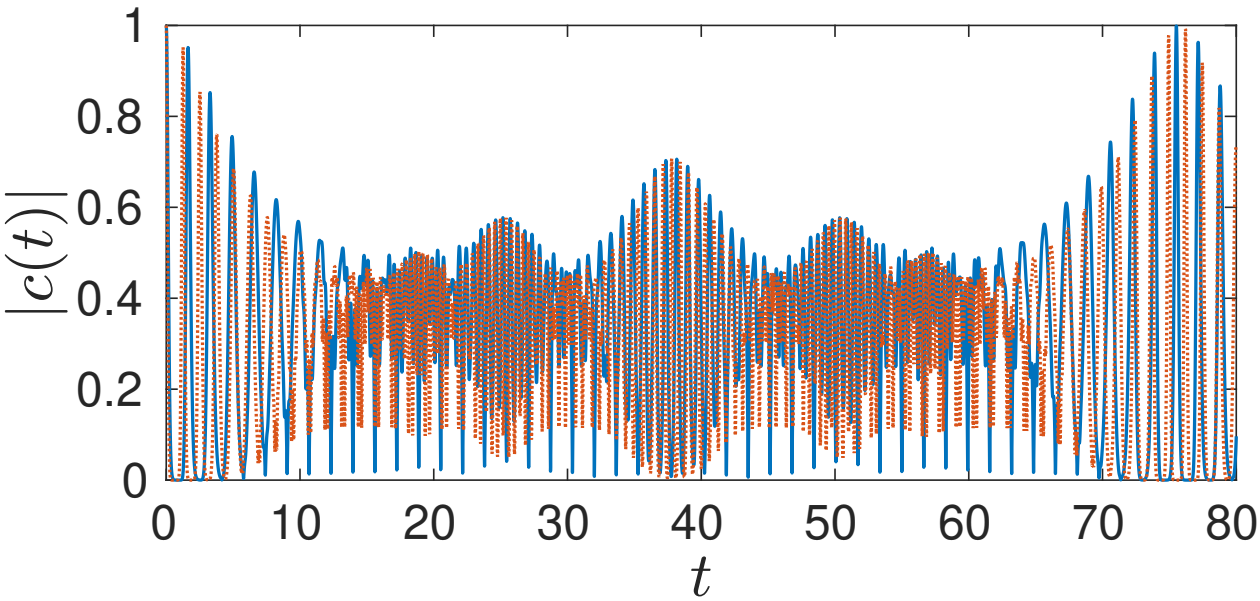

Figure 3.2.: Comparison of two different analytical autocorrelation time series (absolute value is displayed). The faster oscillating (dotted orange) curve uses artificial eigenvalues, whereas the slower oscillating (solid blue) curve uses the true Morse eigenvalues.

Before continuing with the numerical result, we stress that, in the case based on the energies from (3.24), the sum in (3.23) can be performed analytically using the Poisson sum formula according to

$$\begin{aligned} c(t) &= \sum_{n=-\infty}^{+\infty} \mathrm{e}^{-\frac{n^2}{\delta n^2}} \mathrm{e}^{-\mathrm{iE_n t}} \\ &= \sum_{k=-\infty}^{+\infty} \int \mathrm{d}\eta \mathrm{e}^{2\pi \mathrm{ik}\eta} \mathrm{e}^{-\frac{\eta^2}{\delta n^2}} \mathrm{e}^{-\mathrm{i}\left(\omega_\mathrm{M}\eta - \frac{\alpha^2}{2}\eta^2\right)\mathrm{t}} \\ &= \frac{\sqrt{2\pi}}{\sqrt{\tilde{\alpha}(t)}} \sum_{k=-\infty}^{+\infty} \mathrm{e}^{-(\omega_\mathrm{M} t - 2k\pi)^2/2\tilde{\alpha}(t)} \end{aligned} \tag{3.25}$$

with $\tilde{\alpha}(t) = -\mathrm{i}\alpha^2\mathrm{t} + \frac{2}{\delta \mathrm{n}^2}$. Using the definition of time scales in (3.18) and (3.22), we get

$$c(t) = \frac{1}{\sqrt{\alpha(t)}} \sum_{k=-\infty}^{+\infty} \mathrm{e}^{-\pi\left[t/T_\mathrm{cl} - k^2\right]/\alpha(t)} \tag{3.26}$$

with $\alpha(t) = \mathrm{i}\frac{\mathrm{t}}{\mathrm{T_{rev}}} + \frac{1}{\pi\delta \mathrm{n}^2}$. Looking at times $t = T_{rev}$, we get $\alpha(t) = \mathrm{i} + \frac{1}{\pi\delta \mathrm{n}^2}$ and $|\alpha(t)| \approx 1$ and thus

$$c(t \approx T_{rev}) \propto \sum_{k=-\infty}^{+\infty} \mathrm{e}^{-\mathrm{i}\pi[\mathrm{t}/\mathrm{T_{cl}} - \mathrm{k}]^2} \mathrm{e}^{-\left[t/T_{cl} - k^2\right]/\delta n^2} \tag{3.27}$$

The second term limits the sum to $k \approx k_0 = \mathrm{nint}\left(\frac{T_{rev}}{T_{cl}}\right)$ and for $t = \left(k_0 + \frac{1}{2}\right) T_{cl}$ and with $\tilde{k} = k - k_0$,

we find

$$c(t \approx T_{rev}) \propto \sum_{\tilde{k}} \mathrm{e}^{\mathrm{i}\pi\left[\tilde{\mathrm{k}}+\frac{1}{2}\right]^2} = \cdots \mathrm{e}^{\mathrm{i}\pi/4} + \mathrm{e}^{\mathrm{i}\pi/4} + \mathrm{e}^{\mathrm{i}\pi/4} \cdots \tag{3.28}$$

which is a sum of equal terms, explaining the appearance of revivals.

3.2. Numerical Case Study

After the introduction of the model and its parameters, the methods from chapter 2 like the CCS, SCS and HK will first be discussed with respect to the complexity of the underlying equations as well as the initial choice of the coherent state parameters and, apart from TGWD, will be applied to the revival dynamics. In Table 3.1, we compare the nature of the ordinary differential equations to be solved. For increasing degree of approximation, the equations become less coupled and less nonlinear. A related table can be found in [57].

Where appropriate and known to us, we will also discuss the scaling of the numerical effort of the methods with respect to the number of basis function (i.e., on the degrees of freedom). We start with the method with the highest degree of approximation. Not taking into account any variant of TGWD in this section, this is the HK method.

3.2.1. HK results and FFT benchmark

Our benchmark here and in all other cases will be a numerically exact solution of the TDSE on a position space grid using the split-operator fast Fourier transform (FFT) technique discussed in 2.1.1, where one switches between position and momentum grid to ease propagation. For converged results, we used a grid of 128 points extending from $x_{\min} = -5$ to $x_{\max} = 10$ and time-steps of $\Delta t = 0.01$. The FFT results in Fig. 3.3 coincide with the analytical ones from the previous section and display an initial oscillation with the *local* period. Then the oscillation becomes twice faster and fractional revivals can be observed whereas around the full revival the local period sets in again.

The necessary numerical phase space integration for the HK method can be made very efficiently

Methods	$a_i(t)$	$z_i(t)$
VCS	Nonlinear, coupled to all z_i and a_j	Nonlinear, coupled to all a_i and z_j
CCS	Linear, time-dependent coeff., coupled	Nonlinear, uncoupled
SCS	Linear, constant coeff., coupled	Stationary
HK	Linear, uncoupled	Nonlinear, uncoupled
TGWD	n/a	One nonlinear equation

Table 3.1.: Nature of ordinary differential equations for the different methods in the case of a generic (non harmonic oscillator), time-independent Hamiltonian. "Uncoupled" indicates that equations of motion with different index do not talk to each other (no "inter-coupling"). In the HK case the equations of motion for a specific a_i is, however, coupled to the z_i with the same index ("intra-coupling")

using the Box-Muller algorithm [148] based on pseudo-random numbers [55], as proposed in [101] and [38] and calculated the time-evolved wavefunction

$$|\Psi_\alpha(t)\rangle = \frac{2}{M}\sum_{l=1}^{M}\bar{b}_l(t)|z_l(t)\rangle, \tag{3.29}$$

where M is the multiplicity (or the number of propagated trajectories) and where

$$\bar{b}(t) = \bar{a}(t)F^{-1}, \tag{3.30}$$

as well as

$$\bar{a}(t) = R\left(p,q,t\right)\mathrm{e}^{\frac{\mathrm{i}}{\hbar}S(p,q,t)}\langle z\left(p,q\right)|\Psi_\alpha\left(0\right)\rangle. \tag{3.31}$$

Here the sampling function F is part of the overlap of the initial Gaussian centered at (p_α, q_α) with the coherent states i.e., $\langle z\left(p,q\right)|\Psi_\alpha\left(0\right)\rangle$

$$F = \exp\left[-\frac{\gamma}{4}(q-q_\alpha)^2 - \frac{1}{4\gamma\hbar^2}(p-p_\alpha)^2\right] = \exp\left[-\tilde{\alpha}|z-z_\alpha|^2\right] \tag{3.32}$$

which is the absolute value (real part) of (2.69) and which corresponds to the special case of compression parameter $\tilde{\alpha}$ equal to $1/2$ in Eq. (8) of [75][2]. The trajectories are thus initially close to the support of the initial wavefunction, centered around (p_α, q_α) and at $t = 0$ all the corresponding coefficients

$$\bar{b}(0) = \exp\left[\frac{\mathrm{i}}{2\hbar}(q-q_\alpha)(p+p_\alpha)\right] \tag{3.33}$$

were therefore nonzero and had an absolute value of unity. One may ask where the inverse overlap matrix appears in the HK approach. By implicitly assuming that we can discretize the phase space integral with a single phase space sum, i.e., by assuming the representation of unity in the form

$$\sum_l |z_l(0)\rangle\langle z_l(0)| \sim 1 \tag{3.34}$$

also discussed in Appendix C, the coherent states have been used as if they formed a tight frame [77] and the inverse overlap is not encountered [78]. Hence, we can say that one has used the non-orthogonal Gaussians "painlessly". There is a difference between the tight frames used in the HK case compared to the SCS case which is discussed in the Appendix C. In the HK case we choose random initial phase space points dense enough to form a tight frame, and perform the Monte Carlo integration in order to discretize the phase space integral. Whereas in the SCS case we take a fixed

[2]The phase space integral of the sampling function is $4\pi\hbar$, which together with the factor $1/\left(2\pi\hbar\right)$ in (2.68) simplified for a single degree of freedom gives the factor of 2 in Eq. (3.29)

rectangular grid of initial phase space points, so that the phase space integral is discretized simply by calculating the total phase space volume. It remains to be tested if the use of the double sum in Eq. (2.26) is of any advantage in the HK case.

For convergence of the semiclassical results at almost all times shown in Fig. 3.3, we needed around 10^4 trajectories, which is in the same ballpark as mentioned in [101], where the dynamics was monitored over 12 vibrational periods and where 50000 coherent states were used and it was stated that the results are still very good for 5000 trajectories but not for only 500. Similar orders of magnitude have been reported in [38]. The random choice of initial conditions leads to a favorable scaling of the methodology with the number of degrees of freedom (subexponential), which comes, however, at the expense of slow convergence [75]. In a MATLAB implementation, we realized that it is favorable to propagate all trajectories in parallel (not propagating the trajectories individually until the end) as then the scaling of the numerical effort with the number of trajectories is sublinear!

A more recent mathematical exposition of the errors encountered by Monte Carlo and quasi Monte Carlo discretization of the phase space integral is given in [149]. Usage of grid based discretization is possible in 1D but does not present a viable scheme for more degrees of freedom because in the HK case, the grid has to represent a tight frame [78], which leads to rather densely spaced grids and thus large numbers of trajectories to be propagated.

For the common propagation of Hamilton's equations of motion as well as the action and the stability information, we used symplectic (leap frog) integration [150], see also Appendix D. The time step used was the same as in the split-operator calculations. Numerical results up to the time of the first revival (corresponding to about 60(!) (classical) vibrational periods) are shown in Fig. 3.3. Here we have refrained from normalization of the results, which is frequently performed because the

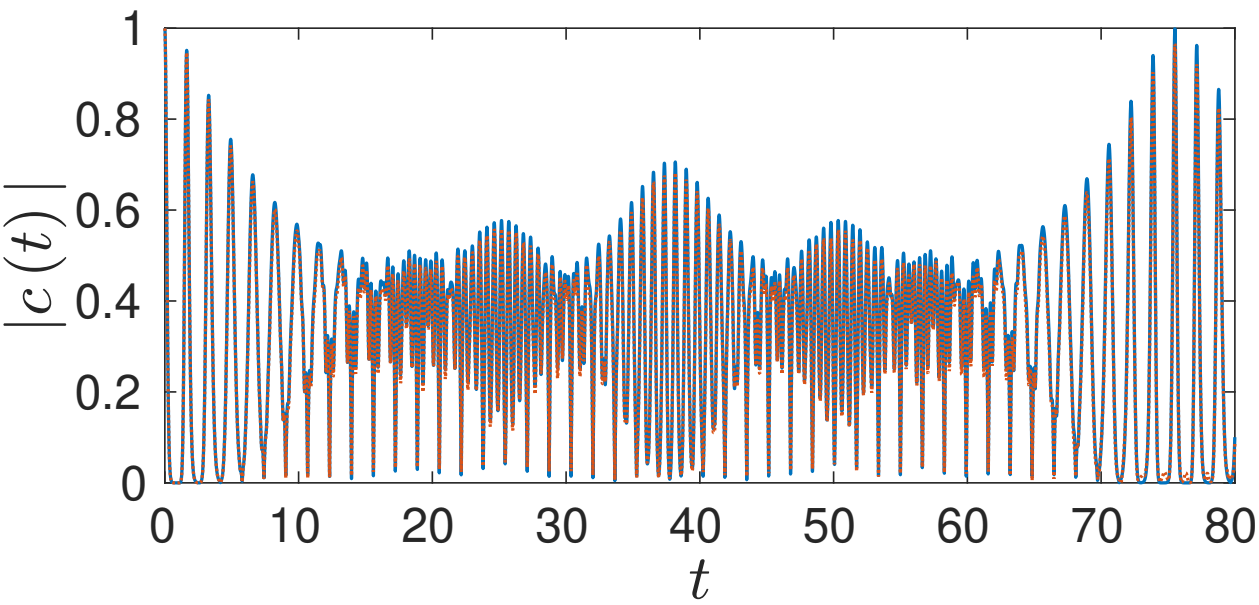

Figure 3.3.: Absolute value of the autocorrelation function using the HK method (dotted red line) with a (sub-)random grid of initial points in phase space, compared to results of a FFT calculation (solid blue).

HK propagator is unitary only analytically in the stationary phase approximation [91], but not in numerical calculations [38]. Still, the HK result very closely follows the fully converged FFT result and shows the revival, which is in accord with the results presented in [99]. By using 50000 trajectories also the small discrepancies at low values of $|c(t)|$ at long times visible in Fig. 3.3 can be converged to the FFT results (not shown). The lack of norm conservation of the HK results can only be cured by renormalization, however [151].

In a MATLAB implementation [152], it was found that the use of a Halton sequence of random numbers seems favorable compared to a Sobol sequence, if the options of skip and leap are not used. With those options comparable results can be gained by the two methods. To make the comparison, the relative maximum of the absolute value of the autocorrelation at $t = 75.52$, close to the analytical revival time $T_{\text{rev}} \approx 75.75$ and almost identical to 60 times the classical period, defined in Section 3.1, was looked at. The results are given in Table 3.2. The corresponding result from the FFT calculation is 0.9990.

skip,leap	$0,0$	$1000,10$	$1000,100$	$1000,1000$	$1000,10,000$
Sobol	0.9456	0.9598	0.9741	0.9757	0.9703
Halton	0.9607	0.9802	0.9611	0.9581	0.9600

Table 3.2.: Absolute value of the autocorrelation at $t = 75.52$ for an implementation of HK propagation with 10000 trajectories and two different choices of quasi random number generators. Skip=1000 leaves out the first 1000 random numbers and leap=100 takes only every 100th entry.

3.2.2. SCS results

Because we are taking into account the inverse overlap and solve Eq. (2.57), a relatively sparse static grid may be employed. The grid we are using has the extension in q-direction from $q_{\min} + q_\alpha$ to $q_{\max} = -q_{\min} + q_\alpha$ with $q_{\min} = -3\sqrt{\pi}$ and in p-direction from $p_{\min} = -5\sqrt{\pi}$ to $p_{\max} = -p_{\min}$. The number of equally spaced grid points in both directions was 9, leading to a grid with $M = 81$ points and the PBBGK completeness-criterion for the spacing of the z-grid was met [62, 64] and the initial state is a member of the set (an odd number of grid points is necessary to this end). Other workers have also experimented with randomly distributed static grid points [33, 153] with, at least in the first reference, less satisfactory results. This might be due to the fact that in [33] a 1D single particle system was studied, whereas in [153] the system had two degrees of freedom and Monte Carlo methods perform the better the higher-dimensional the integral.

In implementing the matrix exponential [154] that occurs in Eq. (2.57) one has to first invert the overlap matrix. This has to be done only once at the very beginning, however, for a static grid of coherent states and requires regularization in the form of the addition of a unit matrix times a very small number (10^{-8}, larger values would lead to noisy results at longer times) to the overlap matrix before inversion. A judicious choice of the small regularization parameter allows a closer approach to the von Neumann limit of the spacing of grid points. We have not tried to optimize the grid in this respect, but this might become necessary in high-dimensional applications. The propagation matrix is then established and used iteratively to advance the wavefunction vector in time. A cutoff of high

energy basis functions was not necessary for the grid used. Our results are shown in Fig. 3.4. There is no problem with norm conservation and the revival is displayed completely.

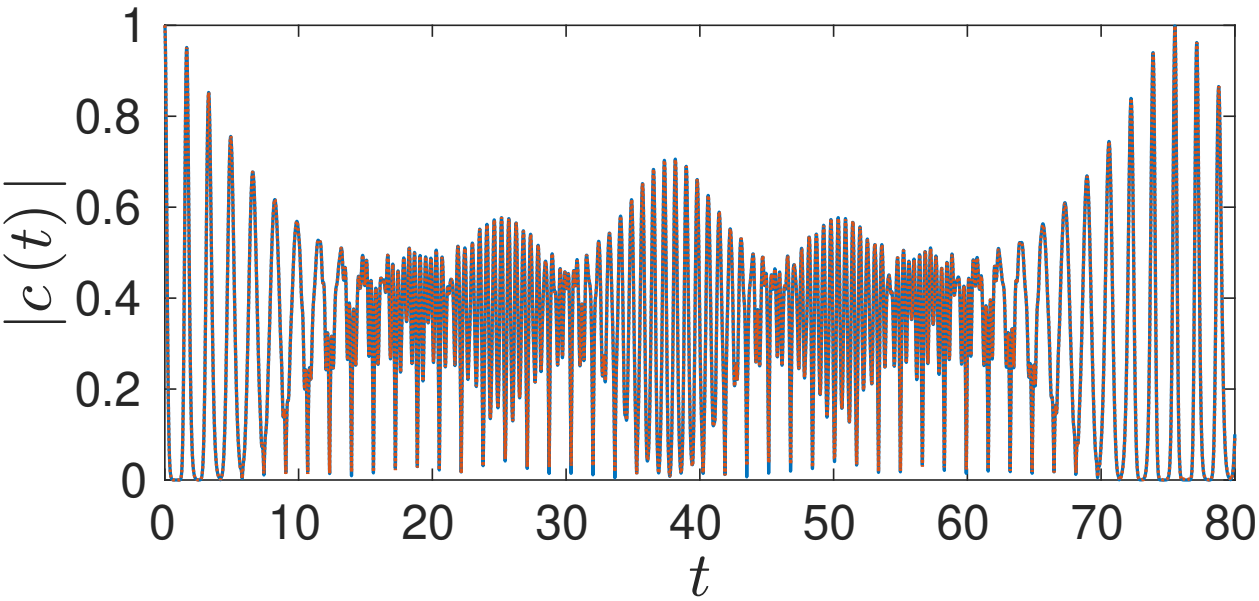

Figure 3.4.: Absolute value of the autocorrelation function using the SCS method (dotted red line) with a fixed rectangular grid compared to results of a FFT calculation (solid blue line).

In Fig. 3.5, we display the absolute value of the a coefficients at the revival time as a function of the phase space variables. We see from this figure that the a coefficients do not come back to their initial values but the individual Gaussians interfere in such a way that the position space wavefunction shows the revival, see also the HK implementation in [99].

Setting up the propagation matrix in SCS was much more time consuming than in the FFT case (where only vectors have to be set up, due to the locality of the potential and kinetic energy operators in position and momentum space, respectively!). With the propagation matrix set up, the total program execution time up to the first revival was less than one second on a modern laptop computer in a MATLAB implementation in both cases, SCS and FFT, though. Comparing to the studies in [33], we used very similar grids but we also note that we did not use second order differencing for time propagation but used matrix exponentiation and subsequently iterative propagation via multiplication of a vector by a matrix. Our procedure also conserves the norm and is very stable, as long as the overlap matrix is regularized by adding a small unit matrix. We note in passing that solving the differential equation for the coefficients with an adaptive step-size Runge-Kutta method results in an order of magnitude longer computation times.

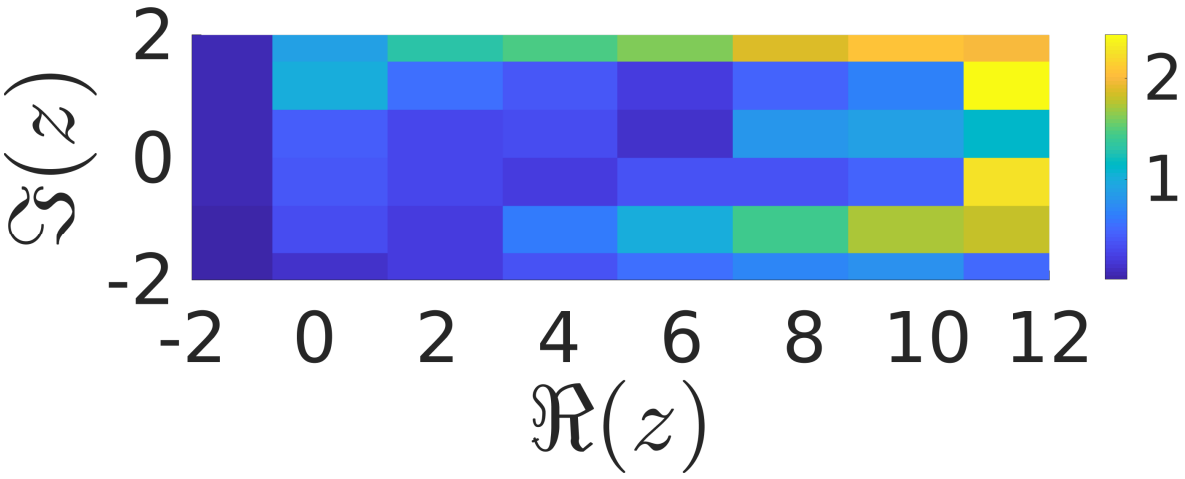

Figure 3.5.: Absolute value of the a coefficients at the numerical revival time $T = 75.52$ for the static rectangular grid used in the SCS case as a function of the real and imaginary part of z. The color of each face depends on the color at one of its four surrounding vertices. Of the four vertices, the one that comes first in the x-y grid determines the color of the face [152].

Shalashilin and Child have tried to reduce the numerical effort by coupling to nearest or up to next nearest neighbors only [33]. This could become very relevant for the treatment of larger numbers of degrees of freedom. Alternatively, the scaling of matrix multiplication with the square of the number of basis functions M could be reduced by employing the sparsity of the propagation matrix. Then a scaling even more favorable than the highly efficient FFT methodology, that scales with $M \log M$ [55] might be possible. It might also be worthwhile to not calculate the matrix exponential at all but just its action on the wavefunction vector [155].

In passing, we note that, for the present potential and initial state parameters, we could not get any reasonable results if the inverse overlap matrix was set proportional to the unit matrix, in contrast to the parameters used in [33] (see Appendix C). Furthermore, in contrast to the split-operator FFT approach, the present method allows for very large time steps, as there is no split-operator approximation involved, similar to the Chebyshev-polynomial method [156]. The drawback, however, is that time-dependent Hamiltonians cannot be treated in the presented way by using a precompiled matrix exponential.

3.2.3. CCS results

Now let us turn to moving CS grids, where the grid points are determined using importance sampling and follow classical equations of motion very similar to the ones that are followed by the HK trajec-

tories. We used a set of 121 trajectories, which are a lot less than used in the HK case (the central trajectory starting at (q_α, p_α) has to be present though).

We can draw the trajectories' initial conditions from the distribution (3.32). For the calculation of the wavefunction in the case of CCS with importance sampling, we then get

$$|\Psi_\alpha(t)\rangle = \sum_{l=1}^{M} a_l(t)|z_l(t)\rangle, \tag{3.35}$$

with the randomly sampled initial conditions for the real and imaginary part of z_l. In contrast to the HK case (where we had discretized an integral) there is only one single coefficient $a_l(0)|_{l=\alpha} = 1$ nonzero initially, however, assuming that the coherent basis states have the same width parameters as the initial state. In the course of time because of the coupled equations of motion, different trajectories will start to contribute to the wavefunction by developing nonzero a coefficients. Using a different compression parameter, which was here chosen to be the natural one that was also used in the HK case, did not improve the results. Furthermore, we stress that by starting from the Ansatz (2.16), we are not implicitly using a tight frame assumption as done in Eq. (29) in [33], where (in the present notation) the set $\{\bar{a}_l\}$ is propagated.

Using symplectic integration (leap frog) for the momenta and positions explained in appendix D, we found that the determination of the trajectories was an order of magnitude faster than if an adaptive step-size Runge-Kutta method for evolution of the complex-valued z-variable was used.

After approximately half the revival time the evolved trajectories are displayed in Fig. 3.6 together with the initial state. The reasons why one should use a random grid are holding true especially for many particle problems and are detailed in [75]. There also the optimal choice of the compression parameter $\tilde{\alpha}$, which we here took to be $1/2$, is discussed. In higher-dimensional problems one has the additional freedom to choose $\tilde{\alpha}$ differently for the different degrees of freedom. This then leads to the notion of "pancake sampling".

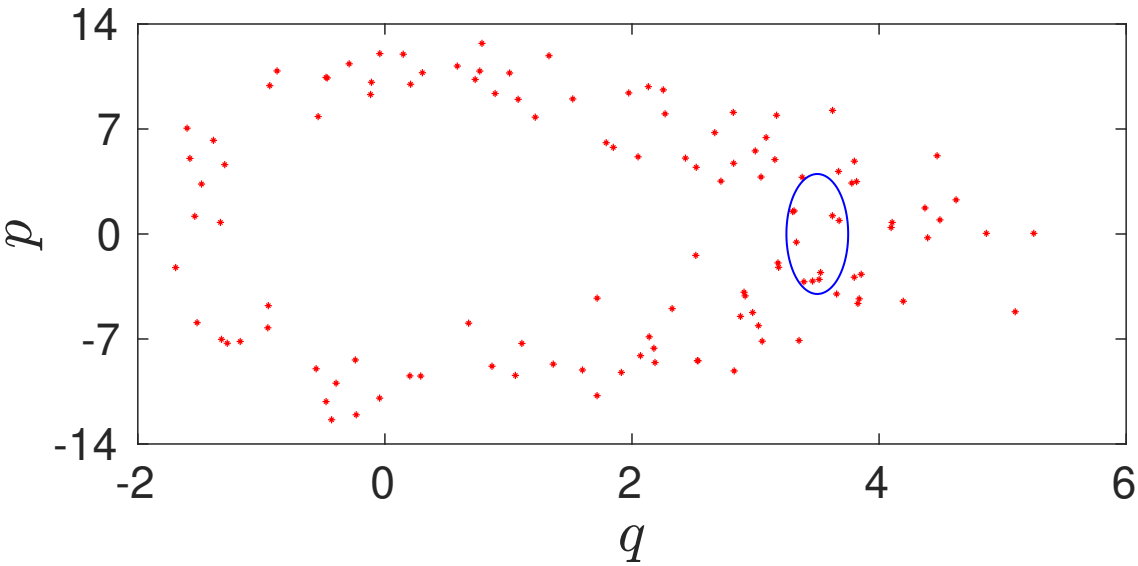

Figure 3.6.: Positions and momenta of the 121 random points used for the CCS calculation at time $t = 40$. Inserted into the plot is a blue ellipse that visualizes the location and extend of the initial sampling function (real part of Eq. (2.69)), by showing its decay to the value $1/e$.

The corresponding correlation function is exactly on top of the FFT result, as can be seen in Fig. 3.7. Due to the coupling between the coherent states and the fact that they are moving, which renders all overlaps time-dependent and thus also the coherent state matrix elements of the Hamiltonian, the present scheme in 1D is quite demanding numerically. Although we did not explicitly use matrix inversion (scaling cubically with the number of basis functions), but solved for the linear system of equations for the coefficients by using a mass matrix, the program was two orders of magnitude slower than the FFT calculation.

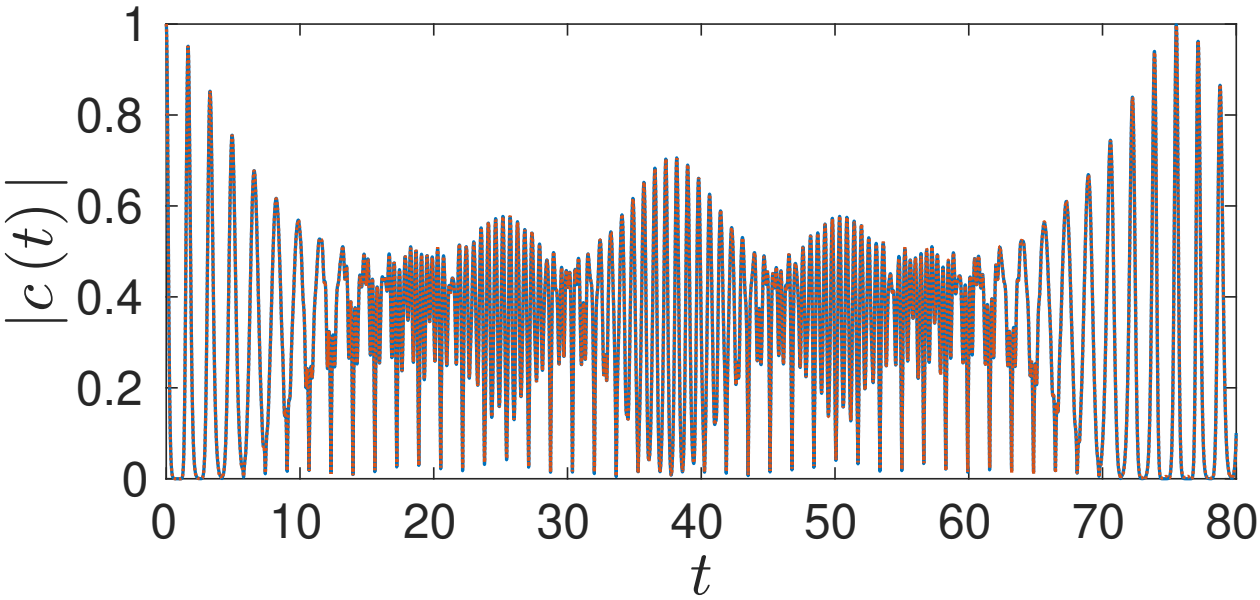

Figure 3.7.: Absolute value of the autocorrelation function using the CCS method (dotted red line) compared to the converged results of a FFT calculation (solid blue line).

3.3. Different potentials and their Hamiltonian matrix in the CS basis

Here we will collect the expressions for the Hamiltonian matrix of the three potentials considered in this thesis namely, Morse, harmonic and quartic. The Hamiltonian matrix is needed to calculate the variational equations of motion as in the VCS, CCS and SCS cases. The kinetic energy operator for all the three potentials will be the same for unit mass

$$\hat{T} = \frac{\hat{p}^2}{2}. \tag{3.36}$$

Therefore, the normal-ordered form of the kinetic energy operator is given by

$$\hat{T}_{\text{ord}}(\hat{a}^\dagger, \hat{a}) = -\frac{\gamma}{4}(\hat{a}^\dagger - \hat{a})^2 = -\frac{\gamma}{4}\left[(\hat{a}^\dagger)^2 - 2\hat{a}^\dagger\hat{a} - 1 + \hat{a}^2\right] \tag{3.37}$$

and the normal-ordered form of the kinetic energy needed to calculate the matrix elements of the Hamilton operator between the coherent states is thus

$$T_{\text{ord}}(z_k^*, z_l) = -\frac{\gamma}{4}\left[(z_k^* - z_l)^2 - 1\right]. \tag{3.38}$$

The potential energy operator and the normal-ordered form of the potential energy for all the three potentials considered in this thesis are given in the following table:

Potentials	$\hat{V}$	$V_{\text{ord}}(z_k^*, z_l)$
Morse	$D(1-\mathrm{e}^{-\alpha\hat{x}})^2$	$D\left(1 - 2\mathrm{e}^{\alpha_1^2/2}\mathrm{e}^{-\alpha_1(z_k^*+z_l)} + \mathrm{e}^{2\alpha_1^2}\mathrm{e}^{-2\alpha_1(z_k^*+z_l)}\right)$
Harmonic	$\frac{1}{2}\omega^2\hat{x}^2$	$\frac{\gamma}{4}\left[(z_k^* + z_l)^2 + 1\right]$
Quartic	$\frac{a}{4}\hat{x}^4$	$\frac{a}{16\gamma^2}\left[(z_k^* + z_l)^4 + 6\,(z_k^* + z_l)^2 + 3\right]$

Table 3.3.: Expressions for the normal-ordered form of potential energy in terms of coherent state parameters for some general potentials.

Here we consider the trivial case for the harmonic potential i.e., the harmonic oscillator frequency ω_0 is equal to the frequency ω of the harmonic oscillator that defines the coherent state basis. The more general expression for the normal-ordered Hamiltonian of the harmonic oscillator is given in Appendix B. The calculation of the normal-ordered form of the potential energy for the quartic oscillator is given in detail in Appendix G. Therefore, the normally ordered Hamiltonian for all the three potentials are given by

$$H_{\text{ord}}(z_k^*, z_l) = T_{\text{ord}}(z_k^*, z_l) + V_{\text{ord}}(z_k^*, z_l). \tag{3.39}$$

4. Staying Probability: Husimi Version

In the previous chapter the HK method was shown to be a powerful tool for solving the TDSE. For many-body systems, the favorable scaling of the Monte Carlo integration is promising. In the case that time-dependent correlation functions of the form

$$C_{AB}(t) = \mathrm{Tr}\left[\hat{A}\hat{B}(t)\right] = \mathrm{Tr}\left[\hat{A}\mathrm{e}^{\frac{\mathrm{i}}{\hbar}\hat{H}t}\hat{B}\mathrm{e}^{-\frac{\mathrm{i}}{\hbar}\hat{H}t}\right] \tag{4.1}$$

are sought for, already in 1D two propagators are needed, one forward and one backwards in time, however. This fact calls for additional approximations, which we will discuss in the present chapter.

Along similar lines, in the chemical physics community, a classical Wigner dynamics was introduced early on by Heller [157], with a precursor in reaction rate theory by Miller [158]. Historically, the heuristic introduction of this Wigner method, based on classical trajectories preceded its derivation from a semiclassical initial value representation of the propagator by Cao and Voth [159] by two decades. Nowadays, the classical Wigner method in chemical physics is also referred to as linearized semiclassical initial value representation and is prominently used by the Miller group [45, 95, 160]. Technically, the LSC-IVR method is much easier to apply than the full semiclassical initial value representation of, e.g., Herman and Kluk [37], as it linearizes the phase difference between interfering classical trajectories and does not contain any oscillating terms in the integrand (no sign problem). In addition to the application to (reactive) single surface dynamics, also the application of LSC-IVR to electronically nonadiabatic processes i.e., those involving transitions between different potential energy surfaces was shown by Miller and co-authors [42, 161]. Furthermore, LSC-IVRs are close in spirit to the diagonal approximation that is used to calculate the smooth part of the semiclassical spectral density in chaotic systems [162].

Whereas in the pioneering works of the Heller as well as the Miller groups, Wigner transforms in the LSC-IVR are used, a new semiclassical framework, introduced by Antipov, Ye and Ananth [47], based on Husimi functions, see also [163, 164], can be tuned to reproduce existing quantum-limit and classical-limit SC approximations to quantum real-time correlation functions. So far, the applicability of the Husimi LSC-IVR is restricted to correlation functions $C_{AB}(t) = \langle\hat{A}\hat{B}(t)\rangle$ with operators $\hat{B}$ that do not contain exponential terms [47]. In the present chapter, we will extend the usability of the Husimi based LSC-IVR to the calculation of survival probabilities, that is, we will choose identical (projection) operators $\hat{A} = \hat{B} = |\Psi\rangle\langle\Psi|$, where the involved wavefunctions are Gaussians. We will discuss, however, also other more common choices for the operators.

In this chapter, we will show comparisons of numerical results for survival probabilities using three different approaches (Wigner LSC-IVR, Husimi LSC-IVR and full SC-IVR) with the full quantum

mechanical results. The system for which we perform the investigations is again the Morse oscillator from Chap. 3 and we will especially focus on the revival phenomenon which is present in the full quantum dynamics. If the Morse oscillator is coupled to a harmonic oscillator (acting as a bath for the system) the revival phenomenon is expected to vanish also in the full quantum result.

4.1. Theory

In the following, we will introduce the general form of correlation functions that are to be studied and then we will compare different implementations thereof based on classical trajectories.

4.1.1. General Correlation Functions

The time correlation function of two arbitrary operators $\hat{A}$ and $\hat{B}$ with a (Heisenberg) time-evolved operator $\hat{B}(t)$ is defined as in Eq. (4.1) where

$$\hat{H} = \sum_{i=1}^{f} \frac{p_i^2}{2m_i} + V(\mathbf{q}) \tag{4.2}$$

is the Hamiltonian of the system under consideration. This system shall have $2f$ degrees of freedom in phase space, denoted by $(\mathbf{p}, \mathbf{q})$.

Dynamic phenomena in complex systems can be described in terms of real-time correlation functions. The general time correlation function has various applications based on the choice of the arbitrary operators $\hat{A}$ and $\hat{B}$. Different possible choices for the operators of the correlation function are as follows:

- $\hat{A} = |\Psi_\alpha\rangle\langle\Psi_\alpha|$, $\hat{B} = |\Psi_\alpha\rangle\langle\Psi_\alpha|$
  $|\Psi_\alpha\rangle\langle\Psi_\alpha|$ is a projection operator on the initial state $|\Psi_\alpha\rangle$. This leads to the survival probability which is equivalent to the absolute value squared of the auto-correlation function. In the following, we will assume the initial states to be Gaussian wavefunctions.

- $\hat{A} = Q^{-1} \exp\left\{-\beta\hat{H}\right\} \hat{\mathbf{r}}$, $\hat{B} = \hat{\mathbf{r}}$,
  Where Q is the partition function, $\beta = 1/kT$ is the inverse temperature and $\hat{\mathbf{r}}$ the position operator. This is the temperature dependent dipole-dipole correlation function used to study IR spectra. Semiclassical investigations for this case have been performed in [163, 165, 166] in the high temperature limit $\beta \to 0$.

- $\hat{A} = |\Psi_\alpha\rangle\langle\Psi_\alpha|$, $\hat{B} = |\mathbf{r}\rangle\langle\mathbf{r}|$
  This choice leads to the reduced density. For the case of a Caldeira-Leggett model, the transition to classicality and the blue shift of the system oscillator have been investigated in [146], see also [46].

- $\hat{A} = |\Psi_\alpha\rangle\langle\Psi_\alpha|$, $\hat{B} = \hat{x}, \hat{x^2}, ...$

Here $\hat{x}$ is the position operator in one dimension. This choice is used to calculate time-dependent moments of $\hat{x}$.

We will be evaluating the dipole-dipole correlation function and the survival probability using both Wigner LSC-IVR and Husimi LSC-IVR methods in the following subsection.

4.1.2. Comparison between Wigner LSC-IVR and Husimi LSC-IVR

For the following comparison, we restrict the discussion to the case $f = 1$, i.e., a single degree of freedom. The generalization to arbitrary f is straightforward.

In the classical, so-called LSC-IVR employing Wigner functions, the expression for the general time-correlation function is given by [157, 159]

$$C_{AB}^{W}(t) = \int \frac{\mathrm{d}p\mathrm{d}q}{2\pi\hbar} A_W(p,q)\, B_W(p_t,q_t)\,, \tag{4.3}$$

where $A_W(p,q)$ and $B_W(p_t,q_t)$ are the Wigner-Weyl transforms of operators $\hat{A}$ and $\hat{B}$ and (p_t,q_t) are classical trajectories in phase space that evolve from the initial conditions (p,q) according to Hamilton's equations of motion

$$\dot{q}_t = \frac{\partial H}{\partial p_t} \qquad \dot{p}_t = -\frac{\partial H}{\partial q_t}. \tag{4.4}$$

$A_W(p,q)$ is defined as:

$$A_W(p,q) = \int \mathrm{d}\Delta q \mathrm{e}^{-\mathrm{i}\frac{\mathrm{p}\Delta\mathrm{q}}{\hbar}} \left\langle q + \frac{\Delta q}{2} \middle| \hat{A} \middle| q - \frac{\Delta q}{2} \right\rangle. \tag{4.5}$$

Now in the case of the coherent state based LSC-IVR method employing Husimi functions, the general time-correlation function is given by [47]

$$C_{AB}^{H}(t) = \int \frac{\mathrm{d}p\mathrm{d}q}{2\pi\hbar} A_H(p,q)\, B_H(p_t,q_t)\,, \tag{4.6}$$

where $A_H(p,q)$ and $B_H(p_t,q_t)$ are the Husimi transforms of the operators $\hat{A}$ and $\hat{B}$ defined as [167]

$$A_H(p,q) = \langle z(p,q)|\hat{A}|z(p,q)\rangle, \tag{4.7}$$

where $|z(p,q)\rangle$ represents a coherent state with width parameter $\tilde{\gamma}$, given in position representation by

$$\langle x|z(p,q)\rangle = \left(\frac{\tilde{\gamma}}{\pi}\right)^{1/4} \mathrm{e}^{-\frac{\tilde{\gamma}}{2}(x-q)^2 + \frac{\mathrm{i}}{\hbar}p(x-q)}, \tag{4.8}$$

with a phase convention slightly different from Klauder's [58].

We stress that although the Wigner expression is generally valid, the Husimi version of the correla-

tion function only holds for operators $\hat{B}$ that do not contribute to the phase [47]. In passing, we note that a proof that any operator is determined by its expectation in all coherent states is given in [168].

Now we will examine two cases with the help of both LSC-IVR methods (Wigner and Husimi). Firstly this will be the dipole-dipole correlation function and secondly the survival probability.

The Dipole-Dipole Correlation Function

For the case of the dipole-dipole correlation function, we choose the operators $\hat{A}$ and $\hat{B}$ as: $\hat{A} = \exp\left\{-\beta\hat{H}\right\}\hat{q}/Q$ and $\hat{B} = \hat{q}$. Here

$$\hat{\rho} = \exp\left\{-\beta\hat{H}\right\}/Q \tag{4.9}$$

is the canonical density-operator. Therefore, the Wigner-Weyl transform [169] is given by (we are neglecting the partition function Q in the following)

$$A_W(p,q) = \int \mathrm{d}\Delta q \mathrm{e}^{-\mathrm{i}\frac{p\Delta q}{\hbar}} \langle q + \frac{\Delta q}{2}| \exp\left\{-\beta\hat{H}\right\}\hat{q}|q - \frac{\Delta q}{2}\rangle \tag{4.10}$$

and the canonical density-operator matrix element is

$$\rho(y,z) = \langle y|\mathrm{e}^{-\beta\hat{H}}|z\rangle. \tag{4.11}$$

Because we are investigating the classical limit of correlation functions, a high temperature limit seems justified. For high temperatures, i.e, for small β, a short time approximation to the "imaginary time propagator" $\mathrm{e}^{-\beta\hat{H}}$ is possible [170] and it leads to the expression

$$\rho(y,z) \approx \sqrt{\frac{m}{2\pi\beta\hbar^2}}\mathrm{e}^{-\frac{m}{2\beta\hbar^2}(y-z)^2}\mathrm{e}^{-\beta V\left(\frac{y+z}{2}\right)} \tag{4.12}$$

for the position matrix element of the canonical density-operator. Applying the short-time approximation to the canonical density-operator and neglecting an additive term proportional to β, the Wigner-Weyl transform thus becomes

$$\begin{aligned}
A_W(p,q) &\approx \int \mathrm{d}\Delta q \mathrm{e}^{-\mathrm{i}\frac{\mathrm{p}\Delta\mathrm{q}}{\hbar}} \rho\left(q + \frac{\Delta q}{2}, q - \frac{\Delta q}{2}\right) q \\
&= \int \mathrm{d}\Delta q \mathrm{e}^{-\mathrm{i}\frac{\mathrm{p}\Delta\mathrm{q}}{\hbar}} \sqrt{\frac{m}{2\pi\beta\hbar^2}}\mathrm{e}^{-\frac{m}{2\beta\hbar^2}\Delta q^2}\mathrm{e}^{-\beta V(q)} q \\
&= q\mathrm{e}^{-\beta V(q)}\sqrt{\frac{m}{2\pi\beta\hbar^2}}\int \mathrm{d}\Delta q \exp\left\{-\frac{m}{2\beta\hbar^2}\Delta q^2 - \mathrm{i}\frac{\mathrm{p}\Delta\mathrm{q}}{\hbar}\right\} \\
&= q\mathrm{e}^{-\beta V(q)}\sqrt{\frac{m}{2\pi\beta\hbar^2}}\sqrt{\frac{2\pi\beta\hbar^2}{m}}\mathrm{e}^{-\frac{\beta p^2}{2m}} \\
&= q\mathrm{e}^{-\beta H}.
\end{aligned} \tag{4.13}$$

Similarly, it can be shown that

$$B_W\left(p_t, q_t\right) = q_t. \tag{4.14}$$

Hence, the dipole-dipole correlation function comes out to be

$$C_{AB}^W\left(t\right) = \int \frac{\mathrm{d}p\mathrm{d}q}{2\pi\hbar} q \mathrm{e}^{-\beta H} q_t, \tag{4.15}$$

see also [171].

Now, we will calculate the dipole-dipole correlation function using coherent states. The Husimi transform of operator $\hat{A}$ is given by

$$\begin{aligned} A_H\left(p,q\right) &= \langle z(p,q)|\mathrm{e}^{-\beta\hat{H}}\hat{q}|z(p,q)\rangle. \\ &\approx \int \mathrm{d}x \int \mathrm{d}x' \langle z(p,q)|x'\rangle\langle x'|\mathrm{e}^{-\beta\hat{H}}|x\rangle\langle x|z(p,q)\rangle q, \end{aligned} \tag{4.16}$$

where we used a stationary phase argument that allows to treat the operator $\hat{q}$ like a constant [163]. Again applying the short-time approximation to the canonical density-operator and substituting the explicit expressions for $\langle z(p,q)|x'\rangle$ and $\langle x|z(p,q)\rangle$ we get,

$$\begin{aligned} A_H\left(p,q\right) \approx & \int \mathrm{d}x \int \mathrm{d}x' q \left(\frac{\tilde{\gamma}}{\pi}\right)^{\frac{1}{2}} \exp\left\{-\frac{\tilde{\gamma}}{2}\left(x'-q\right)^2 - \frac{\mathrm{i}p}{\hbar}\left(x'-q\right)\right\} \\ & \sqrt{\frac{m}{2\pi\beta\hbar^2}} \exp\left\{-\frac{m}{2\beta\hbar^2}\left(x'-x\right)^2 - \beta V\left(\frac{x'+x}{2}\right)\right\} \exp\left\{-\frac{\tilde{\gamma}}{2}\left(x-q\right)^2 + \frac{\mathrm{i}p}{\hbar}\left(x-q\right)\right\} \\ & = q\left(\frac{\tilde{\gamma}}{\pi}\right)^{\frac{1}{2}} \sqrt{\frac{m}{2\pi\beta\hbar^2}} \int \mathrm{d}x \int \mathrm{d}x' \exp\Bigg(- x'^2\left(\frac{\tilde{\gamma}}{2} + \frac{m}{2\beta\hbar^2}\right) + x'\left(\tilde{\gamma}q - \frac{\mathrm{i}p}{\hbar}\right) \\ & - x^2\left(\frac{\tilde{\gamma}}{2} + \frac{m}{2\beta\hbar^2}\right) + x\left(\tilde{\gamma}q + \frac{\mathrm{i}p}{\hbar}\right) + \frac{m}{\beta\hbar^2}x'x - \tilde{\gamma}q^2\Bigg)\mathrm{e}^{-\beta V\left(\frac{x'+x}{2}\right)}. \end{aligned} \tag{4.17}$$

Now, we approximate the potential $V\left(\frac{x'+x}{2}\right)$ by its value at $x = x' = q$ [163], which is constant and hence can be taken out of the integral. Therefore, we have

$$\begin{aligned} A_H\left(p,q\right) \approx & q\left(\frac{\tilde{\gamma}}{\pi}\right)^{\frac{1}{2}} \sqrt{\frac{m}{2\pi\beta\hbar^2}} \mathrm{e}^{-\beta V(q)} \int \mathrm{d}x \int \mathrm{d}x' \exp\Bigg(- x'^2\left(\frac{\tilde{\gamma}}{2} + \frac{m}{2\beta\hbar^2}\right) + x'\left(\tilde{\gamma}q - \frac{\mathrm{i}p}{\hbar}\right) \\ & - x^2\left(\frac{\tilde{\gamma}}{2} + \frac{m}{2\beta\hbar^2}\right) + x\left(\tilde{\gamma}q + \frac{\mathrm{i}p}{\hbar}\right) + \frac{m}{\beta\hbar^2}x'x - \tilde{\gamma}q^2\Bigg). \end{aligned} \tag{4.18}$$

The total exponent E inside the integral can now be written in the form

$$E = -\left(x', x\right)\mathbf{A}\begin{pmatrix} x' \\ x \end{pmatrix} + \mathbf{b}^{\mathsf{T}}\begin{pmatrix} x' \\ x \end{pmatrix} + c, \tag{4.19}$$

with matrix $\mathbf{A}$, vector $\mathbf{b}$ and scalar c. For the matrix we find

$$\mathbf{A} = \begin{pmatrix} \frac{\tilde{\gamma}}{2} + \frac{m}{2\beta\hbar^2} & -\frac{m}{2\beta\hbar^2} \\ -\frac{m}{2\beta\hbar^2} & \frac{\tilde{\gamma}}{2} + \frac{m}{2\beta\hbar^2} \end{pmatrix} \tag{4.20}$$

and for the vector

$$\mathbf{b} = \begin{pmatrix} \tilde{\gamma}q - \frac{\mathrm{i}}{\hbar}p \\ \tilde{\gamma}q + \frac{\mathrm{i}}{\hbar}p \end{pmatrix} \tag{4.21}$$

and finally the scalar is given by

$$c = -\tilde{\gamma}q^2. \tag{4.22}$$

The value of the Gaussian integral in terms of the quantities just defined is

$$\int \mathrm{d}x \int \mathrm{d}x' \exp\{E\} = \sqrt{\frac{\pi^2}{\det \mathbf{A}}} \exp\left\{\frac{\mathbf{b}^\intercal \mathbf{A}^{-1}\mathbf{b}}{4} + c\right\}, \tag{4.23}$$

where

$$\mathbf{b}^\intercal \mathbf{A}^{-1}\mathbf{b} = \frac{1}{\det \mathbf{A}}\left(b_1^2 a_{22} + b_2^2 a_{11} - 2b_1 b_2 a_{12}\right) \tag{4.24}$$

and

$$\det \mathbf{A} = a_{11}a_{22} - a_{12}^2 = \frac{\tilde{\gamma}^2}{4} + \frac{m\tilde{\gamma}}{2\beta\hbar^2}. \tag{4.25}$$

Applying the short-time approximation $\beta \to 0$ to the expression of $\mathbf{b}^\intercal \mathbf{A}^{-1}\mathbf{b}$ and also to $\det \mathbf{A}$, we arrive at the final result for the Husimi transform

$$\begin{aligned} A_H(p,q) &\approx q\left(\frac{\tilde{\gamma}}{\pi}\right)^{\frac{1}{2}} \sqrt{\frac{m}{2\pi\beta\hbar^2}} \mathrm{e}^{-\beta V(q)} \sqrt{\frac{\pi^2}{\frac{m\tilde{\gamma}}{2\beta\hbar^2}}} \exp\left(\tilde{\gamma}q^2 - \beta\frac{p^2}{2m} - \tilde{\gamma}q^2\right). \\ &= q\mathrm{e}^{-\beta H}, \end{aligned} \tag{4.26}$$

independent of the coherent state width parameter $\tilde{\gamma}$. Similarly,

$$B_H(p_t, q_t) = q_t. \tag{4.27}$$

The dipole-dipole correlation function comes out to be

$$C_{AB}^H(t) = \int \frac{\mathrm{d}p\mathrm{d}q}{2\pi\hbar} q\mathrm{e}^{-\beta H} q_t. \tag{4.28}$$

Hence, we can conclude that the expressions for the Wigner-Weyl (4.15) and Husimi (4.28) versions

for the dipole-dipole correlation function case in the high temperature limit coincide.

The Survival Probability

For the case of the survival probability, the operators $\hat{A}$ and $\hat{B}$ are projection operators; i.e., $\hat{A} = \hat{B} = |\Psi_\alpha\rangle\langle\Psi_\alpha|$, and it is assumed that the wavefunctions $\langle x|\Psi_\alpha\rangle$ in position space are Gaussians. Let us first derive the survival probability using Wigner LSC-IVR. For the Wigner-Weyl transform, we get

$$\begin{aligned}
A_W(p,q) &= \int \mathrm{d}\Delta q \mathrm{e}^{-\mathrm{i}\frac{\mathrm{p}\Delta\mathrm{q}}{\hbar}} \langle q + \frac{\Delta q}{2}|\hat{A}|q - \frac{\Delta q}{2}\rangle \\
&= \int \mathrm{d}\Delta q \mathrm{e}^{-\mathrm{i}\frac{\mathrm{p}\Delta\mathrm{q}}{\hbar}} \langle q + \frac{\Delta q}{2}|\Psi_\alpha\rangle\langle\Psi_\alpha|q - \frac{\Delta q}{2}\rangle \\
&= \int \mathrm{d}\Delta q \mathrm{e}^{-\mathrm{i}\frac{\mathrm{p}\Delta\mathrm{q}}{\hbar}} \Psi_\alpha\left(q + \frac{\Delta q}{2}\right)\Psi_\alpha^*\left(q - \frac{\Delta q}{2}\right) \\
&= \int \mathrm{d}\Delta q \mathrm{e}^{-\mathrm{i}\frac{\mathrm{p}\Delta\mathrm{q}}{\hbar}} \left(\frac{\gamma}{\pi}\right)^{\frac{1}{4}} \exp\left\{-\frac{\gamma}{2}\left(q + \frac{\Delta q}{2} - q_\alpha\right)^2 + \frac{\mathrm{i}}{\hbar}p_\alpha\left(q + \frac{\Delta q}{2} - q_\alpha\right)\right\} \\
&\left(\frac{\gamma}{\pi}\right)^{\frac{1}{4}} \exp\left\{-\frac{\gamma}{2}\left(q - \frac{\Delta q}{2} - q_\alpha\right)^2 - \frac{\mathrm{i}}{\hbar}p_\alpha\left(q - \frac{\Delta q}{2} - q_\alpha\right)\right\} \\
&= \left(\frac{\gamma}{\pi}\right)^{\frac{1}{2}} \int \mathrm{d}\Delta q \mathrm{e}^{-\mathrm{i}\frac{\mathrm{p}\Delta\mathrm{q}}{\hbar}} \exp\left\{-\gamma\left[(q-q_\alpha)^2 + \left(\frac{\Delta q}{2}\right)^2\right] + \frac{\mathrm{i}}{\hbar}p_\alpha\Delta q\right\} \\
&= \left(\frac{\gamma}{\pi}\right)^{\frac{1}{2}} \int \mathrm{d}\Delta q \exp\left\{-\frac{\gamma}{4}\Delta q^2 - \frac{\mathrm{i}}{\hbar}\Delta q\,(p - p_\alpha) - \gamma\,(q - q_\alpha)^2\right\}.
\end{aligned} \tag{4.29}$$

Defining $a = \frac{\gamma}{4}$, $b = -\frac{\mathrm{i}}{\hbar}(p - p_\alpha)$ and $c = -\gamma\,(q - q_\alpha)^2$, we can use the 1D version of the Gaussian integral (4.23) and the Wigner-Weyl transform becomes

$$A_W(p,q) = 2\exp\left\{-\gamma\,(q - q_\alpha)^2 - \frac{1}{\gamma\hbar^2}(p - p_\alpha)^2\right\} \tag{4.30}$$

and, similarly,

$$B_W(p_t,q_t) = 2\exp\left\{-\gamma\,(q_t - q_\alpha)^2 - \frac{1}{\gamma\hbar^2}(p_t - p_\alpha)^2\right\}. \tag{4.31}$$

Therefore, the survival probability becomes

$$\begin{aligned}
C_{AB}^W(t) &= \int \frac{\mathrm{d}p\mathrm{d}q}{2\pi\hbar} A_W(p,q)\,B_W(p_t,q_t) \\
&= 2\int \frac{\mathrm{d}p\mathrm{d}q}{\pi\hbar} \exp\left(-\gamma\left[(q-q_\alpha)^2 + (q_t - q_\alpha)^2\right] - \frac{1}{\gamma\hbar^2}\left[(p-p_\alpha)^2 + (p_t - p_\alpha)^2\right]\right).
\end{aligned} \tag{4.32}$$

Now let us try to get a first guess at the survival probability using the Husimi LSC-IVR method. We stress that the Husimi version for the correlation is not applicable to the present case [47] but

we will get a partial answer by using it anyways. Operators $\hat{A}$ and $\hat{B}$ are again projection operators. Their Husimi transforms are thus given by

$$A_H(p,q) = |\langle z(p,q)|\Psi_\alpha\rangle|^2. \tag{4.33}$$

Now,

$$\langle x|z(p,q)\rangle = \left(\frac{\tilde{\gamma}}{\pi}\right)^{\frac{1}{4}} \exp\left\{-\frac{\tilde{\gamma}}{2}(x-q)^2 + \frac{\mathrm{i}}{\hbar}p(x-q)\right\}, \tag{4.34}$$

$$\langle x|\Psi_\alpha\rangle = \left(\frac{\gamma}{\pi}\right)^{\frac{1}{4}} \exp\left\{-\frac{\gamma}{2}(x-q_\alpha)^2 + \frac{\mathrm{i}}{\hbar}p_\alpha(x-q_\alpha)\right\}, \tag{4.35}$$

where Ψ_α is a Gaussian centered around (p_α, q_α) with the width parameter γ. Therefore,

$$\langle z(p,q)|\Psi_\alpha\rangle = \int \mathrm{d}x \left(\frac{\tilde{\gamma}\gamma}{\pi^2}\right)^{\frac{1}{4}} \exp\left\{-\frac{\tilde{\gamma}}{2}(x-q)^2 - \frac{\gamma}{2}(x-q_\alpha)^2 - \frac{\mathrm{i}}{\hbar}\left[p(x-q) - p_\alpha(x-q_\alpha)\right]\right\}. \tag{4.36}$$

To simplify matters, we consider $\tilde{\gamma} = \gamma$ and get

$$\langle z(p,q)|\Psi_\alpha\rangle = \exp\left\{-\frac{\gamma}{4}(q-q_\alpha)^2 - \frac{1}{4\gamma\hbar^2}(p-p_\alpha)^2 + \frac{\mathrm{i}}{2\hbar}(q-q_\alpha)(p+p_\alpha)\right\} \tag{4.37}$$

for the overlap. Similarly,

$$\langle \Psi_\alpha|z(p,q)\rangle = \exp\left\{-\frac{\gamma}{4}(q-q_\alpha)^2 - \frac{1}{4\gamma\hbar^2}(p-p_\alpha)^2 - \frac{\mathrm{i}}{2\hbar}(q-q_\alpha)(p+p_\alpha)\right\}. \tag{4.38}$$

Therefore, the Husimi transforms are given by

$$A_H(p,q) = \exp\left\{-\frac{\gamma}{2}(q-q_\alpha)^2 - \frac{1}{2\gamma\hbar^2}(p-p_\alpha)^2\right\} \tag{4.39}$$

and

$$B_H(p_t,q_t) = \exp\left\{-\frac{\gamma}{2}(q_t-q_\alpha)^2 - \frac{1}{2\gamma\hbar^2}(p_t-p_\alpha)^2\right\}. \tag{4.40}$$

Hence, the survival probability follows to be

$$C_{AB}^H(t) = \int \frac{\mathrm{d}p\mathrm{d}q}{2\pi\hbar} \exp\left(-\frac{\gamma}{2}(q-q_\alpha)^2 - \frac{1}{2\gamma\hbar^2}(p-p_\alpha)^2 - \frac{\gamma}{2}(q_t-q_\alpha)^2 - \frac{1}{2\gamma\hbar^2}(p_t-p_\alpha)^2\right). \tag{4.41}$$

If we compare the Wigner-Weyl transforms and the Husimi transforms, we see that both expressions are quite different. In the Husimi transform (4.39), there is the factor of $\frac{1}{2}$ multiplied to the terms in the exponential, which is not present in the Wigner-Weyl transform (4.30). In addition, in the Wigner-

Weyl transform we have an additional factor of 2 multiplied with the exponential term. Hence, the two expressions for the transforms are different and we find that $A_H = \sqrt{\frac{A_w}{2}}$. Also, the final Husimi result (4.41) does not give unity at initial time as a simple Gaussian integration shows. We note in passing that if we had considered the width parameters of the coherent state ($\tilde{\gamma}$) and that of the Gaussian initial state (γ) to be different would not have resolved matters.

We are therefore led to introduce a new approach of calculating the linearized semiclassical survival probability starting from the Herman-Kluk (HK) propagator.

4.2. Quasiclassical Staying Probability Using the HK Propagator

Here we develop a consistent approach to the linearized survival (or staying) probability, using the HK propagator. We follow the path used by Cao and Voth as well as by Miller and his co-workers to derive the Wigner LSC-IVR i.e, making a sum and difference coordinate transformation of the integration variables. Let us consider an initial Gaussian wavefunction for f degrees of freedom, centered at $(\mathbf{p}_\alpha, \mathbf{q}_\alpha)$, given by

$$\Psi_\alpha(\mathbf{x}, 0) = \left(\frac{\det \boldsymbol{\gamma}}{\pi^f}\right)^{\frac{1}{4}} \exp\left\{-(\mathbf{x}-\mathbf{q}_\alpha)^{\mathrm{T}} \frac{\boldsymbol{\gamma}}{2}(\mathbf{x}-\mathbf{q}_\alpha) + \frac{\mathrm{i}}{\hbar}\mathbf{p}_\alpha^{\mathrm{T}}(\mathbf{x}-\mathbf{q}_\alpha)\right\}, \tag{4.42}$$

where we have defined (column) vectors and a matrix via

$$\mathbf{x} = \begin{pmatrix} x_1 \\ \cdot \\ \cdot \\ x_f \end{pmatrix} \qquad \boldsymbol{\gamma} = \begin{pmatrix} \gamma_1 & 0 & 0 & 0 \\ 0 & \ddots & 0 & 0 \\ 0 & 0 & \ddots & 0 \\ 0 & 0 & 0 & \gamma_f \end{pmatrix} \qquad \mathbf{q}_\alpha = \begin{pmatrix} q_{1\alpha} \\ \cdot \\ \cdot \\ q_{f\alpha} \end{pmatrix} \qquad \mathbf{p}_\alpha = \begin{pmatrix} p_{1\alpha} \\ \cdot \\ \cdot \\ p_{f\alpha} \end{pmatrix}.$$

Subscripts denote the f degrees of freedom. Later, subscript 1 denotes the Morse oscillator coordinate and the other subscript(s) correspond to the harmonic oscillator(s) acting as the bath for the system. We stress that the HK propagator to be used below is based on real classical trajectories and therefore can account for interference effects but for the inclusion of tunneling effects also non-classical trajectories would be needed.

The auto-correlation function is given by

$$c(t) = \langle \Psi_\alpha(0) | \Psi_\alpha(t) \rangle. \tag{4.43}$$

Using the HK propagator [37] to evolve the wavefunction in time, this is given by

$$c(t) = \int \frac{\mathrm{d}^f p \mathrm{d}^f q}{(2\pi\hbar)^f} \langle \Psi_\alpha(0) | \mathbf{z}(\mathbf{p}_t, \mathbf{q}_t) \rangle R(\mathbf{p}, \mathbf{q}, t)\, \mathrm{e}^{\frac{\mathrm{i}}{\hbar} S(\mathbf{p},\mathbf{q},t)} \langle \mathbf{z}(\mathbf{p}, \mathbf{q}) | \Psi_\alpha(0) \rangle, \tag{4.44}$$

with the classical trajectories $(\mathbf{p}_t, \mathbf{q}_t)$ and the classical action

$$S(\mathbf{p}, \mathbf{q}, t) = \int_0^t [\mathbf{p}_{t'} \cdot \dot{\mathbf{q}}_{t'} - H] \, \mathrm{d}t', \tag{4.45}$$

as well as the prefactor

$$R(\mathbf{p}, \mathbf{q}, t) = \frac{1}{2^{f/2}} \left(\det \left\{ \mathbf{m}_{11} + \boldsymbol{\gamma} \mathbf{m}_{22} \boldsymbol{\gamma}^{-1} - \mathrm{i}\hbar \boldsymbol{\gamma} \mathbf{m}_{21} - \frac{1}{\mathrm{i}\hbar} \mathbf{m}_{12} \boldsymbol{\gamma}^{-1} \right\} \right)^{\frac{1}{2}}, \tag{4.46}$$

where $\mathbf{m}_{11}, \mathbf{m}_{12}, \mathbf{m}_{21}$ and $\mathbf{m}_{22}$ are the elements of the so-called monodromy (or stability) matrix $\mathbf{M}$ [49],

$$\mathbf{M} = \begin{pmatrix} \mathbf{m}_{11} & \mathbf{m}_{12} \\ \mathbf{m}_{21} & \mathbf{m}_{22} \end{pmatrix} = \begin{pmatrix} \frac{\partial \tilde{\mathbf{p}}_t}{\partial \tilde{\mathbf{p}}^\intercal} & \frac{\partial \tilde{\mathbf{p}}_t}{\partial \tilde{\mathbf{q}}^\intercal} \\ \frac{\partial \tilde{\mathbf{q}}_t}{\partial \tilde{\mathbf{p}}^\intercal} & \frac{\partial \tilde{\mathbf{q}}_t}{\partial \tilde{\mathbf{q}}^\intercal} \end{pmatrix}. \tag{4.47}$$

explained in detail in Appendix D. The width parameter matrix of the coherent state $|\mathbf{z}(\mathbf{p}, \mathbf{q})\rangle$ is $\tilde{\boldsymbol{\gamma}}$, but here for simplicity we will consider the width parameters for the Gaussian initial state and the ones for the coherent state appearing in the HK propagator to be equal.

In the following, we look for a quantity with a classical analog, therefore we consider the "probability to stay"

$$P(t) = |\langle \Psi_\alpha(0) | \Psi_\alpha(t) \rangle|^2 = |c(t)|^2, \tag{4.48}$$

which is given as the double phase space integral

$$\begin{aligned} P(t) = \int \frac{\mathrm{d}^f p \mathrm{d}^f q}{(2\pi\hbar)^f} \int \frac{\mathrm{d}^f p' \mathrm{d}^f q'}{(2\pi\hbar)^f} & \langle \Psi_\alpha(0) | \mathbf{z}(\mathbf{p}_t, \mathbf{q}_t) \rangle R(\mathbf{p}, \mathbf{q}, t) \, \mathrm{e}^{\frac{\mathrm{i}}{\hbar} S(\mathbf{p}, \mathbf{q}, t)} \langle \mathbf{z}(\mathbf{p}, \mathbf{q}) | \Psi_\alpha(0) \rangle \\ & \langle \mathbf{z}(\mathbf{p}'_t, \mathbf{q}'_t) | \Psi_\alpha(0) \rangle R^*(\mathbf{p}', \mathbf{q}', t) \, \mathrm{e}^{-\frac{\mathrm{i}}{\hbar} S(\mathbf{p}', \mathbf{q}', t)} \langle \Psi_\alpha(0) | \mathbf{z}(\mathbf{p}', \mathbf{q}') \rangle, \end{aligned} \tag{4.49}$$

sometimes referred to as double HK expression. To make progress with the integration, we introduce the sum and difference variables

$$\tilde{\mathbf{q}} = \frac{\mathbf{q} + \mathbf{q}'}{2} \qquad \Delta\mathbf{q} = \mathbf{q} - \mathbf{q}' \tag{4.50}$$

$$\tilde{\mathbf{p}} = \frac{\mathbf{p} + \mathbf{p}'}{2} \qquad \Delta\mathbf{p} = \mathbf{p} - \mathbf{p}', \tag{4.51}$$

with the reverse transformation

$$\mathbf{q} = \tilde{\mathbf{q}} + \frac{\Delta\mathbf{q}}{2} \qquad \mathbf{q}' = \tilde{\mathbf{q}} - \frac{\Delta\mathbf{q}}{2} \tag{4.52}$$

$$\mathbf{p} = \tilde{\mathbf{p}} + \frac{\Delta\mathbf{p}}{2} \qquad \mathbf{p}' = \tilde{\mathbf{p}} - \frac{\Delta\mathbf{p}}{2}. \tag{4.53}$$

For 1 dimension, the Jacobians are:

$$J\left(q,q'\right)=\left|\frac{\partial(\tilde{q},\Delta q)}{\partial(q,q')}\right|=\begin{vmatrix}\frac{1}{2} & \frac{1}{2}\\ 1 & -1\end{vmatrix}=-1$$

$$J\left(p,p'\right)=\left|\frac{\partial(\tilde{p},\Delta p)}{\partial(p,p')}\right|=\begin{vmatrix}\frac{1}{2} & \frac{1}{2}\\ 1 & -1\end{vmatrix}=-1$$

Now, for 2 dimensions, the Jacobians look like this:

$$J\left(\mathbf{q},\mathbf{q}'\right)=\begin{vmatrix}\frac{\partial\tilde{\mathbf{q}}}{\partial\mathbf{q}^{\intercal}} & \frac{\partial\tilde{\mathbf{q}}}{\partial\mathbf{q}'^{\intercal}}\\ \frac{\partial\Delta\mathbf{q}}{\partial\mathbf{q}^{\intercal}} & \frac{\partial\Delta\mathbf{q}}{\partial\mathbf{q}'^{\intercal}}\end{vmatrix}=\begin{vmatrix}\frac{1}{2} & 0 & \frac{1}{2} & 0\\ 0 & \frac{1}{2} & 0 & \frac{1}{2}\\ 1 & 0 & -1 & 0\\ 0 & 1 & 0 & -1\end{vmatrix}=1$$

Similarly,

$$J\left(\mathbf{p},\mathbf{p}'\right)=\begin{vmatrix}\frac{\partial\tilde{\mathbf{p}}}{\partial\mathbf{p}^{\intercal}} & \frac{\partial\tilde{\mathbf{p}}}{\partial\mathbf{p}'^{\intercal}}\\ \frac{\partial\Delta\mathbf{p}}{\partial\mathbf{p}^{\intercal}} & \frac{\partial\Delta\mathbf{p}}{\partial\mathbf{p}'^{\intercal}}\end{vmatrix}=\begin{vmatrix}\frac{1}{2} & 0 & \frac{1}{2} & 0\\ 0 & \frac{1}{2} & 0 & \frac{1}{2}\\ 1 & 0 & -1 & 0\\ 0 & 1 & 0 & -1\end{vmatrix}=1$$

Again, for 3 dimensions, the Jacobians are:

$$J\left(\mathbf{q},\mathbf{q}'\right)=-1$$

$$J\left(\mathbf{p},\mathbf{p}'\right)=-1$$

So for an odd number of degrees of freedom, the Jacobians for positions as well as momenta are always -1 and for an even number they are $+1$, such that their product, appearing in the double phase space integral, is always unity, which means that for general f, the Jacobian for the variable transformation in the double phase space integral is always unity.

We now expand the trajectories around $\tilde{\mathbf{q}}_t\left(\tilde{\mathbf{p}},\tilde{\mathbf{q}}\right)$, $\tilde{\mathbf{p}}_t\left(\tilde{\mathbf{p}},\tilde{\mathbf{q}}\right)$ up to the first order. Using the reverse transformation in (4.52,4.53) this leads to

$$\mathbf{q}_t=\tilde{\mathbf{q}}_t+\frac{\partial\tilde{\mathbf{q}}_t}{\partial\tilde{\mathbf{q}}^{\intercal}}\left(\mathbf{q}-\tilde{\mathbf{q}}\right)+\frac{\partial\tilde{\mathbf{q}}_t}{\partial\tilde{\mathbf{p}}^{\intercal}}\left(\mathbf{p}-\tilde{\mathbf{p}}\right)=\tilde{\mathbf{q}}_t+\mathbf{m}_{22}\frac{\Delta\mathbf{q}}{2}+\mathbf{m}_{21}\frac{\Delta\mathbf{p}}{2}=\tilde{\mathbf{q}}_t+\frac{\delta\mathbf{q}_t}{2}, \tag{4.54}$$

$$\mathbf{q}'_t=\tilde{\mathbf{q}}_t+\frac{\partial\tilde{\mathbf{q}}_t}{\partial\tilde{\mathbf{q}}^{\intercal}}\left(\mathbf{q}'-\tilde{\mathbf{q}}\right)+\frac{\partial\tilde{\mathbf{q}}_t}{\partial\tilde{\mathbf{p}}^{\intercal}}\left(\mathbf{p}'-\tilde{\mathbf{p}}\right)=\tilde{\mathbf{q}}_t-\mathbf{m}_{22}\frac{\Delta\mathbf{q}}{2}-\mathbf{m}_{21}\frac{\Delta\mathbf{p}}{2}=\tilde{\mathbf{q}}_t-\frac{\delta\mathbf{q}_t}{2}, \tag{4.55}$$

$$\mathbf{p}_t=\tilde{\mathbf{p}}_t+\frac{\partial\tilde{\mathbf{p}}_t}{\partial\tilde{\mathbf{p}}^{\intercal}}\left(\mathbf{p}-\tilde{\mathbf{p}}\right)+\frac{\partial\tilde{\mathbf{p}}_t}{\partial\tilde{\mathbf{q}}^{\intercal}}\left(\mathbf{q}-\tilde{\mathbf{q}}\right)=\tilde{\mathbf{p}}_t+\mathbf{m}_{11}\frac{\Delta\mathbf{p}}{2}+\mathbf{m}_{12}\frac{\Delta\mathbf{q}}{2}=\tilde{\mathbf{p}}_t+\frac{\delta\mathbf{p}_t}{2}, \tag{4.56}$$

$$\mathbf{p}'_t=\tilde{\mathbf{p}}_t+\frac{\partial\tilde{\mathbf{p}}_t}{\partial\tilde{\mathbf{p}}^{\intercal}}\left(\mathbf{p}'-\tilde{\mathbf{p}}\right)+\frac{\partial\tilde{\mathbf{p}}_t}{\partial\tilde{\mathbf{q}}^{\intercal}}\left(\mathbf{q}'-\tilde{\mathbf{q}}\right)=\tilde{\mathbf{p}}_t-\mathbf{m}_{11}\frac{\Delta\mathbf{p}}{2}-\mathbf{m}_{12}\frac{\Delta\mathbf{q}}{2}=\tilde{\mathbf{p}}_t-\frac{\delta\mathbf{p}_t}{2}. \tag{4.57}$$

Then we expand the action up to the first order around $\tilde{S}$, as the second order difference vanishes. This yields

$$\begin{aligned} S\left(\mathbf{q}_t\left(\mathbf{p},\mathbf{q}\right),\mathbf{q}\right) &= \tilde{S}\left(\tilde{\mathbf{q}}_t\left(\tilde{\mathbf{p}},\tilde{\mathbf{q}}\right),\tilde{\mathbf{q}}\right) + \frac{\partial \tilde{S}}{\partial \tilde{\mathbf{p}}^{\intercal}}\left(\mathbf{p}-\tilde{\mathbf{p}}\right) + \frac{\partial \tilde{S}}{\partial \tilde{\mathbf{q}}^{\intercal}}\left(\mathbf{q}-\tilde{\mathbf{q}}\right) \\ &= \tilde{S} + \frac{\partial \tilde{S}}{\partial \tilde{\mathbf{p}}^{\intercal}}\frac{\Delta\mathbf{p}}{2} + \frac{\partial \tilde{S}}{\partial \tilde{\mathbf{q}}^{\intercal}}\frac{\Delta\mathbf{q}}{2} \end{aligned} \tag{4.58}$$

and an analogous formula for S' (which denotes the action depending on the primed variables). From classical mechanics we have

$$\frac{\partial \tilde{S}}{\partial \tilde{\mathbf{p}}^{\intercal}} = \frac{\partial \tilde{S}}{\partial \tilde{\mathbf{q}}_t^{\intercal}}\frac{\partial \tilde{\mathbf{q}}_t}{\partial \tilde{\mathbf{p}}^{\intercal}} = \tilde{\mathbf{p}}_t^{\intercal}\mathbf{m}_{21}, \tag{4.59}$$

$$\frac{\partial \tilde{S}}{\partial \tilde{\mathbf{q}}^{\intercal}} = \frac{\partial \tilde{S}}{\partial \tilde{\mathbf{q}}_t^{\intercal}}\frac{\partial \tilde{\mathbf{q}}_t}{\partial \tilde{\mathbf{q}}^{\intercal}} + \frac{\partial \tilde{S}}{\partial \tilde{\mathbf{q}}^{\intercal}} = \tilde{\mathbf{p}}_t^{\intercal}\mathbf{m}_{22} - \tilde{\mathbf{p}}^{\intercal} \tag{4.60}$$

for the first derivatives and therefore the action difference becomes

$$\begin{aligned} S - S' &= \tilde{S} + \tilde{\mathbf{p}}_t^{\intercal}\mathbf{m}_{21}\frac{\Delta\mathbf{p}}{2} + \tilde{\mathbf{p}}_t{}^{\intercal}\mathbf{m}_{22}\frac{\Delta\mathbf{q}}{2} - \tilde{\mathbf{p}}^{\intercal}\frac{\Delta\mathbf{q}}{2} \\ &\quad - \left(\tilde{S} - \tilde{\mathbf{p}}_t^{\intercal}\mathbf{m}_{21}\frac{\Delta\mathbf{p}}{2} - \tilde{\mathbf{p}}_t^{\intercal}\mathbf{m}_{22}\frac{\Delta\mathbf{q}}{2} + \tilde{\mathbf{p}}^{\intercal}\frac{\Delta\mathbf{q}}{2}\right) \\ &= \tilde{\mathbf{p}}_t^{\intercal}\mathbf{m}_{21}\Delta\mathbf{p} + \tilde{\mathbf{p}}_t^{\intercal}\mathbf{m}_{22}\Delta\mathbf{q} - \tilde{\mathbf{p}}^{\intercal}\Delta\mathbf{q} \\ &= \tilde{\mathbf{p}}_t^{\intercal}\delta\mathbf{q}_t - \tilde{\mathbf{p}}^{\intercal}\Delta\mathbf{q}. \end{aligned} \tag{4.61}$$

The prefactor in zeroth order is given by

$$\begin{aligned} R\left(\mathbf{p},\mathbf{q},t\right)R^*\left(\mathbf{p}',\mathbf{q}',t\right) &= \left|R\left(\tilde{\mathbf{p}},\tilde{\mathbf{q}},t\right)\right|^2 \\ &= \frac{1}{2^f}\Bigg(\det\left\{\mathbf{m}_{11} + \boldsymbol{\gamma}\mathbf{m}_{22}\boldsymbol{\gamma}^{-1} + \mathrm{i}\hbar\boldsymbol{\gamma}\mathbf{m}_{21} + \frac{1}{\mathrm{i}\hbar}\mathbf{m}_{12}\boldsymbol{\gamma}^{-1}\right\} \\ &\quad \det\left\{\mathbf{m}_{11} + \boldsymbol{\gamma}\mathbf{m}_{22}\boldsymbol{\gamma}^{-1} - \mathrm{i}\hbar\boldsymbol{\gamma}\mathbf{m}_{21} - \frac{1}{\mathrm{i}\hbar}\mathbf{m}_{12}\boldsymbol{\gamma}^{-1}\right\}\Bigg)^{\frac{1}{2}}. \end{aligned} \tag{4.62}$$

Collecting terms, the total expression for the staying probability is

$$P^{cl}\left(t\right) = \int\frac{\mathrm{d}^f\tilde{p}\mathrm{d}^f\tilde{q}}{\left(2\pi\hbar\right)^f}\int\frac{\mathrm{d}^f\Delta p\mathrm{d}^f\Delta q}{\left(2\pi\hbar\right)^f}\left|R\left(\tilde{\mathbf{p}},\tilde{\mathbf{q}},t\right)\right|^2\exp\left\{E\right\}, \tag{4.63}$$

where the exponent E has still to be defined. From

$$\begin{aligned}\langle z\left(\mathbf{p},\mathbf{q}\right)|\Psi_\alpha\rangle\langle\Psi_\alpha|z\left(\mathbf{p}',\mathbf{q}'\right)\rangle = \exp\Bigg(&-\frac{1}{4}\left[\left(\mathbf{q}-\mathbf{q}_\alpha\right)^\intercal\boldsymbol{\gamma}\left(\mathbf{q}-\mathbf{q}_\alpha\right)+\left(\mathbf{q}'-\mathbf{q}_\alpha\right)^\intercal\boldsymbol{\gamma}\left(\mathbf{q}'-\mathbf{q}_\alpha\right)\right]\\&-\frac{1}{4\hbar^2}\left[\left(\mathbf{p}-\mathbf{p}_\alpha\right)^\intercal\boldsymbol{\gamma}^{-1}\left(\mathbf{p}-\mathbf{p}_\alpha\right)+\left(\mathbf{p}'-\mathbf{p}_\alpha\right)^\intercal\boldsymbol{\gamma}^{-1}\left(\mathbf{p}'-\mathbf{p}_\alpha\right)\right]\\&+\frac{\mathrm{i}}{2\hbar}\left[\left(\mathbf{q}-\mathbf{q}_\alpha\right)^\intercal\left(\mathbf{p}+\mathbf{p}_\alpha\right)-\left(\mathbf{q}'-\mathbf{q}_\alpha\right)^\intercal\left(\mathbf{p}'+\mathbf{p}_\alpha\right)\right]\Bigg)\end{aligned} \tag{4.64}$$

using (4.52,4.53), we find the contributions

$$\left(\mathbf{q}-\mathbf{q}_\alpha\right)^\intercal\boldsymbol{\gamma}\left(\mathbf{q}-\mathbf{q}_\alpha\right)+\left(\mathbf{q}'-\mathbf{q}_\alpha\right)^\intercal\boldsymbol{\gamma}\left(\mathbf{q}'-\mathbf{q}_\alpha\right)=2\left(\tilde{\mathbf{q}}-\mathbf{q}_\alpha\right)^\intercal\boldsymbol{\gamma}\left(\tilde{\mathbf{q}}-\mathbf{q}_\alpha\right)+2\left(\frac{\Delta\mathbf{q}}{2}\right)^\intercal\boldsymbol{\gamma}\left(\frac{\Delta\mathbf{q}}{2}\right) \tag{4.65}$$

as well as

$$\begin{aligned}\left(\mathbf{p}-\mathbf{p}_\alpha\right)^\intercal\boldsymbol{\gamma}^{-1}\left(\mathbf{p}-\mathbf{p}_\alpha\right)+\left(\mathbf{p}'-\mathbf{p}_\alpha\right)^\intercal\boldsymbol{\gamma}^{-1}\left(\mathbf{p}'-\mathbf{p}_\alpha\right)&=2\left(\tilde{\mathbf{p}}-\mathbf{p}_\alpha\right)^\intercal\boldsymbol{\gamma}^{-1}\left(\tilde{\mathbf{p}}-\mathbf{p}_\alpha\right)\\&\quad+2\left(\frac{\Delta\mathbf{p}}{2}\right)^\intercal\boldsymbol{\gamma}^{-1}\left(\frac{\Delta\mathbf{p}}{2}\right)\end{aligned} \tag{4.66}$$

and

$$\left(\mathbf{q}-\mathbf{q}_\alpha\right)^\intercal\left(\mathbf{p}+\mathbf{p}_\alpha\right)-\left(\mathbf{q}'-\mathbf{q}_\alpha\right)^\intercal\left(\mathbf{p}'+\mathbf{p}_\alpha\right)=\Delta\mathbf{q}^\intercal\left(\tilde{\mathbf{p}}+\mathbf{p}_\alpha\right)+\left(\tilde{\mathbf{q}}-\mathbf{q}_\alpha\right)^\intercal\Delta\mathbf{p}. \tag{4.67}$$

The total exponent (including the action difference) thus is

$$\begin{aligned}E=&\frac{\mathrm{i}}{2\hbar}\left[\Delta\mathbf{q}^\intercal\left(\mathbf{p}_\alpha-\tilde{\mathbf{p}}\right)+\left(\tilde{\mathbf{q}}-\mathbf{q}_\alpha\right)^\intercal\Delta\mathbf{p}\right]-\frac{\mathrm{i}}{2\hbar}\left[\delta\mathbf{q}_t{}^\intercal\left(\mathbf{p}_\alpha-\tilde{\mathbf{p}}_t\right)+\left(\tilde{\mathbf{q}}_t-\mathbf{q}_\alpha\right)^\intercal\delta\mathbf{p}_t\right]\\&-\frac{1}{2}\left[\left(\tilde{\mathbf{q}}-\mathbf{q}_\alpha\right)^\intercal\boldsymbol{\gamma}\left(\tilde{\mathbf{q}}-\mathbf{q}_\alpha\right)+\left(\frac{\Delta\mathbf{q}}{2}\right)^\intercal\boldsymbol{\gamma}\left(\frac{\Delta\mathbf{q}}{2}\right)+\left(\tilde{\mathbf{q}}_t-\mathbf{q}_\alpha\right)^\intercal\boldsymbol{\gamma}\left(\tilde{\mathbf{q}}_t-\mathbf{q}_\alpha\right)+\left(\frac{\delta\mathbf{q}_t}{2}\right)^\intercal\boldsymbol{\gamma}\left(\frac{\delta\mathbf{q}_t}{2}\right)\right]\\&-\frac{1}{2\hbar^2}\Bigg(\left(\tilde{\mathbf{p}}-\mathbf{p}_\alpha\right)^\intercal\boldsymbol{\gamma}^{-1}\left(\tilde{\mathbf{p}}-\mathbf{p}_\alpha\right)+\left(\frac{\Delta\mathbf{p}}{2}\right)^\intercal\boldsymbol{\gamma}^{-1}\left(\frac{\Delta\mathbf{p}}{2}\right)\\&+\left(\tilde{\mathbf{p}}_t-\mathbf{p}_\alpha\right)^\intercal\boldsymbol{\gamma}^{-1}\left(\tilde{\mathbf{p}}_t-\mathbf{p}_\alpha\right)+\left(\frac{\delta\mathbf{p}_t}{2}\right)^\intercal\boldsymbol{\gamma}^{-1}\left(\frac{\delta\mathbf{p}_t}{2}\right)\Bigg).\end{aligned} \tag{4.68}$$

Remembering the defining equations of the stability matrix (see Appendix D)

$$\delta\mathbf{p}_t=\mathbf{m}_{11}\Delta\mathbf{p}+\mathbf{m}_{12}\Delta\mathbf{q}, \tag{4.69}$$

$$\delta\mathbf{q}_t=\mathbf{m}_{22}\Delta\mathbf{q}+\mathbf{m}_{21}\Delta\mathbf{p}, \tag{4.70}$$

we can now do the $\Delta\mathbf{p}$ and $\Delta\mathbf{q}$ integrations as they are simple Gaussian integrations. To this end,

we write the exponent in the form

$$E = -\left(\Delta\mathbf{q}^{\mathrm{T}}, \Delta\mathbf{p}^{\mathrm{T}}\right)\mathbf{A}\begin{pmatrix}\Delta\mathbf{q}\\ \Delta\mathbf{p}\end{pmatrix} + \mathbf{b}^{\mathrm{T}}\begin{pmatrix}\Delta\mathbf{q}\\ \Delta\mathbf{p}\end{pmatrix} + c, \tag{4.71}$$

where

$$\mathbf{A} = \begin{pmatrix} \frac{1}{2}\left(\frac{\boldsymbol{\gamma}}{4} + \frac{\mathbf{m}_{22}^{\mathrm{T}}\boldsymbol{\gamma}\mathbf{m}_{22}}{4}\right) + \frac{1}{2\hbar^2}\frac{\mathbf{m}_{12}^{\mathrm{T}}\boldsymbol{\gamma}^{-1}\mathbf{m}_{12}}{4} & \frac{1}{2}\frac{\mathbf{m}_{22}^{\mathrm{T}}\boldsymbol{\gamma}\mathbf{m}_{21}}{4} + \frac{1}{2\hbar^2}\frac{\mathbf{m}_{12}^{\mathrm{T}}\boldsymbol{\gamma}^{-1}\mathbf{m}_{11}}{4} \\ \frac{1}{2}\frac{\mathbf{m}_{21}^{\mathrm{T}}\boldsymbol{\gamma}\mathbf{m}_{22}}{4} + \frac{1}{2\hbar^2}\frac{\mathbf{m}_{11}^{\mathrm{T}}\boldsymbol{\gamma}^{-1}\mathbf{m}_{12}}{4} & \frac{1}{2\hbar^2}\left(\frac{\boldsymbol{\gamma}^{-1}}{4} + \frac{\mathbf{m}_{11}^{\mathrm{T}}\boldsymbol{\gamma}^{-1}\mathbf{m}_{11}}{4}\right) + \frac{1}{2}\frac{\mathbf{m}_{21}^{\mathrm{T}}\boldsymbol{\gamma}\mathbf{m}_{21}}{4} \end{pmatrix} \tag{4.72}$$

is a $2f \times 2f$ matrix and

$$\mathbf{b} = -\frac{\mathrm{i}}{2\hbar}\begin{pmatrix} (\tilde{\mathbf{p}} - \mathbf{p}_\alpha) - \mathbf{m}_{22}^{\mathrm{T}}(\tilde{\mathbf{p}}_t - \mathbf{p}_\alpha) + \mathbf{m}_{12}^{\mathrm{T}}(\tilde{\mathbf{q}}_t - \mathbf{q}_\alpha) \\ -(\tilde{\mathbf{q}} - \mathbf{q}_\alpha) - \mathbf{m}_{21}^{\mathrm{T}}(\tilde{\mathbf{p}}_t - \mathbf{p}_\alpha) + \mathbf{m}_{11}^{\mathrm{T}}(\tilde{\mathbf{q}}_t - \mathbf{q}_\alpha) \end{pmatrix} \tag{4.73}$$

is a $2f$ element column vector, whereas

$$\begin{aligned} c = &-\frac{1}{2}\left[(\tilde{\mathbf{q}} - \mathbf{q}_\alpha)^{\mathrm{T}}\boldsymbol{\gamma}(\tilde{\mathbf{q}} - \mathbf{q}_\alpha) + (\tilde{\mathbf{q}}_t - \mathbf{q}_\alpha)^{\mathrm{T}}\boldsymbol{\gamma}(\tilde{\mathbf{q}}_t - \mathbf{q}_\alpha)\right] \\ &-\frac{1}{2\hbar^2}\left[(\tilde{\mathbf{p}} - \mathbf{p}_\alpha)^{\mathrm{T}}\boldsymbol{\gamma}^{-1}(\tilde{\mathbf{p}} - \mathbf{p}_\alpha) + (\tilde{\mathbf{p}}_t - \mathbf{p}_\alpha)^{\mathrm{T}}\boldsymbol{\gamma}^{-1}(\tilde{\mathbf{p}}_t - \mathbf{p}_\alpha)\right] \end{aligned} \tag{4.74}$$

is a constant term. Hence the Gaussian integration gives

$$\int \frac{\mathrm{d}^f\Delta p\mathrm{d}^f\Delta q}{(2\pi\hbar)^f}\exp\{E\} = \frac{1}{(2\pi\hbar)^f}\sqrt{\frac{\pi^{2f}}{\det\mathbf{A}}}\exp\left\{\frac{\mathbf{b}^{\mathrm{T}}\mathbf{A}^{-1}\mathbf{b}}{4} + c\right\}. \tag{4.75}$$

The exact analytic calculation of $\det\mathbf{A}$ using the method of factorization, as shown in the Appendix F.1, following the lines of Herman's 1986 paper [172], finally gives

$$\begin{aligned} \det\mathbf{A} = &\left(\frac{1}{8\hbar}\right)^{2f}\det\left\{\mathbf{m}_{11} + \boldsymbol{\gamma}\mathbf{m}_{22}\boldsymbol{\gamma}^{-1} + \mathrm{i}\hbar\boldsymbol{\gamma}\mathbf{m}_{21} + \frac{1}{\mathrm{i}\hbar}\mathbf{m}_{12}\boldsymbol{\gamma}^{-1}\right\} \\ &\det\left\{\mathbf{m}_{11} + \boldsymbol{\gamma}\mathbf{m}_{22}\boldsymbol{\gamma}^{-1} - \mathrm{i}\hbar\boldsymbol{\gamma}\mathbf{m}_{21} - \frac{1}{\mathrm{i}\hbar}\mathbf{m}_{12}\boldsymbol{\gamma}^{-1}\right\}. \end{aligned} \tag{4.76}$$

This cancels the HK-prefactor absolute square.

$$|R(\tilde{\mathbf{p}}, \tilde{\mathbf{q}}, t)|^2\frac{1}{(2\pi\hbar)^f}\sqrt{\frac{\pi^{2f}}{\det\mathbf{A}}} = 2^f. \tag{4.77}$$

Therefore, the remaining integral over $\tilde{\mathbf{p}}$ and $\tilde{\mathbf{q}}$ is:

$$P^{cl}(t) = C_{AB}^{H}(t) = 2^f\int\frac{\mathrm{d}^f\tilde{p}\mathrm{d}^f\tilde{q}}{(2\pi\hbar)^f}\exp\left\{\frac{\mathbf{b}^{\mathrm{T}}\mathbf{A}^{-1}\mathbf{b}}{4} + c\right\}. \tag{4.78}$$

Before evaluating this expression numerically some remarks are in order:

- The result is a linearized semiclassical result and we therefore can call it an LSC-IVR result.
- Because it is based on Gaussian basis functions it is the correct Husimi version in the case of the survival (or staying) probability, $\hat{A} = \hat{B} = |\Psi_\alpha\rangle\langle\Psi_\alpha|$.
- In contrast to a straightforward application of (4.41), in addition to the Husimi exponent c, there is a term $\frac{\mathbf{b}^\intercal \mathbf{A}^{-1}\mathbf{b}}{4}$ in the exponent that contains stability information, similar in spirit to the semiclassical hybrid dynamics, where part of the degrees of freedom are treated using the thawed Gaussian approximation [67].
- Furthermore also an overall factor of 2^f appears naturally, ensuring normalization at the initial time $t = 0$.

4.3. Numerical Results

For the following numerical investigations, we again consider a Morse oscillator as our system of interest. The potential is given by Eq. (3.2) of section 3.1.1, the mass of the system is chosen to be unity. The values of the dimensionless potential parameters that we use here are again: $D = 150$ and $\alpha = 0.288$, leading to $\omega = 4.988$ for the frequency of (harmonic) oscillations around the minimum. We choose the value for the phase-space center of the Gaussian wavefunction $|\Psi_\alpha\rangle$ to be $q_\alpha = 3.5$ and $p_\alpha = 0$ and we take the width parameter of the Gaussian as $\gamma = 4$.

We note that Hamilton's equations are solved with the classical Hamiltonian in all cases. Using instead the Hamiltonian matrix element between coherent states that is sometimes used for the Husimi case would lead to almost identical results for the potential parameters considered here. The phase space coordinates, as well as the stability matrix elements are then determined numerically by using a symplectic leap frog method [49].

The quantity of interest in the following is the survival probability $P(t)$ that will be followed up to the first full revival time, $T_{\text{rev}} = 2\pi/\alpha^2$ which, in the present case, is around 60 times the classical period of the Morse oscillator, given by $T_{\text{cl}} = 2\pi/\omega = 2\pi/(\sqrt{2D}\alpha) \approx 2\pi/5$.

The number of trajectories used for the full HK as well as for the LSC-IVR results was 10^4. The time step chosen in all dynamical calculations was $\Delta t = 2\pi/(100 \times \omega) = T_{\text{cl}}/100$.

4.3.1. Uncoupled Case

In Figure 4.1, we compare the full numerical solution to the time-dependent Schrödinger equation (TDSE) with the corresponding semiclassical HK result. Analogously to Fig. 3.3, where the absolute value squared is plotted, it can be seen that the two results coincide very nicely, although the HK result due to the loss of norm is not coming back to unity fully at the revival time, which is around $t = 75$. The fact that the semiclassical HK propagator can reproduce the interference based revival in a Morse oscillator has been investigated in detail by Wang and Heller [99].

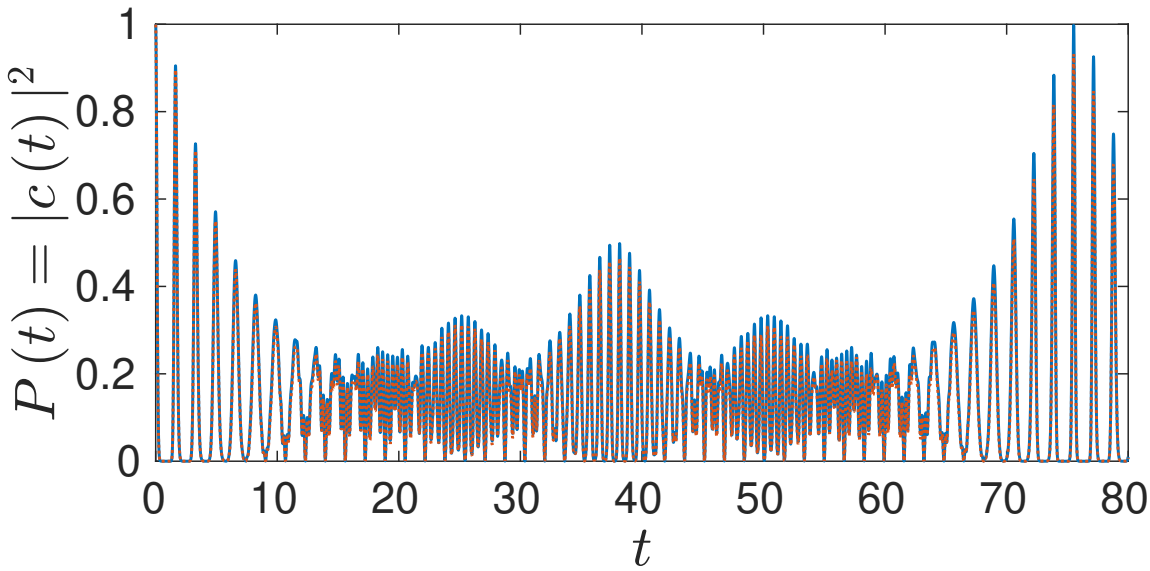

Figure 4.1.: Survival probability for the 1D Morse oscillator up to first full revival time using a split-operator method with fast Fourier transform (FFT) to solve the time-dependent Schrödinger equation (TDSE) (full blue line) and full Herman-Kluk (HK) result (dashed red line).

In Figure 4.2, we now compare several LSC-IVR results. The Wigner and Husimi results differ as well as does the Husimi without the additional exponential term. For short times all three results are identical. For times when all three results have decayed to small values, differences become visible. The new Husimi and the Wigner result are very close, though. The revival visible in the full quantum result is not displayed in any of the linearized approaches, though.

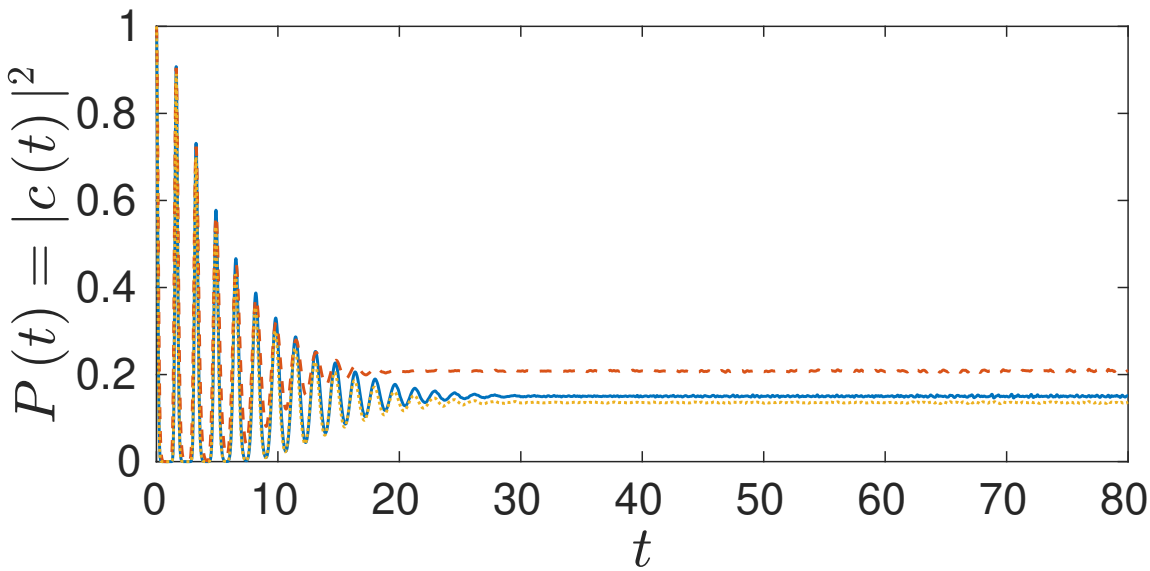

Figure 4.2.: Survival probability for the 1D Morse oscillator using Wigner (full blue curve) and Husimi linearized semiclassical initial value representation (LSC-IVR) (dotted yellow curve) as well as Husimi version without the term $\frac{\mathbf{b}^\intercal \mathbf{A}^{-1}\mathbf{b}}{4}$ but with an additional factor of two (dashed orange curve).

4.3.2. Coupling to a Harmonic Bath Degree of Freedom

Now we proceed and ask the question what happens to the revival dynamics, if we couple the Morse oscillator to a very heavy harmonic oscillator of mass $m_y = 20$ such that the total Hamiltonian reads

$$H = \frac{p_x^2}{2} + \frac{p_y^2}{2m_y} + V_M(x) + \frac{1}{2}m_y\omega_y^2 y^2 + \lambda xy, \tag{4.79}$$

with $\omega_y = 1.17$ and the initial width parameter for the ground state wavepacket in the harmonic degree $\gamma_y = m_y\omega_y$. The very heavy oscillator shall mimic the interaction with a many degree of freedom bath with smaller masses, i.e., a "condensed phase" environment, see also [47].

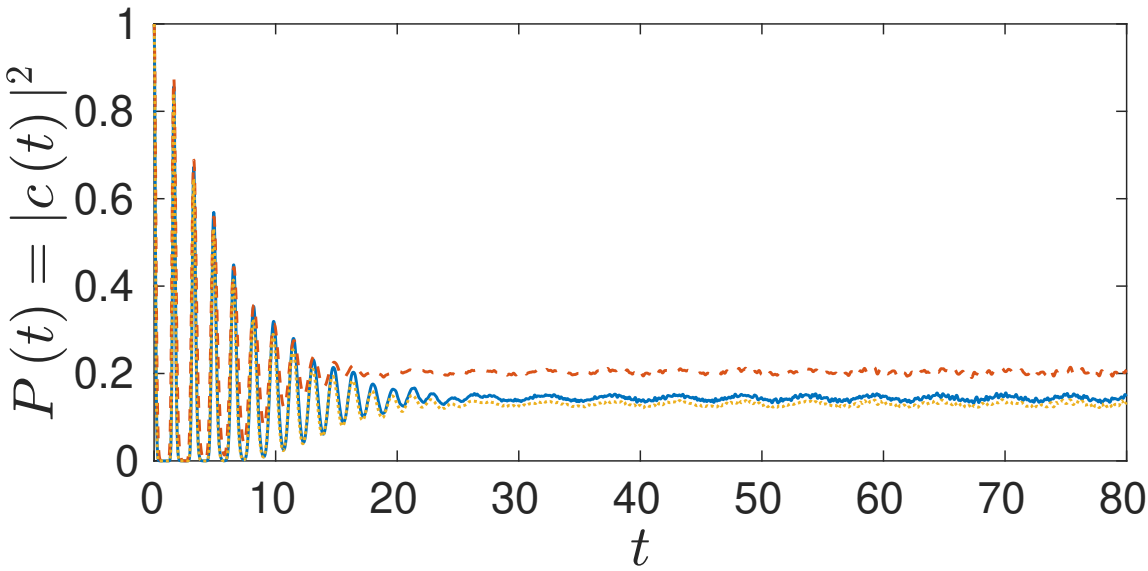

Figure 4.3.: Survival probability for the Morse oscillator coupled to a harmonic degree of freedom with coupling strength $\lambda = 1$, up to first full revival time (in the uncoupled case) using Wigner (full blue line) and Husimi LSC-IVR (dotted yellow curve) as well as Husimi version without the term $\frac{\mathbf{b}^\intercal\mathbf{A}^{-1}\mathbf{b}}{4}$ (dashed orange curve).

First, we look at a moderate coupling strength of $\lambda = 1$. The corresponding results from the Wigner and the Husimi approach as well as the Husimi without the $\frac{\mathbf{b}^\intercal\mathbf{A}^{-1}\mathbf{b}}{4}$ term in the exponent are contrasted in Figure 4.3. It can be seen that the additional term brings the Husimi result closer to the Wigner one, rather similar to the uncoupled case. At longer times there is just a small amplitude wiggling in the signal due to the coupling.

In Figure 4.4, we turn to a higher coupling strength of $\lambda = 9$ and first compare the full solution to the TDSE with the corresponding semiclassical HK result. It can be seen that, as in the uncoupled case, the two results again coincide very nicely, even the small oscillations are reproduced until around $t = 75$. The revival is not visible any more, due to the strong coupling to the harmonic degree, however.

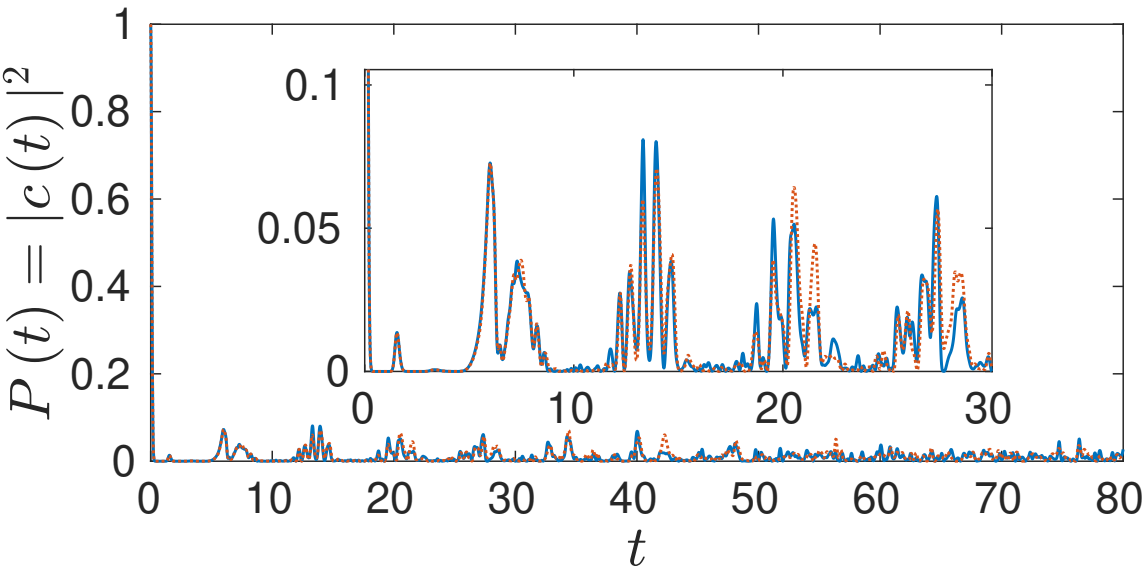

Figure 4.4.: Survival probability for the Morse oscillator coupled to a harmonic degree of freedom with coupling strength $\lambda = 9$, up to first full revival time (in the uncoupled case) using split operator FFT to solve the TDSE (full blue line) and full HK result (dashed red line).

In Figure 4.5, the results from the LSC-IVR calculations (Wigner as well as Husimi) in the strong coupling case are displayed. It can be seen that both also show no revivals, as to be expected. For the very strong coupling the underlying classical dynamics becomes strongly chaotic and the numerical inversion of the **A** matrix turns singular at certain times for a lot of the 10000 trajectories we propagated. In order to circumvent this singularity problem, we treated the problematic trajectories without the additional term in the exponent from the time on, when the inversion is problematic.

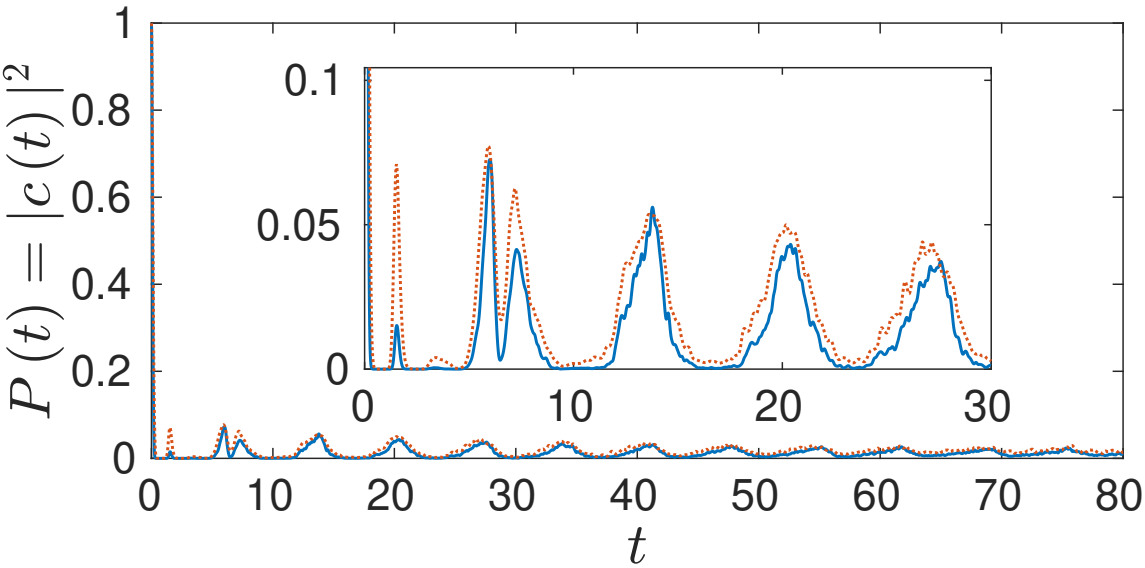

Figure 4.5.: Survival probability for the Morse oscillator coupled to a harmonic degree of freedom with $\lambda = 9$, up to first full revival time (in the uncoupled case) using Wigner LSC-IVR (full blue line) and Husimi LSC-IVR (dotted red line).

5. Thermalization

With the methodological experience laid out in Chapters 3 and 4, we are now able to tackle the problem which is at the heart of this thesis. This is the puzzle of energy exchange between subsystems. Ever since the pioneering works of Fermi, Pasta, Ulam and Tsingou (FPUT) [6], the puzzle of energy exchange between subsystems, eventually leading to equilibration and thermalization in closed systems with a finite number of degrees of freedom has intrigued researchers in the fields of classical [7–15], as well as semiclassical [17, 18] and quantum mechanics [2, 7, 19–27].

In classical systems the prerequisite for thermalization seems to be the (hard) chaoticity of the underlying dynamics [8, 9]; this fact being one possible reason that by investigating a weakly anharmonic system, FPUT did not succeed in finding thermalization but were surprised by a dynamics that showed pronounced revivals [173]. For dynamical chaos to appear, the phase space has to be at least three dimensional. The question therefore arises if it is enough to increase the interaction strength between the different degrees of freedom in order to fully develop chaos, or if, in addition, the number of those degrees of freedom has to be increased (possibly all the way to the thermodynamic limit) in order to observe thermalization. In two more recent contributions from the realm of classical mechanics it has been shown by solving Newton's equations for coupled harmonic oscillator systems, comprising a few hundreds [11] up to a few thousand degrees of freedom [14] that, for a suitably chosen initial configuration, a (large enough) subsystem may indeed reach thermal equilibrium, without coupling to an (external) thermostat and even without nonlinear interactions (i. e. without chaos). In the light of these results, another possible reason that FPUT saw no signs of thermalization is the closeness of their model to the noninteracting case [14].

Although semiclassical approaches may be helpful to tackle such problems [143], this large number of degrees of freedom seems elusive if one is interested in a full quantum description of the process. From this perspective it comes as a relief that also small numbers of degrees of freedom (below ten) can lead to thermalization in long-time dynamics of quantum systems, as shown long ago for spin systems [19] and discussed more recently in the seminal book by Gemmer, Michel and Mahler [2] and the article by Reimann [23]. For a more recent reference on spin systems realized in graphene quantum dots, see [174] and for energy exchange in quantum systems with continuous degrees of freedom, see [21]. There it is claimed that as little as ten to twenty harmonic degrees of freedom are necessary to observe energy loss to the bath without backflow on the observed time scales. In addition, in [20], the thermalization of eight valence electrons inside a small sodium cluster has been investigated quantum mechnically. Furthermore, whereas in [19] it was argued that both integrable as well nonintegrable systems exhibit statistical behavior for long times, in [22] it was pointed out that, in a Bose-Hubbard dynamics, thermalization is only observed if the system starts from a chaotic region of phase space

but not if the system is launched from a quasi-integrable region.

In the present chapter, we will investigate the toppling pencil model, studied recently by Dittrich and Pena Martínez (DPM) [15]. In their classical mechanics study, they focused on a particle on top of the barrier in a quartic double well that is coupled to a small (from just one single up to the order of ten and higher) number of harmonic oscillators. It is well known that the transition from integrable to chaotic motion sets in first around the separatrix of the double well's phase space, when the interaction strength with an external sinusoidal field is tuned higher [175]. In the light of the findings in [22], this makes an initial condition starting on top of the double well's barrier an ideal candidate to search for (quick [23]) thermalization under the interaction with a relatively small number of harmonic degrees of freedom, although the interaction with a sinusoidal field is a crude approximation to the interaction with harmonic degrees of freedom, whose dynamics is influenced by "back action" of the system.

In contrast to DPM, in the following, we will investigate the system dynamics fully quantum mechanically, making use of the method of coupled coherent states, introduced by Shalashilin and Child [33]. By being based on an expansion of the total wavefunction in terms of coherent states (Gaussians), whose initial positions in phase space are chosen randomly, the exponential wall that one usually experiences in grid based approaches to the quantum dynamics can be overcome or at least be pushed to rather larger numbers of degrees of freedom. For a recent review of the CCS and related methods, we refer to [34]. The main focus of the present work is on the question of how many bath degrees will be needed to ensure thermalization and how strong the interaction has to be and how the speed of thermalization depends on the coupling and/or the number of degrees of freedom. The toppling pencil model setup seems to be ideally suited to answer all those questions. Earlier the phenomenon of tunneling was investigated for a symmetric double-well potential perturbed by a monochromatic driving force using the Floquet formalism and the concept of quasienergies [176]. In contrast to [176], we investigate here thermalization for the symmetric quartic double-well potential.

5.1. Quartic Double Well coupled to a Finite Heat Bath

Our model system of interest is a double well, which is bilinearly coupled to a finite number f of harmonic oscillators [15]. A quartic double-well is a bistable system with two symmetry related minima. It has many physical realizations, one of the most prominent of which is the ammonia molecule, first discussed in the quantum (tunneling) context by Hund as early as 1927 [177]. A solid state realization of a non quartic but symmetric double-well potential is given by a suitably parametrized rf-SQUID, where the role of the coordinate is played by the flux through the ring [178]. More recently bistable potentials have been discussed in cold atom physics in connection with Bose-Einstein condensation [179]. In the following, we first discuss the bare quartic bistable system before coupling it to a finite heat bath.

5.1.1. Quartic Double Well

The potential of a symmetric quartic oscillator double well with a parabolic barrier around its relative maximum can be written as

$$V_S(x) = -\frac{a}{2}x^2 + \frac{b}{4}x^4, \qquad a, b \in \mathbb{R}^+. \tag{5.1}$$

It has quadratic minima at $x_\pm = \pm\sqrt{\frac{a}{b}}$ and a quadratic maximum at $x_0 = 0$ of relative height $E_B = \frac{a^2}{4b}$. The Hamiltonian of the quartic double well is then given by

$$H_S(p_x, x) = \frac{p_x^2}{2m_x} + V_S(x). \tag{5.2}$$

Its classical dynamics consists of harmonic oscillations with the frequency $\omega = \sqrt{\frac{2a}{m_x}}$ close to the minima at $x_\pm$. These oscillations become increasingly anharmonic as the energy rises towards the top of the barrier. The phase space portrait of the dynamics contains the prototypical separatrix, shaped like the number eight, as well as a hyperbolic fixed point at $p_x = 0, x = 0$ on that separatrix and two elliptic fixed points at $p_x = 0, x = x_\pm$ [180]. If the available energy is higher than the barrier, in the case of the NH_3 molecule, the corresponding motion is referred to as umbrella motion.

For an understanding of the corresponding quantum dynamics, we first calculate the energy spectrum of the quartic double well potential, using a finite difference representation of the Laplacian to solve the TISE

$$\hat{H}_S\phi_n(x) \equiv \left[-\frac{\hbar^2}{2m_x}\Delta + V_S(x)\right]\phi_n(x) = E_n\phi_n(x). \tag{5.3}$$

The first few eigenvalues for the parameters $m_x = 1$ and $a = 2, b = 1$ and in units, where $\hbar = 1$ are gathered in Table 5.1. In the numerical work to be shown later, we will use a Gaussian of the form

$$\Psi(x, 0) = \left(\frac{\gamma_x}{\pi}\right)^{1/4} \mathrm{e}^{-\frac{\gamma_x}{2}x^2} \tag{5.4}$$

that is located at the top of the barrier as the initial state. Together with the potential and its first eigenstate it is shown in Figure 5.1. The base lines for the two wavefunctions are at their corresponding energy expectation values, which in the case of the Gaussian is $E_G = \gamma_x/4 - 1/(2\gamma_x) + 3/(16\gamma_x^2)$, leading to $E_G = 0.3$ for a width parameter of $\gamma_x = 2$. Although both, initial position as well as momentum

	$n = 1$	$n = 2$	$n = 3$	$n = 4$	$n = 5$
E_n	-0.300	0.046	1.23	2.46	3.94
$\lvert c_n\rvert^2$	0.654	0	0.323	0	0.0225

Table 5.1.: Eigenvalues E_n and squared overlap $|c_n|^2 := |\langle\phi_n|\Psi(0)\rangle|^2$ of eigenstates with the initial Gaussian of Eq. (5.4) for $\gamma_x = 2$ of the bare quartic double well with $a = 2$, $b = 1$. The grid extension for the finite difference calculation was $x \in [-4, 4]$ and 256 grid points were sufficient to achieve convergence to within the number of digits given.

expectations are zero, due to its finite width, there is a finite energy content in the wavepacket. This initial state is the motivation for the naming "toppling pencil"; a pencil balanced tip down on a flat surface, prone to fall over [15].

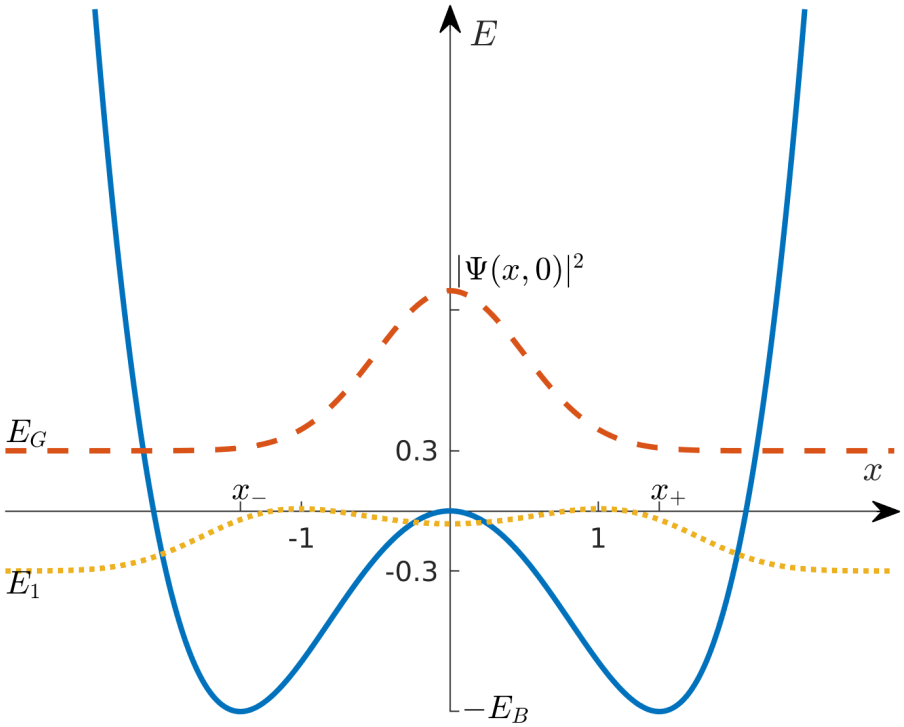

Figure 5.1.: Quartic double well potential with parameters $a = 2$, $b = 1$ (solid blue line), leading to minima at $x_\pm = \pm\sqrt{2}$. Absolute value squared of the initial Gaussian sitting at the top of the barrier with initial energy $E_G = 0.3$ (dashed red line) and absolute value squared of the ground state wavefunction of the quartic double well with ground state energy $E_1 = -0.30$ (dotted yellow line) are overlaid.

For symmetry reasons, it is obvious that the symmetric initial Gaussian does have zero overlap with the eigenfunctions of odd parity (see Table 5.1). Like the odd ones, also almost all higher even eigenstates (from the fifth eigenstate on) are not taking part in the dynamics. The dynamics of the Gaussian in the bare potential will then be an oscillation with the frequency corresponding to the difference of the first and the third eigenvalue see above. We stress that this is not the usual tunneling scenario, where a Gaussian is sitting in one of the two wells initially and is then moving to the other well and back with a (usually very small) frequency given by the difference $E_2 - E_1$ of the two lowest eigenvalues. Here we focus on the symmetric initial condition, however, and have chosen the potential parameters such that just the eigenstates with eigenvalues E_1 and E_3 are appreciably populated.

5.1.2. Coupling to a Finite Heat Bath

Coupling a double well to a harmonic oscillator heat bath with infinitely many degrees of freedom with continuous spectral density will lead to decoherence and dissipation in the dynamics. In the case that only the two lowest states of the bistable system play a role, the tunneling rate will be severely influenced by the system bath coupling [181]. A lot of work has been done on that so-called spin-boson model in the 80s of the last century, as documented by the impressive review by Leggett et al [182]. More recently, this model has been studied deeply by different numerical methods, with a focus on correctly mimicking infinite baths by either a discretization in frequency of the harmonic oscillator spectral density or by a correct description of the bath correlation function in the time domain [144]. Furthermore, also the influence of a sinusoidal driving on the tunneling effect in a two-level system has been studied, yielding surprising localization effects [183, 184].

Here we are not restricting ourselves to the spin-boson case but will consider the total Hamiltonian to be that of the full bistable system coupled to an environment with a large but finite number of degrees of freedom, given by

$$H(\mathbf{R},\mathbf{r}) = H_S(\mathbf{R}) + H_E(\mathbf{r}) + H_{SE}(\mathbf{R},\mathbf{r}) \tag{5.5}$$

where $\mathbf{R} = (p_x, x)$ denotes the phase-space vector of the central system of interest, whereas $\mathbf{r} = (p_1, p_2, ..., p_f, y_1, y_2, ..., y_f)$ denotes the $2f$-dimensional phase space vector of all the environmental degrees of freedom. The dynamics of the bare central system of interest (index S) is governed by the Hamiltonian of the quartic double well given in Eq. (5.2). The environment (index E) consists of f harmonic oscillators, whose Hamiltonian is given by

$$H_E(\mathbf{r}) = \sum_{n=1}^{f} \left(\frac{p_n^2}{2m} + \frac{m\omega_n^2}{2} y_n^2 \right). \tag{5.6}$$

The choice of a discrete set of frequencies ω_n, $n = 1, ..., f$ will be discussed below in the numerical results section. As each oscillator should exert a force on the system, hence their interaction can be modeled as the position-position coupling

$$H_{SE}(\mathbf{R},\mathbf{r}) = -x \sum_{n=1}^{f} g_n y_n \tag{5.7}$$

with coupling constant $g_n = \frac{g}{\sqrt{f}}$, which is renormalized by $\sqrt{f}$ in order to make the results for different number of oscillators comparable. Using linear response theory, this scaling has been derived in [12].

The bilinear coupling does not break the invariance of the total Hamiltonian under a parity transformation (spatial reflection) $P : (\mathbf{R},\mathbf{r}) \to (-\mathbf{R},-\mathbf{r})$. However, it drives the two bistable minima apart from $x_\pm = \pm\sqrt{\frac{a}{b}}$ to $x_\pm = \pm\sqrt{\frac{1}{b}(a + \sum_{n=1}^{f} \frac{g_n^2}{m\omega_n^2})}$, an effect which is not intended by the coupling to the environment [15, 185], see Fig 5.2a for a quartic double well coupled to a single harmonic (bath) degree of freedom. This driving apart can, however, be compensated by including the so-called

counter term proportional to the square of the system coordinate in the potential of the total Hamiltonian (system plus bath) to complete the squares with respect to the dependence on the oscillator coordinates, which is shown below in Fig 5.2b for a single environmental (bath) oscillator. One thus replaces the total potential by [15, 185, 186]

$$\begin{aligned} V_S + V_E + H_{SE} + V_C &= V_S(x) + \sum_{n=1}^{f} \frac{m\omega_n^2}{2} y_n^2 - x \sum_{n=1}^{f} g_n y_n + x^2 \sum_{n=1}^{f} \frac{g_n^2}{2m\omega_n^2} \\ &= V_S(x) + \sum_{n=1}^{f} \frac{m\omega_n^2}{2} \left(y_n - \frac{g_n}{m\omega_n^2} x \right)^2 . \end{aligned} \tag{5.8}$$

The counter term

$$V_C = x^2 \sum_{n=1}^{f} \frac{g_n^2}{2m\omega_n^2} \tag{5.9}$$

now renormalizes the factor a in front of the quadratic term in the system coordinate according to $a \to a - \sum_{n=1}^{f} \frac{g_n^2}{m\omega_n^2}$ [187], thus exactly undoing the renormalization (shift of the minima) mentioned above and the minima are at their uncoupled positions, see also Fig. 2 of [15]. In the section on the numerical results, we will display the time evolution of the counter term V_C. Even more importantly, we will start the bath in its ground state (in the thermodynamic limit $f \to \infty$ this would correspond to zero temperature) and will focus on the evolution of the system dynamics away from the excited state on top of the barrier. To this end we will need a numerical method that allows us to treat a multitude of degrees of freedom quantum mechanically. The method of our choice is the CCS method that was reviewed in section 2.1.2.

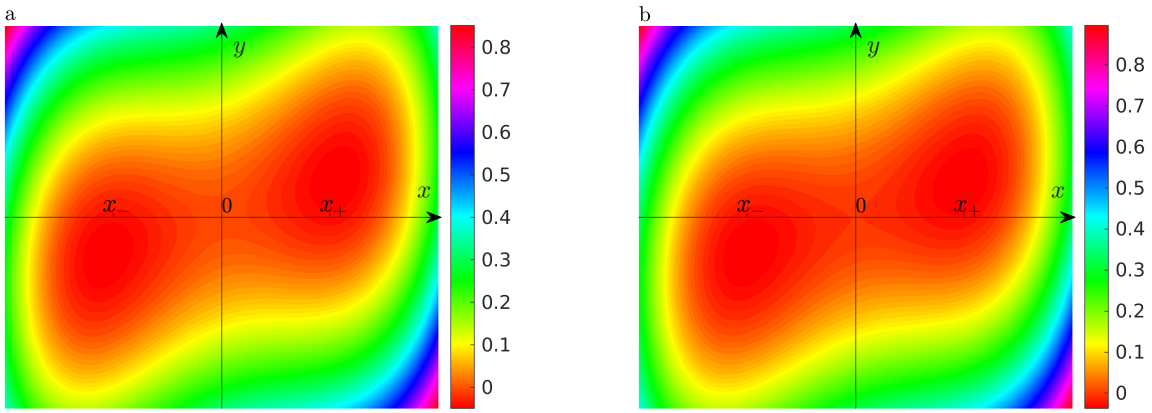

Figure 5.2.: Contour plots of the potential (5.8) for a single bath degree of freedom with phase-space coordinates (y, p_y). Quartic double well potential parameters $a = b = 0.15$; harmonic oscillator parameters $m = 1, \omega = 0.4$ and coupling $g = 0.06$. Panel (a) includes the bilinear coupling term but excluding the counter term (5.9); whereas panel (b) includes both coupling and the counter term.

5.2. Long-time dynamics of the coupled system

In the following, we will present numerical results for the time-evolution of the composite system using the CCS method to solve the time-dependent Schrödinger equation. In addition, for up to a total of 4 degrees of freedom, i.e., $f = 3$, we also corroborated our results by using the split-operator FFT technique for quantum propagation [50][1]. Our focus will be on the question if the coupling to the environmental degrees of freedom, which are all starting in their ground states

$$\Psi(y_n, 0) = \left(\frac{\gamma_n}{\pi}\right)^{1/4} \exp\left\{-\frac{\gamma_n}{2} y_n^2\right\}, \tag{5.10}$$

will eventually lead to a "thermalization" of the quartic degree towards its ground state (which is depicted in Fig. 5.1 as the dotted yellow line). We stress that previous treatements of the double well dynamics using CCS [188] have focussed on the description of quantum tunneling, where the initial state is made up of an equal weight superposition of the two lowest energy eigenstates, whereas herein, the initial states consists mostly of state one and state three (see Table 5.1).

In the following, the potential parameters for the double well are $a = 2$ and $b = 1$ and the mass m_x is set equal to unity. The choice of frequencies of the environmental degrees of freedom will be detailed below. All masses of the oscillators are taken to be equal and given by $m = 0.1$.

In order to make use of the CCS method to solve quantum dynamics of this composite system of $(f + 1)$ degrees of freedom as in the previous section 5.1, we represent the $(f + 1)$-mode CS by a $(f + 1)$-fold tensor product given as

$$|\boldsymbol{z}_l\rangle = \bigotimes_{j=0}^{f} |z_{lj}\rangle \tag{5.11}$$

of normalized one-dimensional CS $|z_{lj}\rangle$. Here the zeroth degree of freedom denotes the system of interest, which in the present case is the double well with phase-space coordinates (x, p_x), whereas the remaining 1 to f represents the bath degrees of freedom. The Appendix G contains details of the implementation of the CCS method, including a derivation for the normally ordered Hamiltonian of the composite system along with the classical equations of motion.

[1] We note that the number of grid points in the x direction needed for convergence was just 32 (for the grid extension $x \in [-4, 4]$) and thus much less than in the finite difference approach in 5.1.1. Furthermore, the number of grid points we took for the harmonic degrees varied between 128 for the low frequency oscillators and 64 for the high frequency ones. The time-step for propagation was $\Delta t = 0.01$.

5.2.1. Different numerical measures

As a first measure of the possible deviation of the time-evolved wavefunction away from the initial state, we use the autocorrelation function, defined in 1D as

$$\begin{aligned} c(t) = \langle \Psi^{\mathrm{M}}_{\mathrm{CS}}(0)|\Psi^{\mathrm{M}}_{\mathrm{CS}}(t)\rangle &= \sum_{l=1}^{M} a_l(t)\langle \Psi^{\mathrm{M}}_{\mathrm{CS}}(0)|z_l(t)\rangle \\ &= \sum_{k,l} a_k^*(0)\langle z_k(0)|z_l(t)\rangle a_l(t). \end{aligned} \tag{5.12}$$

For a multitude of degrees of freedom, an analogous quantity could be defined by just replacing the scalars z_k, z_l by the corresponding vectors $\boldsymbol{z}_k, \boldsymbol{z}_l$, which would, however, not serve our purpose. Our goal is to find an autocorrelation measure, irrespective of the dynamics of the environment. Therefore, we first define the probability density of the system degree of freedom, by integrating the absolute value squared of the full wavefunction over all f environmental degrees of freedom

$$\rho_S(x,t) = \int \mathrm{d}y_1 \ldots \mathrm{d}y_f |\Psi^{\mathrm{M}}_{\mathrm{CS}}(x, y_1, \ldots, y_f, t)|^2 \tag{5.13}$$

to arrive at the probability density of the quartic degree of freedom. The explicit expression for the probability density $\rho_S(x,t)$ in terms of the time-dependent complex coefficients $a_l(t)$ and time-dependent $(f+1)$-dimensional complex displacement vectors $\boldsymbol{z}_l(t)$ is given in Appendix H. This then allows to calculate the quantity

$$c_S(t) = \int \mathrm{d}x \Psi(x,0)\sqrt{\rho_S(x,t)}, \tag{5.14}$$

which (if the initial state is real (and positive) as herein) has no phase anymore and is thus the analogue of the absolute value of the correlation function of Eq. (5.12). For the pure quartic (1D) case and the initial state we use, the time evolution of the quantities defined Eq. (5.12) and Eq. (5.14) is similar but not idential. The oscillation period is identical though.

This can be seen explicitly by looking at the time-evolved initial state (5.4), which to a large degree is given by ($\hbar$ is set to unity)

$$|\Psi(t)\rangle = \sum_n c_n |n\rangle \mathrm{e}^{-\mathrm{iE_n t}} \approx c_1|1\rangle \mathrm{e}^{-\mathrm{iE_1 t}} + c_3|3\rangle \mathrm{e}^{-\mathrm{iE_3 t}}. \tag{5.15}$$

The autocorrelation thus is

$$c(t) \approx |c_1|^2 \mathrm{e}^{-\mathrm{iE_1 t}} + |c_3|^2 \mathrm{e}^{-\mathrm{iE_3 t}} \tag{5.16}$$

and its absolute value is given by

$$\begin{aligned}|c(t)| =& \sqrt{c^*(t)c(t)} \\ =& \left\{|c_1|^4 + |c_3|^4 + 2|c_1|^2|c_3|^2\cos(E_3 - E_1)t\right\}^{\frac{1}{2}}\end{aligned} \tag{5.17}$$

Using the values of the c_n coefficients gathered in Table 5.1, it can be corroborated that $|c(t)|$ varies between unity and 0.33, as can be seen in the numerical results to be presented below.

For the density, which appears in the alternative measure, we find (assuming real-valued eigenfunctions)

$$\rho(x,t) = |\Psi(x,t)|^2 = |c_1|^2\rho_1^2(x) + |c_3|^2\rho_3^2(x) + 2|c_1||c_3|\cos(E_3 - E_1)t, \tag{5.18}$$

leading to the same oscillation frequency of $|c_S(t)|$ as the one observed in $|c(t)|$.

An even more stringent measure to decide if the time evolved state is approaching the ground state is the energy expectation value, defined by

$$\begin{aligned}\langle E\rangle(t) =& \langle\Psi^{\mathrm{M}}_{\mathrm{CS}}(t)|\hat{H}_{\mathrm{ord}}|\Psi^{\mathrm{M}}_{\mathrm{CS}}(t)\rangle \\ =& \sum_{k,l} a_k^*(t)H_{\mathrm{ord}}(\boldsymbol{z}_k^*, \boldsymbol{z}_l)\langle\boldsymbol{z}_k(t)|\boldsymbol{z}_l(t)\rangle a_l(t).\end{aligned} \tag{5.19}$$

The different terms in the total Hamiltonian can be disentangled and their respective contribution to the total energy can be looked at separately. The conservation of the total energy will also serve as a convergence check for the CCS method [74]. In passing, we note that the norm of the total wavefunction was well conserved in all the numerical calculations that we present. This is in contrast to the semiclassical Herman-Kluk case, where often a normalization of the results has to be performed. This is not necessary for CCS.

5.2.2. Numerical results

First, we consider the autocorrelation of the initial state at the top of the barrier in the uncoupled 1D case in Fig. 5.3. For the CCS calculations, a multiplicity of $M = 299$ was enough to converge the result to the converged split operator FFT result. Because the initial state mainly contains only two eigenstates (see Table 5.1), the local spectrum [49], i. e., the Fourier transform of the autocorrelation contains just two major peaks. From the figure, it can be seen that the absoulte value of the autocorrelation correspondingly oscillates back and forth between unity and around 0.3 with a period of around $T = 2\pi/(E_3 - E_1) \approx 4$ in the dimensionless units used. This fact has been corroborated in the previous subsection, see Eq. (5.17).

The initial state that will be used in the propagation of the coupled system is the (direct) product of the Gaussian on top of the barrier of the double well, given in Eq. (5.4), times the ground state Gaussians of Eq. (5.10) which amounts to zero temperature of the environment as shown in Appendix I. Before showing the alteration of the results by the coupling of the double well to several oscillators,

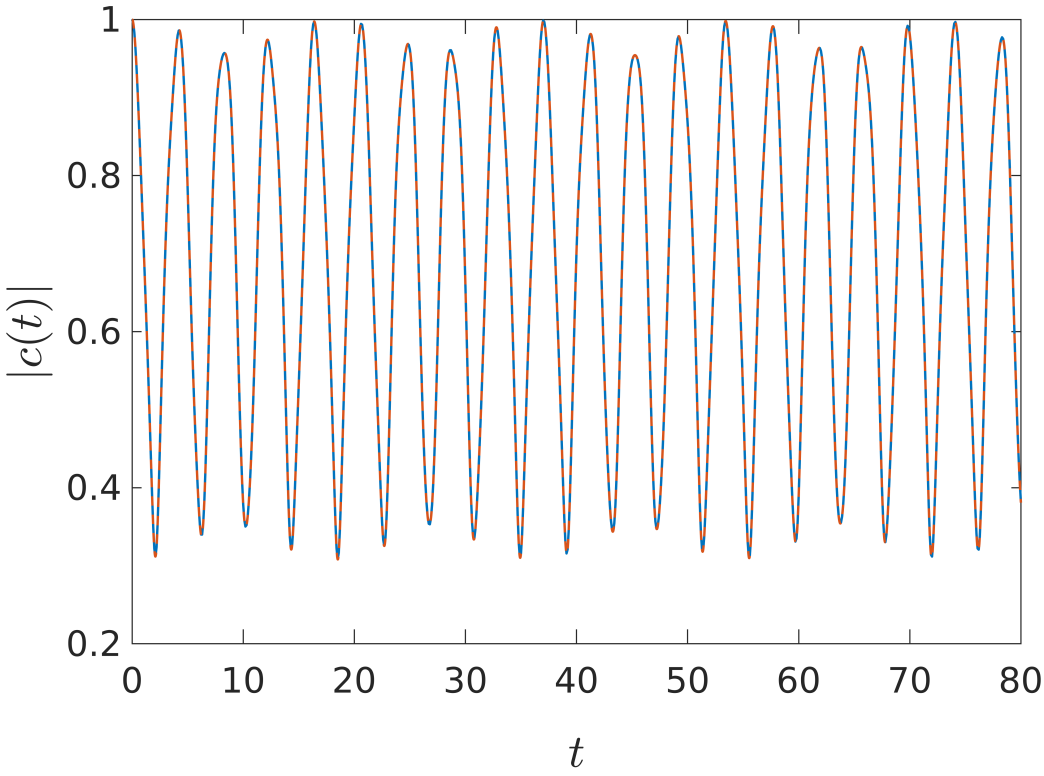

Figure 5.3.: Absolute value of the autocorrelation for the 1D system (double well only) from a CCS calculation (solid blue line) and from a split-operator FFT calculation (dashed red line). The two curves coincide to within line thickness.

we have to elaborate on the choice of frequencies of those oscillators, however. This choice will be crucial for the energy flow between the double well and the environment. We again follow the work of DPM [15] and choose the frequencies from the (normalized) density

$$\rho_{\mathrm{f}}(\omega) = \frac{1}{\omega_{\mathrm{co}}} \exp\left\{-\frac{\omega}{\omega_{\mathrm{co}}}\right\}, \tag{5.20}$$

with a parameter ω_{co} to be fixed below, according to

$$\int_0^{\omega_k} \mathrm{d}\omega \rho_{\mathrm{f}}(\omega) \stackrel{!}{=} \frac{k}{f_{\mathrm{co}}}. \tag{5.21}$$

This leads to the explicit expression

$$\omega_k = -\omega_{\mathrm{co}} \ln\left(1 - \frac{k}{f_{\mathrm{co}}}\right) \qquad k = 1, ..., f \tag{5.22}$$

for the frequencies and we here choose the second parameter $f_{\mathrm{co}} > f$, such that extremely high frequencies which would not exchange energy with the system (not shown) are not considered. Other frequency distributions have been used in [144] as well as in [189], while the present one has been found favorable also in MCTDH calculations [190]. Now one could choose the coupling strength between system and environment according to a specific (continuous) spectral distribution, which is usually taken as Ohmic or sub- or super-Ohmic. Here, however, we again adhere to DPM and take equal coupling strengths $g = 0.1$ for all oscillators, just suitably normalized by the total number of environmental degrees of freedom (see remark after Eq. (5.7)) to make the results for different values of f comparable. In Table 5.2, we give the parameters that were used in Eq. (5.22) for the calculation of the discretized frequencies for different values of f. We note in passing that for the number of oscillators that we will use, and for the present frequencies and couplings there is no transition to monostability of the combination of the bare potential plus the counter term, mentioned in [187]. In the following several different quantities will be looked at for increasing numbers of environmental degrees of freedom.

To start with, for the system's "autocorrelation" $c_S(t)$ defined in Eq. (5.14), we found the results displayed in Fig. 5.4. For the 3D results ($f = 2$) we used 799 trajectories, whereas for the 4D case ($f = 3$) we used 2999 trajectories. From Fig. 5.4 and by comparison to the 1D case displayed in Fig. 5.3, it can be seen that by the coupling to the environmental degrees of freedom, the oscillation frequency is only marginally increased (as to be expected by comparison to Rabi oscillations in a two level system) but the oscillation amplitude becomes decisively smaller. Furthermore, a damping

f	2	3	4	5
ω_{co}	4	4	4	4
f_{co}	10	12	14	16

Table 5.2.: Parameters needed for the calculation of the discretized bath frequencies according to Eq. (5.22) for different values of f.

of the oscillations for long times can be observed, which becomes more prominent, the higher the number of environmental degrees of freedom. This observation is in line with the expectation that the time-evolved state moves towards the ground state for large times $t \to \infty$. Then

$$\sqrt{\rho(x,t)} \overset{t\to\infty}{\approx} \rho_1(x) \tag{5.23}$$

and we get

$$\begin{aligned} c_S(\infty) &= \int_{-\infty}^{+\infty} \mathrm{d}x \Psi(x,0) \sqrt{\rho(x,\infty)} \\ &\approx \int_{-\infty}^{+\infty} \mathrm{d}x \left(c_1\rho_1(x) + c_3\rho_3(x)\right) \rho_1(x) \\ &= c_1 \approx 0.8 \end{aligned} \tag{5.24}$$

The expected value of 0.8 for $c_S(\infty)$ is close to the long-time average of the numerical result displayed in Fig. 5.4.

The most important measure to decide about the propagated density's possible evolution towards

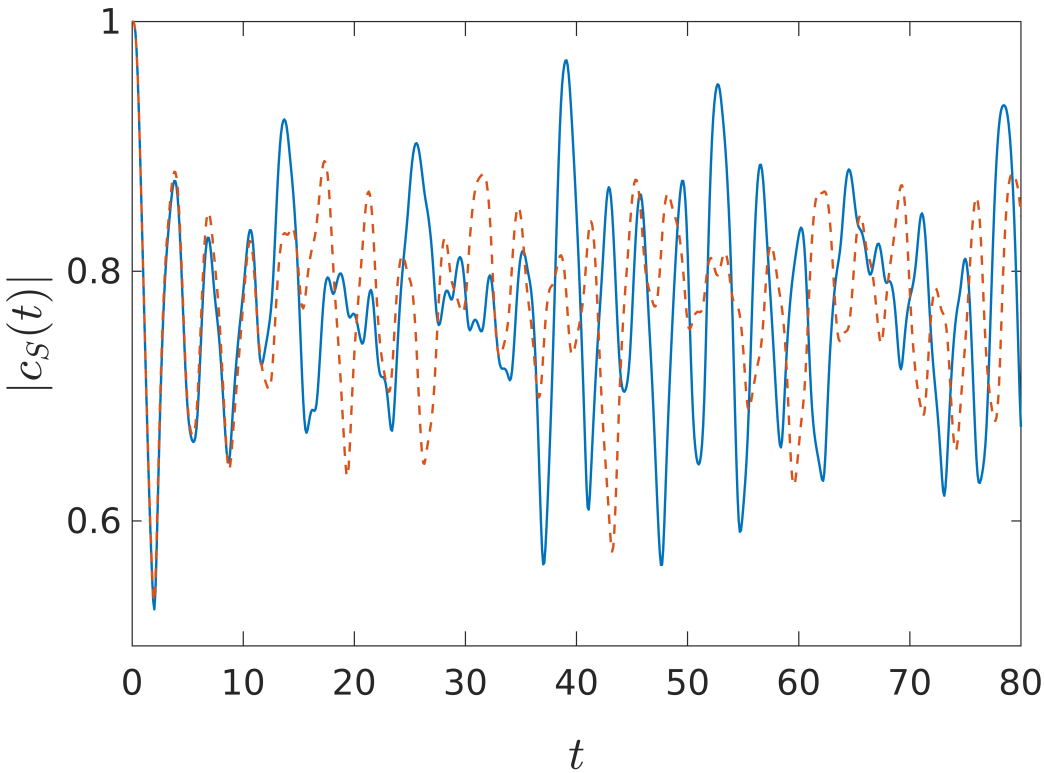

Figure 5.4.: Absolute value of the autocorrelation-like quantity defined in Eq. (5.14) from a CCS calculation for different numbers of environmental oscillators: $f = 2$ (solid blue) and $f = 3$ (dashed red)

the ground state is the energy expectation value. In Fig. 5.5 the energy expectations for all the five degrees of freedom in the case of $f = 4$ as well as the coupling and the counter term are displayed for times up to $t = 300$, whereby panel (a) contains the total energy, the double well energy as well as the coupling and the counter term and panel (b) contains all the different oscillator energies. The total energy is conserved very well, although a small tendency towards an energy drift is visible (panel (a)). For the presented results we have used a multiplicity of $M = 5999$ and we did not increase this number because the convergence is becoming exceedingly slow with the number of trajectories and the presented calculation took already several days on a modern computer cluster using several cores. As displayed in panel (b), the different oscillators clearly show an increase in their energy, away from their ground state value and the ω_1 oscillator even overtakes the ω_2 oscillator in terms of energy at certain times. We stress that the oscillators' energies never fall below their ground state energies as it should be [191]. Furthermore, the oscillator with the highest frequency is still showing appreciable variations in its energy. If even higher frequencies would have been chosen, the energy transfer would start to diminish, however (not shown). We stress that the environment, by consisting of a finite number of degrees of freedom, does heat up, in contrast to the case of infinitely many environmental oscillators described by a continuous spectral density [192]. As shown in panel (a), the counter term shows high frequency oscillations with a period similar to the total double well energy and the interaction energy is large and negative. Most importantly, the total double well energy shows a clear tendency to decrease below its initial value of 0.3. In addition, for large times, the amplitude of oscillation of the double well energy around its average value is rather small and we do not observe any revival in the relatively long time span that we display.

This last finding led us to investigate the long-time average value of the double well energy expec-

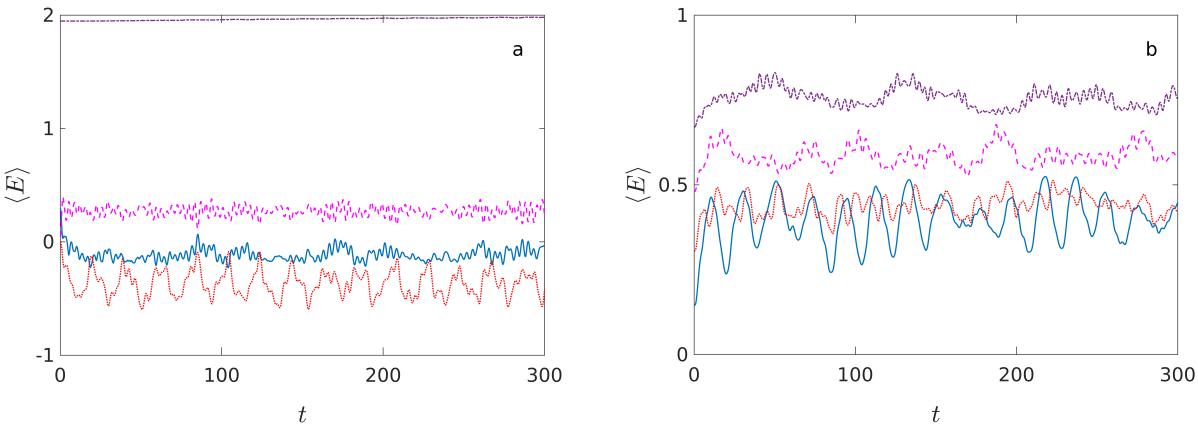

Figure 5.5.: Different energy expectation values for the case $f = 4$: (a) Total energy (dashed-dotted), counter term (dashed), double well (solid), coupling term (dotted), (b) kinetic plus potential energy of the different harmonic degrees of freedom: $\omega_1 = 0.29$ (solid), $\omega_2 = 0.61$ (dotted), $\omega_3 = 0.96$ (dashed) $\omega_4 = 1.34$ (dashed-dotted)).

tation

$$\overline{\langle E \rangle} = \frac{1}{T_{\text{tot}}} \int_0^{T_{\text{tot}}} \mathrm{d}t \langle E \rangle(t) \tag{5.25}$$

as a function of the number of environmental oscillators for the relatively long total time of $T_{\text{tot}} = 300$. As shown in Fig. 5.6, the average energy of the double well oscillator indeed decreases as a function of the number of environmental oscillators, indicating a clear trend towards the ground state energy. In [193], a video of the time evolution of the probability density $\rho_S(x,t)$ of the double well is given. This video shows that for long times, the time-evolved density, due to the coupling (in the presented case to three harmonic degrees of freedom) approaches the (static) ground state density (also displayed in the movie) to a substantial degree.

Finally, it is worthwhile to mention that we have tried different values for the coupling strength g and found (not shown) that larger values lead to too much initial energy from the counter term (the coupling itself has zero expectation value at $t = 0$) and thus eventually in the system, whereas smaller values of g, due to the small coupling decrease the flow away from the quartic into the harmonic degrees of freedom. So the value $g = 0.1$ that we used was close to optimal if the cooling of the quartic degree of freedom is to be achieved.

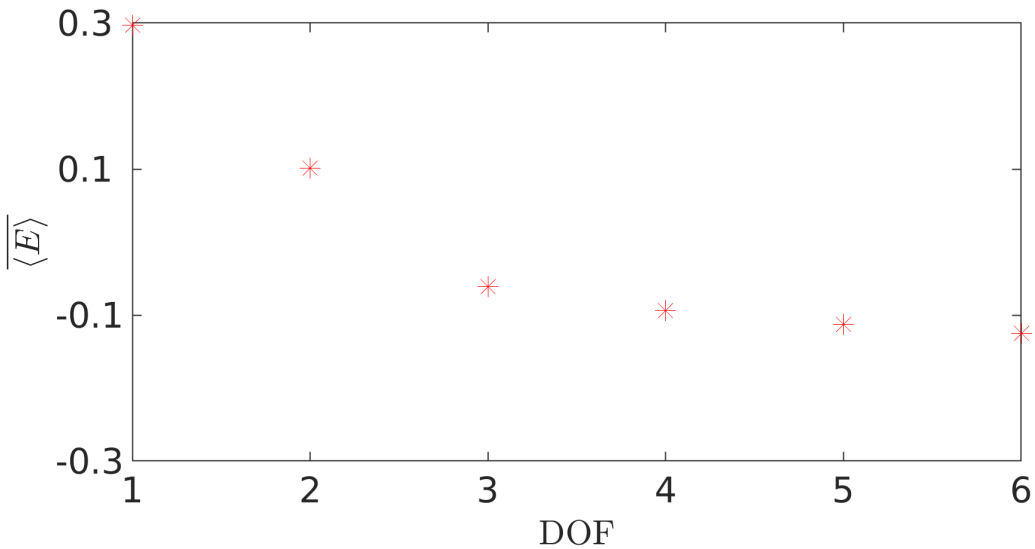

Figure 5.6.: Long-time average energy of the double well as a function of the total number of degrees of freedom (degree of freedom).

6. Summary and Outlook

The main objective of this work was to investigate thermalization in finite quantum systems where the system of interest has a continuous variable, using coherent state-based approaches to solve the TDSE. The objective is achieved and it has been shown that quantum mechanics may lead to thermalization even if the number of degrees of freedom is relatively small, which is not the case in classical mechanics. Earlier there has been quite a lot of work done in the quantum realm to study thermalization in spin systems, but not much is known in the case of continuous systems. Here we studied the zero temperature thermalization i.e., we considered the ground states of the bath oscillators (environment).

In order to study the quantum dynamics of the system under investigation, we first explained different methods to solve the TDSE in Chapter 2. We used the method of split-operator FFT as a benchmark to compare our numerical results obtained from other methods like the CCS, SCS and the semiclassical HK propagator. We studied the case of a one dimensional Morse oscillator to look into its revival dynamics in Chapter 3. We also discussed about other model potentials that have been studied using CSs. We also provided a discussion about three very common potentials namely, Morse, harmonic and quartic and their Hamiltonian matrix elements that are used in calculating the CCS equations of motion in order to study the quantum dynamics. A comprehensive comparison of *all* the methods studied in this thesis has been given in [34], although Shalashilin and coworkers have done a lot of ground breaking work in a similar spirit [57, 73, 108]. The first of the given references also contains an alternative method, called coupled coherent state trajectories, that we have not touched in this thesis.

As a conclusion from Chapter 3, decisive for the understanding of the differences between the methods is the notion of tight frames that is used implicitly in HK and can be used explicitly, e.g., in the static grid case, as shown in Appendix C, but is almost never used in the fully variational VCS (not discussed herein, but in [194]) as well as CCS, with the exception of [33]. The use of the tight frame assumption in the HK case reflects itself in the fact that all initial values of $\bar{a}_l(t)$ are nonzero initially. In the other trajectory based method, CCS, usually only a single coefficient $a_l(t)|_{l=\alpha}$ is nonzero initially and all the others acquire nonzero values eventually during the course of coupled propagation. The fact that $\bar{a}_l$ and a_l have to be distinguished is necessary due to the nonorthogonality of the CS basis functions. If a phase space integral is discretized by a single phase space sum, then, in the present context, one has used the tight frame assumption.

Starting the exposition of the numerical results for the Morse oscillator with the most approximate HK method, as usual, we have used the tight frame assumption, that allows to avoid using the inverse overlap. A densely sampled random grid of 10000 points in phase space is then required for converged results until the revival time. Because the initial points are chosen randomly, the method

can well be applied also to large systems (not shown here). Especially promising for high-dimensional applications is the parallel propagation of all trajectories together with their stabilities and actions as this scales sublinearly with the number of trajectories. The combination of HK with more crude semiclassical methods like TGWD in the semiclassical hybrid dynamics is favorably applied to system-bath Hamiltonians [67]. The biggest argument in favor of HK is that, by its being based on classical dynamical information, it allows for an intuitive understanding of quantum effects [115, 125].

In the SCS case in 1D, also regular grids (with 81 points) can be used but the tight frame assumption was not a viable option here (but worked for the case considered by Shalashilin and Child [33], as discussed in Appendix C) and inversion of the (regularized) overlap matrix had to be done. While it is advantageous to invert the overlap matrix $\mathbf{\Omega}$ for the SCS method where it is time-independent and the propagator for time-independent Hamiltonians reads $\exp\left[-i\mathbf{\Omega}^{-1}\mathbf{H}t\right]$, it is of no obvious benefit in the SCS and in the VCS method. Computation of $\mathbf{\Omega}^{-1}$ and subsequent application to the right-hand side scales worse and is more unstable than direct solution of the linear system with a non-unit "mass matrix". In higher dimensional systems, favorably, random static grids are used [153]. In CCS 121 random points were needed for convergence and the direct solution of the linear algebra problem with a non-diagonal mass matrix has been employed.

Some statements regarding extensions of the CS formalism and possible future work are worthwhile. Firstly, throughout most of the Chapters 2 and 3, we have used CS with a fixed width parameter γ, with the single exception of TGWD. By applying the squeezing operator in addition to the displacement operator, also *multiple* variable width Gaussians (see Section 2.2.2) could be employed as basis functions. This has already been suggested in the HK case [195, 196]. A numerical study uncovered limited success if no further measures are taken [197], however. Also the Davydov-Ansatz has been generalized to include squeezing [61] and further studies are necessary in the other cases. Unpublished work cited in [140], however, points to difficulties for anharmonic systems. Furthermore, generalized coherent states can be used to describe spin systems and particle indistinguishability [198]. A version of CCS for indistinguishable bosons has been published recently [199].

Secondly, most important for the future will be the applicability of the proposed methods to systems with a multitude of degrees of freedom. This has actually already been achieved for the vMCG/VCS case, which is analogous to the multi Davydov-Ansatz in case a bosonic system is coupled to a spin system which is described by its orthogonal basis states [145, 200]. Also for continuous degrees of freedom which are coupled to harmonic baths (see [201] for a recent linearized semiclassical calculation), or for Henon-Heiles systems with an increasing number of degrees of freedom, vMCG without overlap inversion as well as the CCS method are promising workhorses [139]. An alternative method using symmetrized CSs has a very favorable scaling for large systems and was applied for eigenvalue calculations similar in spirit as the work by Davis and Heller [202]. Furthermore, also the dynamics of Bose-Einstein condensates has been tackled with variational Gaussians, see e.g. [203]. Finally, as a conclusion from the Chapters 2 and 3, the Boltzmann operator can be considered as a time-evolution operator in imaginary "time", whose role is played by inverse temperature. Although some efforts using CSs for imaginary time propagation [79, 204] have been made, a lot of work remains to be done.

In Chapter 4, we extended the Husimi (coherent state) based version of LSC-IVRs for the calculation of correlation functions to the case of survival probabilities. This is a case that could be dealt with before only by use of the Wigner version of linearized semiclassical theory. We highlighted that the Wigner-Weyl and Husimi transform version of linearized semiclassical theories can lead to the same final formula in the case of the dipole-dipole correlation, whereas they are quite different in the case of survival probability, where strictly the simple Husimi version is not applicable. This fact then established the goal to find the correct Husimi-like version of the LSC-IVR. This goal was achieved by the straightforward linearization of the double HK expression for the survival (or staying probability). In the course of the derivation, we also slightly generalized a seminal calculation by Herman (appendix of [172]) to the case of width parameter matrices that are not proportional to the unit matrix.

The CS formalism was then applied to the revival dynamics of a Morse oscillator. However, the revival being purely a quantum interference phenomenon, could, apart from the numerically converged quantum results, only be observed in the full HK results. Both LSC-IVR variants show a monotonically decaying envelope and no revival because there is no interference. Coupling the Morse oscillator with a heavy bath oscillator leads to the absence of the revival in the full quantum calculations also. In this case the LSC-IVR results are predicting the correct behavior to a large degree and full quantum calculations are not necessary, as the system dynamics has undergone a quantum to classical transition due to the coupling to the environment, similar to the findings predicted using the semiclassical hybrid dynamics [146]. As a future prospect, it might be worthwhile to look at an even more general correlation function i.e., the so-called out of time order correlators [205] in the (linearized) semiclassical IVR approach.

In Chapter 4, we saw the quantum to classical transition of the system dynamics due to the coupling to the environment (bath harmonic oscillator). This transition can lead ultimately to our final goal of thermalization for long-time dynamics, which is the subject of our study in Chapter 5. The questions then arise are: if it is enough to increase the interaction strength between the different degrees of freedom in order to fully develop chaos which is the classical prerequisite for thermalization, or if, in addition, the number of those degrees of freedom has to be increased (possibly all the way to the thermodynamic limit) in order to observe thermalization. All these questions have been answered for the case of finite quantum systems in Chapter 5, where we investigated thermalization by considering the toppling pencil model [15], i.e., an excited initial state on top of the barrier of a symmetric quartic double well. We investigated if the coupling of the central quartic double well to a finite, environmental bath of harmonic oscillators in their ground states will let the central system evolve towards its uncoupled ground state. This amounts to thermalization i.e., a cooling down to the bath "temperature" (strictly only defined in the thermodynamic limit) of the central system.

By solving the time-dependent Schrödinger equation using the CCS methodology (and also split-operator FFT for small numbers of degrees of freedom), we showed that, indeed, the coupling eventually excites those environmental oscillators and for the relatively long times investigated, there is no appreciable back flow of energy to the system of interest, such that the central degree of freedom (here quartic double well) looses an appreciable amount of energy, monitored by its long-time average,

which we found to be a monotonously decaying function of the number of environmental degrees of freedom. For the largest number $f = 5$ of bath oscillators that we investigated the long-time average of the double well energy decreases from its uncoupled value of 0.3 to -0.125. This tendency of driving the double well towards lower energy via the environmental coupling was corroborated by an autocorrelation function-like measure, which showed a long-time behavior in accord with the estimate assuming a transition to the ground state of the quartic degree of freedom. In the light of these results it is worthwhile to note that the variational approach to solve the TDSE is based on a Lagrangian, see, e.g., [57] and the wavefunction parameters can be viewed as classical generalized coordinates. There are usually many more of them than in the pure classcial approach where there is only a pair of position and momentum variables per degree of freedom.

We have thus been successful in adding a further example to the list of continuous variable systems of interest with (in principle) infinite dimensional Hilbert space that are coupled to a finite bath and show signs of energetic equilibration. Up to now, the focus in the literature was mainly on spin-chain systems [2, 19, 174]. The bath, by consisting of a finite number of degrees of freedom, also has a finite heat capacity, in contrast to treatments in terms of reduced density matrices that hinge on continuous spectral densities of the oscillator bath [192, 206]. By (hypothetically) going to the limit of very large f, due to the scaling of the coupling by the inverse of the square root of f, the coupling to the individual oscillators will be diminished and thus also the energy flow, such that the oscillators will stay close to their initial state, which was here one of zero temperature (all oscillators in their ground states). Due to limited computer resources the explicit fully quantum treatment of all degrees of freedom will be difficult to accomplish in these cases though. Other possible methods to try in the future could be MCTDH [32], matrix product state [24] or different types of semiclassical treatments [34, 67].

Furthermore, so far the dynamics studied does not break the symmetry of the initial state of the quartic double well, because the Hamiltonian as well as the initial state of the bath are symmetric under the parity transformation. In the classical mechanics study by Dittrich and Pena Martínez [15], it has been argued that small asymmetries in the initial condition of the bath lead to a preference of the bistable system to end up in one of the two wells. It will be a worthwhile endeavor to study such asymmetric initial conditions also in a full quantum time evolution.

Another interesting idea to explore in future concerning thermalization in the “toppling pencil” model would be to take finite energy initial states for the bath harmonic oscillators, as in the present study we took zero temperature i.e., the ground states for the environmental oscillators. It would be worthwhile then to see whether we get a canonical distribution for the system energy. Another possibility to explore, would be to take different values for the double well parameters a and b, so that the initial state of the double well has overlap with a much larger set of eigenstates. It would then answer the question if thermalization is more effective with a larger density of system states, or does it only depend on the density of bath states.

On a concluding note, it has been shown in this thesis that thermalization is achieved in finite quantum system with continuous variables using coherent state-based methods to solve the TDSE.

The most important achievement is to witness thermalization by coupling the system to a bath of only few oscillators (less than 10), which has been seen for more than ten to twenty bath oscillators until now [21]. I sincerely hope that the work presented in this thesis will provide strong motivation to future exploration in the topic of thermalization in finite quantum systems.

A. Proof of the relation $\left[\hat{\boldsymbol{a}}, \hat{H}\right] = \frac{\partial \hat{H}_{\text{ord}}}{\partial \hat{\boldsymbol{a}}^\dagger}$ by mathematical induction

Without loss of generality, we assume a normally ordered Hamiltonian of the form $\hat{H} = \left(\hat{\boldsymbol{a}}^\dagger\right)^n$, then the proposition becomes

$$\left[\hat{\boldsymbol{a}}, \left(\hat{\boldsymbol{a}}^\dagger\right)^n\right] = \frac{\partial \left(\hat{\boldsymbol{a}}^\dagger\right)^n}{\partial \hat{\boldsymbol{a}}^\dagger}, \quad \forall n \in \mathbb{N} \tag{A.1}$$

For $n = 1$,

$$\left[\hat{\boldsymbol{a}}, \hat{\boldsymbol{a}}^\dagger\right] = \hat{1} = \frac{\partial \hat{\boldsymbol{a}}^\dagger}{\partial \hat{\boldsymbol{a}}^\dagger} \tag{A.2}$$

So the proposition (A.1) is true for $n = 1$. Let us assume that (A.1) is true for any arbitrary k, i.e., $\left[\hat{\boldsymbol{a}}, \left(\hat{\boldsymbol{a}}^\dagger\right)^k\right] = \frac{\partial \left(\hat{\boldsymbol{a}}^\dagger\right)^k}{\partial \hat{\boldsymbol{a}}^\dagger}$. We need to show that (A.1) is true for $(k+1)$ also. Therefore, now we have

$$\begin{aligned}
\left[\hat{\boldsymbol{a}}, \left(\hat{\boldsymbol{a}}^\dagger\right)^{(k+1)}\right] &= \left[\hat{\boldsymbol{a}}, \left(\hat{\boldsymbol{a}}^\dagger\right)^k \hat{\boldsymbol{a}}^\dagger\right] \\
&= \left[\hat{\boldsymbol{a}}, \left(\hat{\boldsymbol{a}}^\dagger\right)^k\right] \hat{\boldsymbol{a}}^\dagger + \left(\hat{\boldsymbol{a}}^\dagger\right)^k \left[\hat{\boldsymbol{a}}, \hat{\boldsymbol{a}}^\dagger\right] \\
&= \frac{\partial \left(\hat{\boldsymbol{a}}^\dagger\right)^k}{\partial \hat{\boldsymbol{a}}^\dagger} \hat{\boldsymbol{a}}^\dagger + \left(\hat{\boldsymbol{a}}^\dagger\right)^k . \hat{1} \\
&= k \left(\hat{\boldsymbol{a}}^\dagger\right)^k + \left(\hat{\boldsymbol{a}}^\dagger\right)^k \\
&= (k+1) \left(\hat{\boldsymbol{a}}^\dagger\right)^k \\
&= \frac{\partial \left(\hat{\boldsymbol{a}}^\dagger\right)^{(k+1)}}{\partial \hat{\boldsymbol{a}}^\dagger}
\end{aligned} \tag{A.3}$$

The proposition (A.1) is also true for $(k+1)$. Hence, from the principle of mathematical induction, the statement (A.1) is true for all natural numbers n.

B. One dimensional Harmonic oscillator in the SCS, CCS and VCS case

It is very instructive to have a look at the unit mass harmonic oscillator case with Hamiltonian

$$\hat{H} = \frac{\hat{p}^2}{2} + \frac{1}{2}\omega_0^2\hat{x}^2, \tag{B.1}$$

to gain some understanding of the dynamics of the variational parameters. As can be seen below, matters becomes trivial in the case of harmonic oscillator frequency ω_0 identical to ω (and thus to γ in the present system of units), i.e., to the one of the underlying harmonic oscillator that defines the coherent state basis. Therefore we study the general case.

The ordered Hamiltonian is then given by

$$H_{\mathrm{ord}}(z_k^*, z_l) = -\frac{\gamma}{4}[(z_k^* - z_l)^2 - 1] + \frac{\omega_0^2}{4\gamma}[(z_k^* + z_l)^2 + 1], \tag{B.2}$$

boiling down to the standard

$$H_{\mathrm{ord}}(z_k^*, z_l) = \omega\left(z_k^* z_l + \frac{1}{2}\right) \tag{B.3}$$

in the trivial case. For momentum in units of $\sqrt{\omega_0}$ and position in units $1/\sqrt{\omega_0}$, curves of equal energy in units of ω_0 are circles in phase space. A squeezed state, i. e., a coherent state of a harmonic oscillator with a different frequency ω will then "breathe" in position space in the course of time. This is visualized by the phase space dynamics of the corresponding Wigner function [168], displayed in Fig. B.1.

For didactic reasons, firstly, we start with the simple SCS equations. There, the CSs do not move and the *linear* equation of motion for the coefficients repeated here for convenience is

$$\mathrm{i}\sum_{l=1}^{M}\langle z_k|z_l\rangle\dot{a}_l(t) = \sum_{l=1}^{M}\langle z_k|\hat{H}|z_l\rangle a_l(t), \tag{B.4}$$

which shows that due to

$$\langle z_k|\hat{H}|z_l\rangle = H_{\mathrm{ord}}(z_k^*, z_l)\langle z_k|z_l\rangle, \tag{B.5}$$

even in the trivial case, the equations of motion are coupled as they have to allow for the motion of an "excitation" through the CS grid, due to the fact that the Gaussians themselves are immobile.

Secondly, the CCS case will be looked at. The RHS of the equations of motion for the Gaussian's parameters (2.44) is

$$\frac{\partial H}{\partial z^*} = -\frac{\gamma}{2}(z^* - z) + \frac{\omega_0^2}{2\gamma}(z^* + z). \tag{B.6}$$

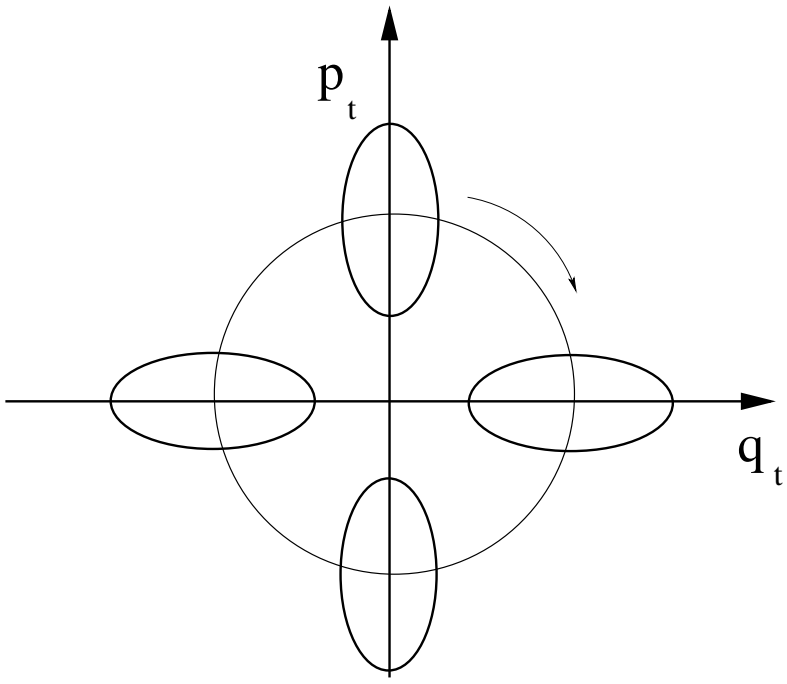

Figure B.1.: Phase space representation of the Wigner function of a squeezed state, i.e., a coherent state of an oscillator with $\omega > \omega_0$ (represented by an ellipse in the scaled phase space coordinates of the ω_0 oscillator), with initial position and momentum $q_\alpha = 0, p_\alpha = \text{const}$ and its dynamics of circling around the line of constant energy (which is a circle centered at the origin).

The solution of the equations of motion is identical to the purely classical solution and is independent of the employed basis function width parameter. It is given in terms of position and momentum as

$$q(t) = q(0)\cos(\omega_0 t) + \frac{p(0)}{\omega_0}\sin(\omega_0 t) \tag{B.7}$$

$$p(t) = p(0)\cos(\omega_0 t) - \omega_0 q(0)\sin(\omega_0 t) \tag{B.8}$$

simplifying to

$$z(t) = z(0)\exp\{-\mathrm{i}\omega t\} \tag{B.9}$$

in the trivial case. In any case the linear classical equations of motion for the complex CS parameters are uncoupled.

The equation of motion for the coefficients (2.47) contains the "tilde Hamiltonian", which becomes

$$\tilde{H}_{kl}(t) = \langle z_k(t)|z_l(t)\rangle\left\{\left(-\frac{\gamma}{4}+\frac{\omega_0^2}{4\gamma}\right)[(z_k^*)^2+(z_l^*)^2]+\left(\frac{\gamma}{2}-\frac{\omega_0^2}{2\gamma}\right)z_k^* z_l^* + \frac{\gamma}{4}+\frac{\omega_0^2}{4\gamma}\right\}, \tag{B.10}$$

for the harmonic oscillator, boiling down to

$$\tilde{H}_{kl}(t) = \langle z_k(t)|z_l(t)\rangle\frac{\omega}{2} \tag{B.11}$$

in the trivial case. From this we see that in the trivial case, the equations for the amplitudes are uncoupled and linear, because it is just the overlap matrix (times a constant) multiplying the vector of coefficients as well as its time-derivative. In the general case, on the RHS of (2.47) the matrix is not just proportional to the overlap matrix and thus the equations become coupled even for the harmonic oscillator. Assuming we start with a single coefficient being nonzero initially this is necessary to describe the "breathing" of the Gaussian wavefunction in addition to its center motion.

Thirdly, in the VCS case, the equations cannot be simplified easily and we just consider the trivial case. By guessing that (i) the equations of the CS parameters are uncoupled and read

$$\mathrm{i}\dot{z}_l = \omega z_l, \tag{B.12}$$

and that (ii) the equations for the coefficients reduce to

$$\mathrm{i}\dot{a}_l = \frac{\omega}{2} a_l \tag{B.13}$$

as in CCS, Eqs. (2.35) and (2.36) can be shown to hold. So there is no difference between VCS and CCS in the trivial case for the harmonic oscillator.

C. SCS in the tight frame case

In this appendix, we briefly review the tight frame equations of motion in the SCS case. One should be able to work with non-orthogonal basis functions "painlessly", in case they are dense enough [77]. Then the representation of unity is given by an expression that resembles the one for orthogonal basis functions

$$\hat{1} = N^{-1} \sum_{l=1}^{M} |z_l\rangle\langle z_l|, \tag{C.1}$$

where $N^{-1} = \frac{\Delta q \Delta p}{2\pi} = V/(2\pi M)$, with the covered phase space volume V [78] and, in contrast to Eq. (2.26), no inverse overlap matrix appears in this straightforward discretization of (2.50). This expression may now be used on the RHS of the TDSE (2.1) and after taking the scalar product with $\langle z_k|$ one gets

$$\mathrm{i}\dot{\bar{a}}_k(t) = N^{-1} \sum_{l} \langle z_k|\hat{H}|z_l\rangle \bar{a}_l(t), \tag{C.2}$$

which can again, in principle, be solved numerically, e.g., by matrix exponentiation, with the initial conditions

$$\bar{a}_l(0) = \langle z_l|\Psi(0)\rangle, \tag{C.3}$$

which is different from the initial conditions for the a_l coefficients in Eq. (2.16) but similar to the ones used in the HK method.

For the Morse potential with the parameters used in [33], reasonable agreement with the FFT results over several oscillation periods for the autocorrelation function using the regular 15x11 grid with $\Delta q \Delta p/2 = (1.2)^2/2$ proposed there, although this grid is much more sparse than the one with $\Delta q = 1/\sqrt{2\gamma}, \Delta p = \sqrt{\gamma/2}$ proposed in [78]. The use of the equations with the inverse overlap allows even sparser grids, however (81 points were enough for the potential and initial state parameters from [33]).

We note that we have not been able to converge the tight frame SCS calculations for the potential and initial state parameters used in the main text, however. It remains to be tested if refinements along the lines of [207], where an iterative scheme to calculate the identity operator (that does not involve inversion of the overlap matrix but instead matrix multiplications, see Eq. (18) in [207]) is proposed is faster than directly using the inverse overlap according to our Eq. (2.52).

D. Stability matrix and symplectic integration

The underlying dynamics of semiclassical methods is classical. Consequently, we need to solve the Hamilton's equations of motion

$$\dot{\mathbf{p}} = -\frac{\partial H}{\partial \mathbf{q}} \tag{D.1}$$

$$\dot{\mathbf{q}} = \frac{\partial H}{\partial \mathbf{p}} \tag{D.2}$$

Numerically, this can be carried out using symplectic integrators [49]. It ensures the preservation of the volume of a propagated region in phase space, which is also known as the Liouville's theorem. The trajectories are then propagated via the symplectic integrator scheme according to

$$\mathbf{p}^{(j)} = \mathbf{p}^{(j-1)} - b_j \Delta t \left.\frac{\partial H}{\partial \mathbf{q}}\right|_{\mathbf{q}^{(j-1)}}, \quad j = 1, 2, \cdots, m \tag{D.3}$$

$$\mathbf{q}^{(j)} = \mathbf{q}^{(j-1)} + a_j \Delta t \left.\frac{\partial H}{\partial \mathbf{p}}\right|_{\mathbf{p}^{(j)}}, \quad j = 1, 2, \cdots, m \tag{D.4}$$

for one time step with step size Δt. The index j denotes the number of iterations. The specific order and scheme of symplectic integration is characterized by the coefficients a_j and b_j, which also set the number of intermediate steps per full time step. Here we have used the second order leapfrog (or position Verlet), where $a_{1/2} = 0.5$ and $b_1 = 0$ and $b_2 = 1$. The coefficients for different symplectic integration schemes are given in [49].

The central ingredient of the prefactor of the semiclassical Herman-Kluk propagator is the stability (or monodromy) matrix.

$$\mathbf{M} = \begin{pmatrix} \mathbf{m}_{11} & \mathbf{m}_{12} \\ \mathbf{m}_{21} & \mathbf{m}_{22} \end{pmatrix} = \begin{pmatrix} \frac{\partial \mathbf{p}_t}{\partial \mathbf{p}^\intercal} & \frac{\partial \mathbf{p}_t}{\partial \mathbf{q}^\intercal} \\ \frac{\partial \mathbf{q}_t}{\partial \mathbf{p}^\intercal} & \frac{\partial \mathbf{q}_t}{\partial \mathbf{q}^\intercal} \end{pmatrix}. \tag{D.5}$$

This matrix determines the time-evolution of small deviations in the initial conditions of a specific trajectory according to

$$\begin{pmatrix} \delta \mathbf{p}_t \\ \delta \mathbf{q}_t \end{pmatrix} = \mathbf{M} \begin{pmatrix} \delta \mathbf{p} \\ \delta \mathbf{q} \end{pmatrix} \tag{D.6}$$

where $\delta \mathbf{p}_t = \tilde{\mathbf{p}}_t - \mathbf{p}_t$ and $\delta \mathbf{q}_t = \tilde{\mathbf{q}}_t - \mathbf{q}_t$. This is represented pictorially for one spatial dimension in Fig. D.1. The area that is spanned by the deviation vectors is not changing in the course of time.

The linear differential equation of first order for the stability matrix thus reads

$$\frac{\mathrm{d}}{\mathrm{d}t}\mathbf{M} = -\mathbf{JHM}, \tag{D.7}$$

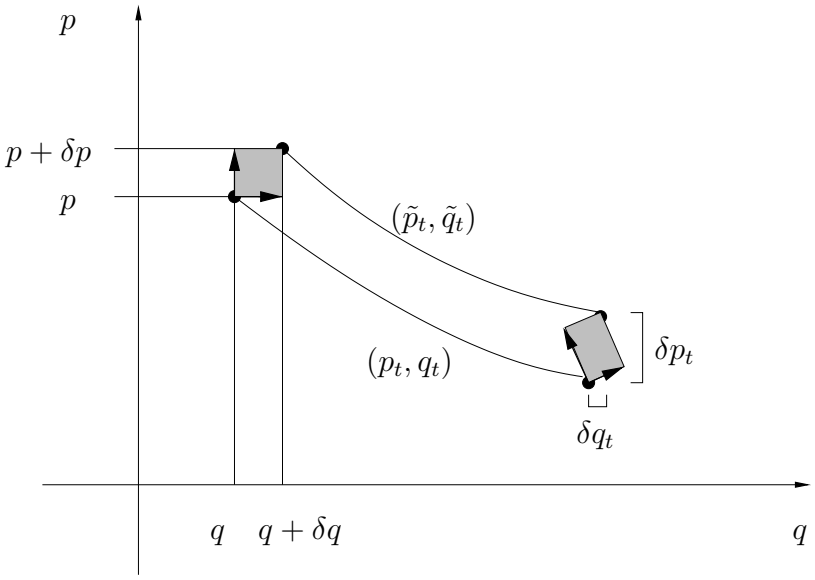

Figure D.1.: Variation of initial conditions in phase space for one degree of freedom. The *shaded area* is constant in time (Liouville's theorem), adapted from [93].

with the skew-symmetric matrix

$$\mathbf{J} = \begin{pmatrix} \mathbf{0} & \mathbf{1} \\ -\mathbf{1} & \mathbf{0} \end{pmatrix}, \tag{D.8}$$

and the Hessian of the Hamiltonian i.e., the matrix of second derivatives with respect to the position and momenta

$$\mathbf{H} = \begin{pmatrix} \frac{\partial^2 H}{\partial \mathbf{p} \partial \mathbf{p}^{\mathrm{T}}} & \frac{\partial^2 H}{\partial \mathbf{p} \partial \mathbf{q}^{\mathrm{T}}} \\ \frac{\partial^2 H}{\partial \mathbf{q} \partial \mathbf{p}^{\mathrm{T}}} & \frac{\partial^2 H}{\partial \mathbf{q} \partial \mathbf{q}^{\mathrm{T}}} \end{pmatrix} \tag{D.9}$$

From the definition of $\mathbf{M}$ in Eq. (D.5), one gets the simple initial condition for the monodromy matrix as

$$\mathbf{M}(0) = \begin{pmatrix} \mathbf{m}_{11}(0) & \mathbf{m}_{12}(0) \\ \mathbf{m}_{21}(0) & \mathbf{m}_{22}(0) \end{pmatrix} = \begin{pmatrix} \mathbf{1} & \mathbf{0} \\ \mathbf{0} & \mathbf{1} \end{pmatrix} \tag{D.10}$$

Using the equation of motion (D.7), it can be shown that

$$\frac{\mathrm{d}}{\mathrm{d}t} \mathbf{M}^{\mathrm{T}} \mathbf{J} \mathbf{M} = 0, \tag{D.11}$$

which ultimately, using the initial condition for $\mathbf{M}$, leads to

$$\mathbf{M}^{\mathrm{T}} \mathbf{J} \mathbf{M} = [\mathbf{M}(0)]^{\mathrm{T}} \mathbf{J} \mathbf{M}(0) = \mathbf{J} \tag{D.12}$$

for all times, i.e., $\mathbf{M}$ is a symplectic matrix. Using the symplectic relation (D.12), we can write out

the relations in terms of the elements of the monodromy matrix more explicitly as

$$\mathbf{m}_{22}^{\mathrm{T}}\mathbf{m}_{11} - \mathbf{m}_{12}^{\mathrm{T}}\mathbf{m}_{21} = \mathbf{1} \quad \forall t, \tag{D.13}$$

$$\mathbf{m}_{11}^{\mathrm{T}}\mathbf{m}_{21} - \mathbf{m}_{21}^{\mathrm{T}}\mathbf{m}_{11} = \mathbf{0} \quad \forall t, \tag{D.14}$$

$$\mathbf{m}_{22}^{\mathrm{T}}\mathbf{m}_{12} - \mathbf{m}_{12}^{\mathrm{T}}\mathbf{m}_{22} = \mathbf{0} \quad \forall t. \tag{D.15}$$

Another property of a symplectic matrix is that if a matrix is symplectic, then its transpose is also symplectic i.e., $\mathbf{M}^{\mathrm{T}}$ is also symplectic. Therefore, if we substitute $\mathbf{M}^{\mathrm{T}}$ in (D.12), we get

$$(\mathbf{M}^{\mathrm{T}})^{\mathrm{T}}\mathbf{J}\mathbf{M}^{\mathrm{T}} = \mathbf{M}\mathbf{J}\mathbf{M}^{\mathrm{T}} = \mathbf{J} \tag{D.16}$$

from where it follows that

$$\mathbf{m}_{22}\mathbf{m}_{11}^{\mathrm{T}} - \mathbf{m}_{12}\mathbf{m}_{21}^{\mathrm{T}} = \mathbf{1} \quad \forall t, \tag{D.17}$$

$$\mathbf{m}_{11}\mathbf{m}_{21}^{\mathrm{T}} - \mathbf{m}_{21}\mathbf{m}_{11}^{\mathrm{T}} = \mathbf{0} \quad \forall t, \tag{D.18}$$

$$\mathbf{m}_{22}\mathbf{m}_{12}^{\mathrm{T}} - \mathbf{m}_{12}\mathbf{m}_{22}^{\mathrm{T}} = \mathbf{0} \quad \forall t. \tag{D.19}$$

The above relations show that the determinant of the stability matrix is unity for all times. This is equivalent to the conservation of phase space volume mentioned previously. Monitoring the determinant of $\mathbf{M}$ thus provides an effective tool for checking the stability of a numerical calculation. It should also be mentioned that the matrix element $\mathbf{m}_{21}$, up to a sign, is the inverse of the second derivative of the action appearing in the prefactor of the VVG propagator.

$$\mathbf{m}_{21} = -\left(\frac{\partial^2 S}{\partial \mathbf{q}_t \partial \mathbf{q}^{\mathrm{T}}}\right)^{-1} \tag{D.20}$$

Because of the symplectic nature of the monodromy matrix, we can apply the following symplectic integration scheme to the elements of the monodromy matrix

$$\mathbf{m}_{11}^{(j)} = \mathbf{m}_{11}^{(j-1)} - b_j \Delta t \left.\frac{\partial^2 H}{\partial \mathbf{q} \partial \mathbf{q}^{\mathrm{T}}}\right|_{\mathbf{q}^{(j-1)}} \mathbf{m}_{21}^{(j-1)} \tag{D.21}$$

$$\mathbf{m}_{12}^{(j)} = \mathbf{m}_{12}^{(j-1)} - b_j \Delta t \left.\frac{\partial^2 H}{\partial \mathbf{q} \partial \mathbf{q}^{\mathrm{T}}}\right|_{\mathbf{q}^{(j-1)}} \mathbf{m}_{22}^{(j-1)} \tag{D.22}$$

$$\mathbf{m}_{21}^{(j)} = \mathbf{m}_{21}^{(j-1)} + a_j \Delta t \left.\frac{\partial^2 H}{\partial \mathbf{p} \partial \mathbf{p}^{\mathrm{T}}}\right|_{\mathbf{p}^{(j)}} \mathbf{m}_{11}^{(j-1)} \tag{D.23}$$

$$\mathbf{m}_{22}^{(j)} = \mathbf{m}_{22}^{(j-1)} + a_j \Delta t \left.\frac{\partial^2 H}{\partial \mathbf{p} \partial \mathbf{p}^{\mathrm{T}}}\right|_{\mathbf{p}^{(j)}} \mathbf{m}_{12}^{(j-1)}. \tag{D.24}$$

E. Eigenstates and eigenvalues of the Morse oscillator

In this appendix the solution of the TISE for the Morse oscillator Hamiltonian in Eq. (3.1) is given without proof and the overlap of the eigenstates with a Gaussian wavepacket is shown.

In his calculation of matrix elements of powers of the position operator between Morse oscillator eigenstates, φ_n, Gallas [208] used the definitions

$$k = \frac{2\omega_{\mathrm{M}}}{\alpha^2}, \tag{E.1}$$

$$z = k \exp\{-\alpha x\}, \tag{E.2}$$

$$b = k - 2n - 1, \tag{E.3}$$

and $N_n = \left(\frac{\alpha b n!}{\Gamma(k-n)}\right)^{1/2}$ in

$$\varphi_n(x) = N_n \mathrm{e}^{-z/2} z^{b/2} L_n^b(z). \tag{E.4}$$

The generalized Laguerre polynomials $L_n^b(z)$ can be constructed according to

$$L_n^b(z) = \frac{1}{n! \mathrm{e}^{-z} z^b} \frac{\mathrm{d}^n}{\mathrm{d}z^n} \left(\mathrm{e}^{-z} z^{n+b}\right), \tag{E.5}$$

and ω_{M} is the Morse oscillator frequency from Eq. (3.17).

The corresponding eigenvalues of the Morse oscillator in Eq. (3.1) then are

$$E_n = \omega_{\mathrm{M}} \left(n + \frac{1}{2}\right) - \frac{\alpha^2}{2} \left(n + \frac{1}{2}\right)^2, \quad 0 \leq n \leq \mathrm{Int}\left(\frac{\omega_{\mathrm{M}}}{\alpha^2} - \frac{1}{2}\right), \tag{E.6}$$

leading to a discrete bound state spectrum with decreasing energy distances up to the dissociation threshold D [49]. For the initial Gaussian wavefunction given Eq. (3.19) and the Morse potential parameters from Sec. 3.1.3, the overlap with the eigenstates, which is given by

$$d_n = \langle \varphi_n | \Psi(0) \rangle, \tag{E.7}$$

can be determined, e.g., using MATLAB [152]. It has a functional dependence on the quantum number that is close to a Gaussian proportional to $\exp\{-(n-n_0)^2/(2\delta n^2)\}$ as can be seen in Fig. E.1.

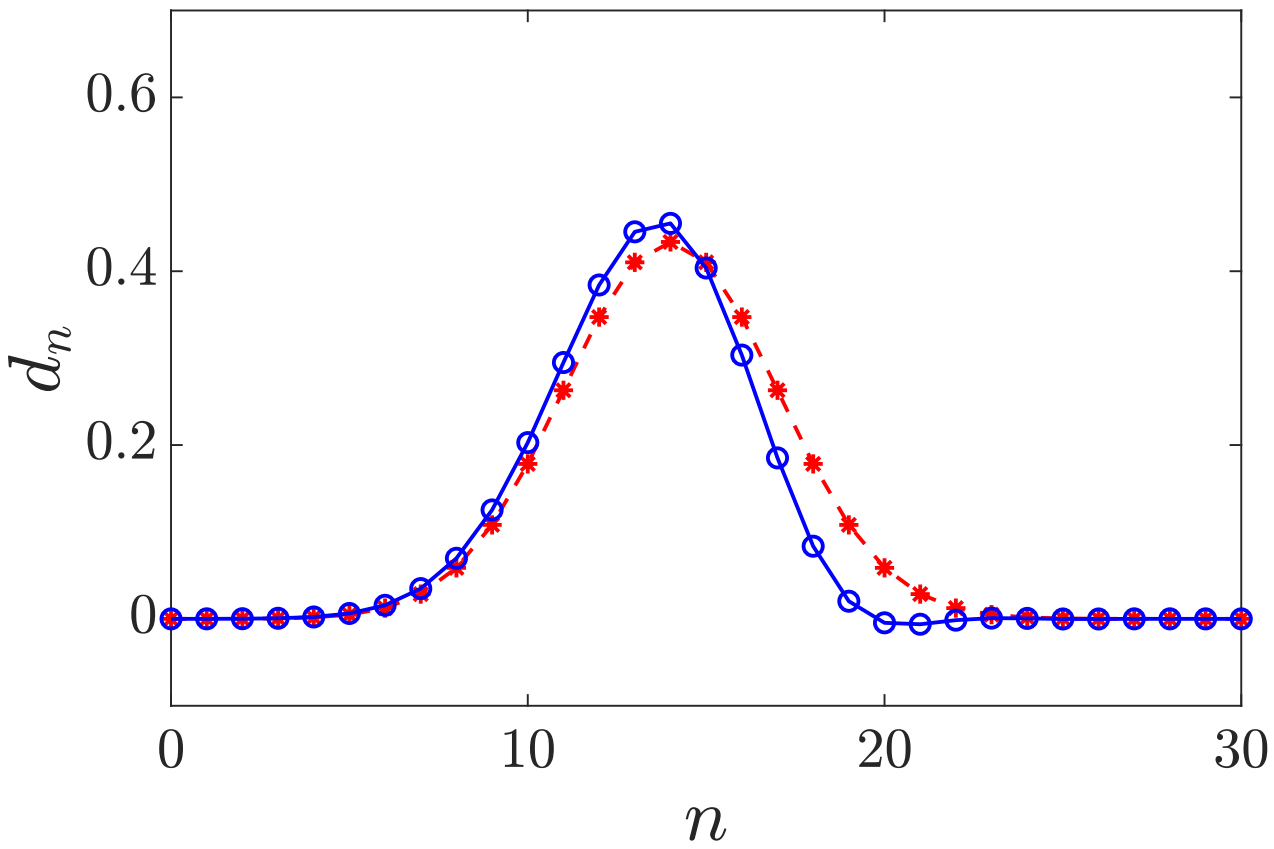

Figure E.1.: Overlap of the Gaussian initial state from Eq. (3.19) with the Morse eigenstates according to Eq. (E.7) (blue dots), compared to a Gaussian function centered around $n_0 = 14$ with width parameter $\delta n = 3$ (red stars)

F. Calculation and Proof of Factorization of det A

F.1. Calculation of det A

In this Appendix we analytically simplify $\det \mathbf{A}$ for the matrix $\mathbf{A}$ in Eq. (4.72) of the main text from the determinant of a $2f \times 2f$ matrix to the product of determinants of two $f \times f$ matrices, so that it cancels out with the HK-prefactor absolute square. We do so, by going along the lines of the appendix of Herman's paper [172]. Our $\det \mathbf{A}$ can be written as

$$\begin{aligned}\det \mathbf{A} &= \left(\frac{1}{8}\right)^{2f} \det \begin{pmatrix} \boldsymbol{\gamma} + \mathbf{m}_{22}^{\intercal}\boldsymbol{\gamma}\mathbf{m}_{22} + \frac{1}{\hbar^2}\mathbf{m}_{12}^{\intercal}\boldsymbol{\gamma}^{-1}\mathbf{m}_{12} & \mathbf{m}_{22}^{\intercal}\boldsymbol{\gamma}\mathbf{m}_{21} + \frac{1}{\hbar^2}\mathbf{m}_{12}^{\intercal}\boldsymbol{\gamma}^{-1}\mathbf{m}_{11} \\ \mathbf{m}_{21}^{\intercal}\boldsymbol{\gamma}\mathbf{m}_{22} + \frac{1}{\hbar^2}\mathbf{m}_{11}^{\intercal}\boldsymbol{\gamma}^{-1}\mathbf{m}_{12} & \frac{\boldsymbol{\gamma}^{-1}}{\hbar^2} + \frac{1}{\hbar^2}\mathbf{m}_{11}^{\intercal}\boldsymbol{\gamma}^{-1}\mathbf{m}_{11} + \mathbf{m}_{21}^{\intercal}\boldsymbol{\gamma}\mathbf{m}_{21} \end{pmatrix} \\ &= \left(\frac{1}{8}\right)^{2f} \det \begin{pmatrix} \mathbf{L} + \boldsymbol{\gamma}\mathbf{I} & \mathbf{M} + \frac{\mathrm{i}}{\hbar}\mathbf{I} \\ \mathbf{M}^{\intercal} + \frac{\mathrm{i}}{\hbar}\mathbf{I} & \frac{\boldsymbol{\gamma}^{-1}}{\hbar^2} + \mathbf{N} \end{pmatrix}. \end{aligned} \tag{F.1}$$

The $f \times f$ matrices $\mathbf{L}$, $\mathbf{M}$ and $\mathbf{N}$ are given by

$$\mathbf{L} = \mathbf{X}_+^{\intercal}\boldsymbol{\gamma}\mathbf{X}_-, \tag{F.2}$$

$$\mathbf{M} = \mathbf{X}_+^{\intercal}\boldsymbol{\gamma}\mathbf{P}_-, \tag{F.3}$$

$$\mathbf{N} = \mathbf{P}_+^{\intercal}\boldsymbol{\gamma}\mathbf{P}_- \tag{F.4}$$

and the matrices $\mathbf{X}_\pm$ and $\mathbf{P}_\pm$ are defined as

$$\mathbf{X}_\pm = \mathbf{m}_{22} \pm \frac{\mathrm{i}}{\hbar}\boldsymbol{\gamma}^{-1}\mathbf{m}_{12}, \tag{F.5}$$

$$\mathbf{P}_\pm = \mathbf{m}_{21} \pm \frac{\mathrm{i}}{\hbar}\boldsymbol{\gamma}^{-1}\mathbf{m}_{11}. \tag{F.6}$$

These matrices obey $\mathbf{P}_+^{\intercal}\boldsymbol{\gamma}\mathbf{P}_- = \mathbf{P}_-^{\intercal}\boldsymbol{\gamma}\mathbf{P}_+$, $\mathbf{X}_+^{\intercal}\boldsymbol{\gamma}\mathbf{X}_- = \mathbf{X}_-^{\intercal}\boldsymbol{\gamma}\mathbf{X}_+$ and $\mathbf{P}_+^{\intercal}\boldsymbol{\gamma}\mathbf{X}_- - \mathbf{P}_-^{\intercal}\boldsymbol{\gamma}\mathbf{X}_+ = \mathbf{X}_-^{\intercal}\boldsymbol{\gamma}\mathbf{P}_+ - \mathbf{X}_+^{\intercal}\boldsymbol{\gamma}\mathbf{P}_- = \left(\frac{2\mathrm{i}}{\hbar}\right)\mathbf{I}$, which follow from the properties of the Lagrange bracket [209] and the fact that the transformation $(\tilde{\mathbf{p}}, \tilde{\mathbf{q}}) \to (\tilde{\mathbf{p}}_t, \tilde{\mathbf{q}}_t)$ is canonical.
Therefore, $\det \mathbf{A}$ can be written as

$$\begin{aligned}\det \mathbf{A} &= \left(\frac{1}{8}\right)^{2f} \begin{vmatrix} \mathbf{L} + \boldsymbol{\gamma}\mathbf{I} & \mathbf{M} + \frac{\mathrm{i}}{\hbar}\mathbf{I} \\ \mathbf{M}^{\intercal} + \frac{\mathrm{i}}{\hbar}\mathbf{I} & \frac{\boldsymbol{\gamma}^{-1}}{\hbar^2} + \mathbf{N} \end{vmatrix} \\ &= \left(\frac{1}{8}\right)^{2f} \begin{vmatrix} \mathbf{X}_+^{\intercal}\boldsymbol{\gamma}\mathbf{X}_- + \boldsymbol{\gamma}\mathbf{I} & \mathbf{X}_+^{\intercal}\boldsymbol{\gamma}\mathbf{P}_- + \frac{\mathrm{i}}{\hbar}\mathbf{I} \\ \mathbf{P}_-^{\intercal}\boldsymbol{\gamma}\mathbf{X}_+ + \frac{\mathrm{i}}{\hbar}\mathbf{I} & \frac{\boldsymbol{\gamma}^{-1}}{\hbar^2} + \mathbf{P}_+^{\intercal}\boldsymbol{\gamma}\mathbf{P}_- \end{vmatrix}. \end{aligned} \tag{F.7}$$

As shown in Appendix F.2, the determinant on the right-hand side of the above equation can be expressed as the product of three determinants, F, G, and $\det(\boldsymbol{\gamma})$, where

$$F = \begin{vmatrix} \frac{1}{2}\mathbf{X}_+^\intercal & \frac{1}{2}\mathbf{X}_-^\intercal \\ \frac{1}{2}\mathbf{P}_+^\intercal & \frac{1}{2}\mathbf{P}_-^\intercal \end{vmatrix} \tag{F.8}$$

$$G = \begin{vmatrix} \boldsymbol{\gamma}\mathbf{X}_-\boldsymbol{\gamma}^{-1} + \mathrm{i}\hbar\boldsymbol{\gamma}\mathbf{P}_- & -\frac{\mathrm{i}}{\hbar}\left(\boldsymbol{\gamma}\mathbf{X}_-\boldsymbol{\gamma}^{-1} + \mathrm{i}\hbar\boldsymbol{\gamma}\mathbf{P}_-\right) \\ \boldsymbol{\gamma}\mathbf{X}_+\boldsymbol{\gamma}^{-1} - \mathrm{i}\hbar\boldsymbol{\gamma}\mathbf{P}_+ & \frac{\mathrm{i}}{\hbar}\left(\boldsymbol{\gamma}\mathbf{X}_+\boldsymbol{\gamma}^{-1} - \mathrm{i}\hbar\boldsymbol{\gamma}\mathbf{P}_+\right) \end{vmatrix}. \tag{F.9}$$

We multiply the transpose of the matrix corresponding to the determinant F from the left by the product matrix

$$\mathbf{Y} = \begin{pmatrix} \mathbf{I} & -\mathbf{P}_+^\intercal\boldsymbol{\gamma}\mathbf{P}_- \\ 0 & \mathbf{I} \end{pmatrix} \begin{pmatrix} \mathbf{P}_-^\intercal\boldsymbol{\gamma} & 0 \\ 0 & \mathbf{P}_-^{-1} \end{pmatrix}, \tag{F.10}$$

whose determinant is $\det(\boldsymbol{\gamma})$ and from the right by $\det\left(\boldsymbol{\gamma}^{-1}\right)$, such that the determinant F is unchanged. Thus we get

$$\begin{aligned} F &= \begin{vmatrix} \frac{1}{2}\mathbf{X}_+^\intercal & \frac{1}{2}\mathbf{X}_-^\intercal \\ \frac{1}{2}\mathbf{P}_+^\intercal & \frac{1}{2}\mathbf{P}_-^\intercal \end{vmatrix} \\ &= \begin{vmatrix} \mathbf{I} & -\mathbf{P}_+^\intercal\boldsymbol{\gamma}\mathbf{P}_- \\ 0 & \mathbf{I} \end{vmatrix} \begin{vmatrix} \mathbf{P}_-^\intercal\boldsymbol{\gamma} & 0 \\ 0 & \mathbf{P}_-^{-1} \end{vmatrix} \begin{vmatrix} \frac{1}{2}\mathbf{X}_+ & \frac{1}{2}\mathbf{P}_+ \\ \frac{1}{2}\mathbf{X}_- & \frac{1}{2}\mathbf{P}_- \end{vmatrix} \det\left(\boldsymbol{\gamma}^{-1}\right) \\ &= \begin{vmatrix} \mathbf{I} & -\mathbf{P}_+^\intercal\boldsymbol{\gamma}\mathbf{P}_- \\ 0 & \mathbf{I} \end{vmatrix} \begin{vmatrix} \frac{1}{2}\mathbf{P}_-^\intercal\boldsymbol{\gamma}\mathbf{X}_+ & \frac{1}{2}\mathbf{P}_-^\intercal\boldsymbol{\gamma}\mathbf{P}_+ \\ \frac{1}{2}\mathbf{P}_-^{-1}\mathbf{X}_- & \frac{1}{2}\mathbf{P}_-^{-1}\mathbf{P}_- \end{vmatrix} \begin{vmatrix} \boldsymbol{\gamma}^{-1} & 0 \\ 0 & 1 \end{vmatrix} \\ &= \begin{vmatrix} \frac{1}{2}\left(\mathbf{P}_-^\intercal\boldsymbol{\gamma}\mathbf{X}_+ - \mathbf{P}_+^\intercal\boldsymbol{\gamma}\mathbf{X}_-\right) & 0 \\ \frac{1}{2}\mathbf{P}_-^{-1}\mathbf{X}_- & \frac{1}{2} \end{vmatrix} \begin{vmatrix} \boldsymbol{\gamma}^{-1} & 0 \\ 0 & 1 \end{vmatrix} \\ &= \begin{vmatrix} -\frac{\mathrm{i}}{\hbar} & 0 \\ \frac{1}{2}\mathbf{P}_-^{-1}\mathbf{X}_- & \frac{1}{2} \end{vmatrix} \begin{vmatrix} \boldsymbol{\gamma}^{-1} & 0 \\ 0 & 1 \end{vmatrix} \\ &= \left(-\frac{\mathrm{i}}{2\hbar}\right)^f \det\left(\boldsymbol{\gamma}^{-1}\right). \end{aligned} \tag{F.11}$$

Now, multiplying the first column in the determinant of $\mathbf{G}$ by $\frac{\mathrm{i}}{\hbar}$ and adding it to the second column we get

$$\begin{aligned} G &= \begin{vmatrix} \boldsymbol{\gamma}\mathbf{X}_-\boldsymbol{\gamma}^{-1} + \mathrm{i}\hbar\boldsymbol{\gamma}\mathbf{P}_- & 0 \\ \boldsymbol{\gamma}\mathbf{X}_+\boldsymbol{\gamma}^{-1} - \mathrm{i}\hbar\boldsymbol{\gamma}\mathbf{P}_+ & \frac{2\mathrm{i}}{\hbar}\left(\boldsymbol{\gamma}\mathbf{X}_+\boldsymbol{\gamma}^{-1} - \mathrm{i}\hbar\boldsymbol{\gamma}\mathbf{P}_+\right) \end{vmatrix} \\ &= \left(\frac{2\mathrm{i}}{\hbar}\right)^f \det\left(\boldsymbol{\gamma}\mathbf{X}_-\boldsymbol{\gamma}^{-1} + \mathrm{i}\hbar\boldsymbol{\gamma}\mathbf{P}_-\right) \det\left(\boldsymbol{\gamma}\mathbf{X}_+\boldsymbol{\gamma}^{-1} - \mathrm{i}\hbar\boldsymbol{\gamma}\mathbf{P}_+\right) \end{aligned} \tag{F.12}$$

and

$$\det\left(\boldsymbol{\gamma}\mathbf{X}_-\boldsymbol{\gamma}^{-1}+\mathrm{i}\hbar\boldsymbol{\gamma}\mathbf{P}_-\right)=\det\left\{\mathbf{m}_{11}+\boldsymbol{\gamma}\mathbf{m}_{22}\boldsymbol{\gamma}^{-1}+\mathrm{i}\hbar\boldsymbol{\gamma}\mathbf{m}_{21}+\frac{1}{\mathrm{i}\hbar}\mathbf{m}_{12}\boldsymbol{\gamma}^{-1}\right\}, \tag{F.13}$$

$$\det\left(\boldsymbol{\gamma}\mathbf{X}_+\boldsymbol{\gamma}^{-1}-\mathrm{i}\hbar\boldsymbol{\gamma}\mathbf{P}_+\right)=\det\left\{\mathbf{m}_{11}+\boldsymbol{\gamma}\mathbf{m}_{22}\boldsymbol{\gamma}^{-1}-\mathrm{i}\hbar\boldsymbol{\gamma}\mathbf{m}_{21}-\frac{1}{\mathrm{i}\hbar}\mathbf{m}_{12}\boldsymbol{\gamma}^{-1}\right\}. \tag{F.14}$$

Therefore,

$$G=\left(\frac{2\mathrm{i}}{\hbar}\right)^f\det\left\{\mathbf{m}_{11}+\boldsymbol{\gamma}\mathbf{m}_{22}\boldsymbol{\gamma}^{-1}+\mathrm{i}\hbar\boldsymbol{\gamma}\mathbf{m}_{21}+\frac{1}{\mathrm{i}\hbar}\mathbf{m}_{12}\boldsymbol{\gamma}^{-1}\right\} \tag{F.15}$$

$$\det\left\{\mathbf{m}_{11}+\boldsymbol{\gamma}\mathbf{m}_{22}\boldsymbol{\gamma}^{-1}-\mathrm{i}\hbar\boldsymbol{\gamma}\mathbf{m}_{21}-\frac{1}{\mathrm{i}\hbar}\mathbf{m}_{12}\boldsymbol{\gamma}^{-1}\right\} \tag{F.16}$$

Hence $\det\mathbf{A}$ is expressed by determinants of $f\times f$ matrices, according to

$$\det\mathbf{A}=\left(\frac{1}{8\hbar}\right)^{2f}\det\left\{\mathbf{m}_{11}+\boldsymbol{\gamma}\mathbf{m}_{22}\boldsymbol{\gamma}^{-1}+\mathrm{i}\hbar\boldsymbol{\gamma}\mathbf{m}_{21}+\frac{1}{\mathrm{i}\hbar}\mathbf{m}_{12}\boldsymbol{\gamma}^{-1}\right\}$$
$$\det\left\{\mathbf{m}_{11}+\boldsymbol{\gamma}\mathbf{m}_{22}\boldsymbol{\gamma}^{-1}-\mathrm{i}\hbar\boldsymbol{\gamma}\mathbf{m}_{21}-\frac{1}{\mathrm{i}\hbar}\mathbf{m}_{12}\boldsymbol{\gamma}^{-1}\right\}. \tag{F.17}$$

In the paper by Herman [172], the width parameter matrix was taken as γ times identity matrix, i.e., the width parameters for all degrees of freedom was chosen to be the same and equal to γ. While, here in this appendix the width parameter matrix can even be taken as a general symmetric and invertible matrix, i.e., the width parameters for all degrees of freedom don't necessarily need to be equal.

F.2. Proof of Factorization of det A

For reasons of completeness, here we briefly sketch the factorization of $\det\mathbf{A}$, i.e., we prove

$$\det\mathbf{A}=\left(\frac{1}{8}\right)^{2f}\begin{vmatrix}\mathbf{X}_+^\intercal\boldsymbol{\gamma}\mathbf{X}_-+\boldsymbol{\gamma}\mathbf{I} & \mathbf{X}_+^\intercal\boldsymbol{\gamma}\mathbf{P}_-+\frac{\mathrm{i}}{\hbar}\mathbf{I}\\ \mathbf{P}_-^\intercal\boldsymbol{\gamma}\mathbf{X}_++\frac{\mathrm{i}}{\hbar}\mathbf{I} & \frac{\boldsymbol{\gamma}^{-1}}{\hbar^2}+\mathbf{P}_+^\intercal\boldsymbol{\gamma}\mathbf{P}_-\end{vmatrix} \tag{F.18}$$

$$=\left(\frac{1}{8}\right)^{2f}FG\det(\boldsymbol{\gamma}), \tag{F.19}$$

with F and G given in (F.8,F.9). Thus,

$$FG=\begin{vmatrix}\frac{1}{2}\mathbf{X}_+^\intercal & \frac{1}{2}\mathbf{X}_-^\intercal\\ \frac{1}{2}\mathbf{P}_+^\intercal & \frac{1}{2}\mathbf{P}_-^\intercal\end{vmatrix}\begin{vmatrix}\boldsymbol{\gamma}\mathbf{X}_-\boldsymbol{\gamma}^{-1}+\mathrm{i}\hbar\boldsymbol{\gamma}\mathbf{P}_- & -\frac{\mathrm{i}}{\hbar}\left(\boldsymbol{\gamma}\mathbf{X}_-\boldsymbol{\gamma}^{-1}+\mathrm{i}\hbar\boldsymbol{\gamma}\mathbf{P}_-\right)\\ \boldsymbol{\gamma}\mathbf{X}_+\boldsymbol{\gamma}^{-1}-\mathrm{i}\hbar\boldsymbol{\gamma}\mathbf{P}_+ & \frac{\mathrm{i}}{\hbar}\left(\boldsymbol{\gamma}\mathbf{X}_+\boldsymbol{\gamma}^{-1}-\mathrm{i}\hbar\boldsymbol{\gamma}\mathbf{P}_+\right)\end{vmatrix}$$
$$=\begin{vmatrix}\mathbf{f}_{11} & \mathbf{f}_{12}\\ \mathbf{f}_{21} & \mathbf{f}_{22}\end{vmatrix}, \tag{F.20}$$

with the block matrices

$$\begin{aligned}\mathbf{f}_{11} &= \frac{1}{2}\left(\mathbf{X}_+^\intercal\boldsymbol{\gamma}\mathbf{X}_- + \mathbf{X}_-^\intercal\boldsymbol{\gamma}\mathbf{X}_+\right)\boldsymbol{\gamma}^{-1} + \frac{\mathrm{i}\hbar}{2}\left(\mathbf{X}_+^\intercal\boldsymbol{\gamma}\mathbf{P}_- - \mathbf{X}_-^\intercal\boldsymbol{\gamma}\mathbf{P}_+\right)\\ &= \left(\mathbf{X}_+^\intercal\boldsymbol{\gamma}\mathbf{X}_- + \boldsymbol{\gamma}\mathbf{I}\right)\boldsymbol{\gamma}^{-1},\end{aligned} \tag{F.21}$$

$$\begin{aligned}\mathbf{f}_{12} &= \frac{1}{2}\left(\mathbf{X}_+^\intercal\boldsymbol{\gamma}\mathbf{P}_- + \mathbf{X}_-^\intercal\boldsymbol{\gamma}\mathbf{P}_+\right) + \frac{\mathrm{i}}{2\hbar}\left(\mathbf{X}_-^\intercal\boldsymbol{\gamma}\mathbf{X}_+ - \mathbf{X}_+^\intercal\boldsymbol{\gamma}\mathbf{X}_-\right)\boldsymbol{\gamma}^{-1}\\ &= \mathbf{X}_+^\intercal\boldsymbol{\gamma}\mathbf{P}_- + \frac{\mathrm{i}}{\hbar}\mathbf{I},\end{aligned} \tag{F.22}$$

$$\begin{aligned}\mathbf{f}_{21} &= \frac{1}{2}\left(\mathbf{P}_+^\intercal\boldsymbol{\gamma}\mathbf{X}_- + \mathbf{P}_-^\intercal\boldsymbol{\gamma}\mathbf{X}_+\right)\boldsymbol{\gamma}^{-1} + \frac{\mathrm{i}\hbar}{2}\left(\mathbf{P}_+^\intercal\boldsymbol{\gamma}\mathbf{P}_- - \mathbf{P}_-^\intercal\boldsymbol{\gamma}\mathbf{P}_+\right)\\ &= \left(\mathbf{P}_-^\intercal\boldsymbol{\gamma}\mathbf{X}_+ + \frac{\mathrm{i}}{\hbar}\mathbf{I}\right)\boldsymbol{\gamma}^{-1},\end{aligned} \tag{F.23}$$

$$\begin{aligned}\mathbf{f}_{22} &= \frac{1}{2}\left(\mathbf{P}_+^\intercal\boldsymbol{\gamma}\mathbf{P}_- + \mathbf{P}_-^\intercal\boldsymbol{\gamma}\mathbf{P}_+\right) + \frac{\mathrm{i}}{2\hbar}\left(\mathbf{P}_+^\intercal\boldsymbol{\gamma}\mathbf{X}_+ - \mathbf{P}_+^\intercal\boldsymbol{\gamma}\mathbf{X}_-\right)\boldsymbol{\gamma}^{-1}\\ &= \frac{\boldsymbol{\gamma}^{-1}}{\hbar^2} + \mathbf{P}_+^\intercal\boldsymbol{\gamma}\mathbf{P}_-.\end{aligned} \tag{F.24}$$

Therefore,

$$\begin{aligned}FG\det(\boldsymbol{\gamma}) &= \begin{vmatrix}\left(\mathbf{X}_+^\intercal\boldsymbol{\gamma}\mathbf{X}_- + \boldsymbol{\gamma}\mathbf{I}\right)\boldsymbol{\gamma}^{-1} & \mathbf{X}_+^\intercal\boldsymbol{\gamma}\mathbf{P}_- + \frac{\mathrm{i}}{\hbar}\mathbf{I}\\ \left(\mathbf{P}_-^\intercal\boldsymbol{\gamma}\mathbf{X}_+ + \frac{\mathrm{i}}{\hbar}\mathbf{I}\right)\boldsymbol{\gamma}^{-1} & \frac{\boldsymbol{\gamma}^{-1}}{\hbar^2} + \mathbf{P}_+^\intercal\boldsymbol{\gamma}\mathbf{P}_-\end{vmatrix}\begin{vmatrix}\boldsymbol{\gamma} & 0\\ 0 & 1\end{vmatrix}\\ &= \begin{vmatrix}\mathbf{X}_+^\intercal\boldsymbol{\gamma}\mathbf{X}_- + \boldsymbol{\gamma}\mathbf{I} & \mathbf{X}_+^\intercal\boldsymbol{\gamma}\mathbf{P}_- + \frac{\mathrm{i}}{\hbar}\mathbf{I}\\ \mathbf{P}_-^\intercal\boldsymbol{\gamma}\mathbf{X}_+ + \frac{\mathrm{i}}{\hbar}\mathbf{I} & \frac{\boldsymbol{\gamma}^{-1}}{\hbar^2} + \mathbf{P}_+^\intercal\boldsymbol{\gamma}\mathbf{P}_-\end{vmatrix},\end{aligned} \tag{F.25}$$

what we had wished to prove.

G. Normally ordered Hamiltonian of Quartic double well coupled to harmonic oscillators and classical equations of motion

The Hamilton operator for the quartic double well potential is given by

$$\hat{H}_S = \hat{T}_S + \hat{V}_S = \frac{\hat{p}_x^2}{2m_x} - \frac{a}{2}\hat{x}^2 + \frac{b}{4}\hat{x}^4. \tag{G.1}$$

To make progress, the position and momentum operators are expressed via creation and annihilation operators, via

$$\hat{x} = \frac{1}{\sqrt{2\gamma_x}}(\hat{a}_x^\dagger + \hat{a}_x), \qquad \hat{p}_x = \mathrm{i}\hbar\sqrt{\frac{\gamma_x}{2}}(\hat{a}_x^\dagger - \hat{a}_x). \tag{G.2}$$

In the following we set $\hbar = 1$. The subscripts to the creation and annihilation operators denote the respective degree of freedom. Using the fundamental commutation relation

$$[\hat{a}_x, \hat{a}_x^\dagger] = \hat{1}, \tag{G.3}$$

the normal ordered form of the kinetic energy operator is found to be

$$\hat{T}_S(\hat{a}_x^\dagger, \hat{a}_x) = \frac{\hat{p}_x^2}{2m_x} = -\frac{\gamma_x}{4m_x}(\hat{a}_x^\dagger - \hat{a}_x)^2 = -\frac{\gamma_x}{4m_x}\left[(\hat{a}_x^\dagger)^2 - 2\hat{a}_x^\dagger\hat{a}_x - 1 + \hat{a}_x^2\right] \tag{G.4}$$

and thus

$$T_S(z_{kx}^*, z_{lx}) = -\frac{\gamma_x}{4m_x}\left[(z_{kx}^* - z_{lx})^2 - 1\right] \tag{G.5}$$

follows for the CS matrix elements of the normally ordered kinetic energy operator.

Now, for the potential energy operator $\hat{V}_S$ of the system, we have

$$\begin{aligned}\hat{x}^2 &= \frac{1}{2\gamma_x}(\hat{a}_x^\dagger + \hat{a}_x)(\hat{a}_x^\dagger + \hat{a}_x) \\ &= \frac{1}{2\gamma_x}\left[(\hat{a}_x^\dagger)^2 + 2\hat{a}_x^\dagger\hat{a}_x + 1 + \hat{a}_x^2\right]\end{aligned} \tag{G.6}$$

and

$$\begin{aligned}\hat{x}^4 = \hat{x}^2\hat{x}^2 &= \frac{1}{4\gamma_x^2}\left[(\hat{a}_x^\dagger)^2 + 2\hat{a}_x^\dagger\hat{a}_x + 1 + \hat{a}_x^2\right]\left[(\hat{a}_x^\dagger)^2 + 2\hat{a}_x^\dagger\hat{a}_x + 1 + \hat{a}_x^2\right] \\ &= \frac{1}{4\gamma_x^2}\Big((\hat{a}_x^\dagger)^4 + \hat{a}_x^4 + (\hat{a}_x^\dagger)^2\hat{a}_x^2 + \hat{a}_x^2(\hat{a}_x^\dagger)^2 + 2(\hat{a}_x^\dagger)^2 + 2\hat{a}_x^2 + 2(\hat{a}_x^\dagger)^3\hat{a}_x \\ &\quad + 2\hat{a}_x^\dagger\hat{a}_x^3 + 2\hat{a}_x^2\hat{a}_x^\dagger\hat{a}_x + 2\hat{a}_x^\dagger\hat{a}_x(\hat{a}_x^\dagger)^2 + 4\hat{a}_x^\dagger\hat{a}_x\hat{a}_x^\dagger\hat{a}_x + 4\hat{a}_x^\dagger\hat{a}_x + 1\Big).\end{aligned} \tag{G.7}$$

Using the differential calculus employed in Theorem II on page 142 of [59], the above equation (G.7)

can be simplified in order to transform all the terms into normal ordered form. To this end one replaces $\hat{a}$ by $z + \partial/\partial z^*$ and $\hat{a}^\dagger$ by z^* and applies the expression to the unit operator to arrive at the matrix elements of the normal form of an operator. $\mathcal{N}$ shall denote the normal ordering operator. Therefore, e.g., from

$$\begin{aligned}\mathcal{N}\left\{\left(z+\frac{\partial}{\partial z^*}\right)^2 (z^*)^2\cdot 1\right\} &= \mathcal{N}\left\{z^2(z^*)^2+4zz^*+2\right\}\\ &= (z^*)^2z^2+4z^*z+2,\end{aligned} \tag{G.8}$$

it follows that

$$\hat{a}_x^2(\hat{a}_x^\dagger)^2 = (\hat{a}_x^\dagger)^2\hat{a}_x^2 + 4\hat{a}_x^\dagger\hat{a}_x + 2 \tag{G.9}$$

and similarly

$$\hat{a}_x^2\hat{a}_x^\dagger\hat{a}_x = \hat{a}_x^\dagger\hat{a}_x^3 + 2\hat{a}_x^2, \tag{G.10}$$

$$\hat{a}_x^\dagger\hat{a}_x\left(\hat{a}_x^\dagger\right)^2 = \left(\hat{a}_x^\dagger\right)^3\hat{a}_x + 2\left(\hat{a}_x^\dagger\right)^2, \tag{G.11}$$

$$\hat{a}_x^\dagger\hat{a}_x\hat{a}_x^\dagger\hat{a}_x = \left(\hat{a}_x^\dagger\right)^2\hat{a}_x^2 + \hat{a}_x^\dagger\hat{a}_x \tag{G.12}$$

for all terms that are not normally ordered already. Hence

$$\begin{aligned}\hat{x}^4 = \frac{1}{4\gamma_x^2}\Bigg(&\left(\hat{a}_x^\dagger\right)^4 + 4\left(\hat{a}_x^\dagger\right)^3\hat{a}_x + 6\left(\hat{a}_x^\dagger\right)^2\hat{a}_x^2 + 4\hat{a}_x^\dagger\hat{a}_x^3 + \hat{a}_x^4\\ &+ 6\left[\left(\hat{a}_x^\dagger\right)^2 + 2\hat{a}_x^\dagger\hat{a}_x + \hat{a}_x^2\right] + 3\Bigg)\end{aligned} \tag{G.13}$$

holds for the normal ordered form of the quartic term in the potential and the CS matrix elements of the total potential energy for the system are given by

$$V_S(z_{kx}^*, z_{lx}) = -\frac{a}{4\gamma_x}\left[(z_{kx}^*+z_{lx})^2+1\right] + \frac{b}{16\gamma_x^2}\left[(z_{kx}^*+z_{lx})^4 + 6\,(z_{kx}^*+z_{lx})^2 + 3\right], \tag{G.14}$$

leading to the corresponding Hamiltonian

$$H_S(z_{kx}^*, z_{lx}) = T_S(z_{kx}^*, z_{lx}) + V_S(z_{kx}^*, z_{lx}) \tag{G.15}$$

with the kinetic energy from Eq. (G.5). Now the environmental Hamilton operator

$$\begin{aligned}\hat{H}_E &= \sum_{n=1}^{f}\left(\frac{\hat{p}_n^2}{2m}+\frac{m\omega_n^2}{2}\hat{y}_n^2\right)\\ &= \sum_{n=1}^{f}-\frac{\gamma_n}{4m}\left[\left(\hat{a}_n^\dagger\right)^2-2\hat{a}_n^\dagger\hat{a}_n-1+\hat{a}_n^2\right]+\frac{\gamma_n}{4m}\left[\left(\hat{a}_n^\dagger\right)^2+2\hat{a}_n^\dagger\hat{a}_n+1+\hat{a}_n^2\right]\\ &= \sum_{n=1}^{f}\omega_n\left(\hat{a}_n^\dagger\hat{a}_n+\frac{1}{2}\right)\end{aligned} \tag{G.16}$$

is already normal ordered, leading to the matrix elements

$$H_E(z_{ky_1}^*,...,z_{ky_n}^*,z_{ly_1},...,z_{ly_n}) = \sum_{n=1}^{f}\omega_n\left(z_{ky_n}^*z_{ly_n}+\frac{1}{2}\right). \tag{G.17}$$

The same holds true for the interaction Hamilton operator

$$\hat{H}_{SE} = -\hat{x}\sum_{n=1}^{f}g_n\hat{y}_n, \tag{G.18}$$

leading to

$$H_{SE}(z_{kx}^*,z_{ky_1}^*,...,z_{ky_n}^*,z_{lx},z_{ly_1},...,z_{ly_n}) = -\frac{(z_{kx}^*+z_{lx})}{2\sqrt{\gamma_x}}\sum_{n=1}^{f}\frac{g_n}{\sqrt{\gamma_n}}\left(z_{ky_n}^*+z_{ly_n}\right). \tag{G.19}$$

Finally, the counter-term operator

$$\hat{V}_C = \hat{x}^2\sum_{n=1}^{f}\frac{g_n^2}{2m\omega_n^2} \tag{G.20}$$

is just quadratic and leads to

$$V_C(z_{kx}^*,z_{lx}) = \left[(z_{kx}^*+z_{lx})^2+1\right]\sum_{n=1}^{f}\frac{g_n^2}{4m\omega_n^2\gamma_x}. \tag{G.21}$$

Therefore, the total normal ordered Hamiltonian is given by the sum of all the terms in Eqs.

(G.15,G.17,G.19,G.21) as

$$
\begin{aligned}
H_{\mathrm{ord}}(\boldsymbol{z}_k^*, \boldsymbol{z}_l) = & -\frac{\gamma_x}{4m_x}\left[(z_{kx}^* - z_{lx})^2 - 1\right] - \frac{a}{4\gamma_x}\left[(z_{kx}^* + z_{lx})^2 + 1\right] \\
& + \frac{b}{16\gamma_x^2}\left[(z_{kx}^* + z_{lx})^4 + 6\,(z_{kx}^* + z_{lx})^2 + 3\right] \\
& + \sum_{n=1}^{f} \omega_n \left(z_{ky_n}^* z_{ly_n} + \frac{1}{2}\right) \\
& - \frac{(z_{kx}^* + z_{lx})}{2\sqrt{\gamma_x}} \sum_{n=1}^{f} \frac{g_n}{\sqrt{\gamma_n}} \left(z_{ky_n}^* + z_{ly_n}\right) \\
& + \left[(z_{kx}^* + z_{lx})^2 + 1\right] \sum_{n=1}^{f} \frac{g_n^2}{4m\omega_n^2\gamma_x}. \qquad \text{(G.22)}
\end{aligned}
$$

The complexified classical equation of motion for the displacements z_x of the quartic degree of freedom is given by

$$
\begin{aligned}
\mathrm{i}\dot{z}_x = \frac{\partial H_{\mathrm{ord}}}{\partial z_x^*} = & -\frac{\gamma_x}{2m_x}\left(z_x^* - z_x\right) + \frac{b}{4\gamma_x^2}\left(z_x^* + z_x\right)^3 - \sum_{n=1}^{f} \frac{g_n}{2\sqrt{\gamma_x\gamma_n}}\left(z_{y_n}^* + z_{y_n}\right) \\
& + \frac{(z_x^* + z_x)}{2\gamma_x}\left[\sum_{n=1}^{f} \frac{g_n^2}{m\omega_n^2} - a + \frac{3b}{2\gamma_x}\right]. \qquad \text{(G.23)}
\end{aligned}
$$

The equations of motion for the displacements z_{y_n} of the harmonic (environmental) degrees of freedom are

$$
\mathrm{i}\dot{z}_{y_n} = \frac{\partial H_{\mathrm{ord}}}{\partial z_{y_n}^*} = \omega_n z_{y_n} - \frac{g_n}{2\sqrt{\gamma_x\gamma_{y_n}}}\left(z_x^* + z_x\right). \qquad \text{(G.24)}
$$

The equations of motion for the coefficients in the CS expansion are given in (2.47).

H. Analytical expression for the probability density of the quartic double well

The probability density of the system degree of freedom is given as

$$\rho_S(x,t) = \int \mathrm{d}y_1 \ldots \mathrm{d}y_f |\Psi^{\mathrm{M}}_{\mathrm{CS}}(x, y_1, \ldots, y_f, t)|^2. \tag{H.1}$$

Using an Ansatz for the wavefunction given in Eq. (2.16) in terms of coherent states of multiplicity M, $|\Psi^{\mathrm{M}}_{\mathrm{CS}}(x, y_1, \ldots, y_f, t)|^2$ can be written for multi-mode coherent states $|\boldsymbol{z}_l\rangle$ as

$$\begin{aligned} |\Psi^{\mathrm{M}}_{\mathrm{CS}}(x, y_1, \ldots, y_f, t)|^2 =& \langle \Psi^{\mathrm{M}}_{\mathrm{CS}}(t)|\boldsymbol{x}\rangle\langle\boldsymbol{x}|\Psi^{\mathrm{M}}_{\mathrm{CS}}(t)\rangle \\ =& \sum_{k,l} a^*_k(t)\langle \boldsymbol{z}_k(t)|\boldsymbol{x}\rangle\langle\boldsymbol{x}|\boldsymbol{z}_l(t)\rangle a_l(t) \end{aligned} \tag{H.2}$$

where the vector $\boldsymbol{x} = (x, y_1, \ldots, y_f)$. Therefore, after separating out each individual degrees of freedom the probability density becomes

$$\begin{aligned} \rho_S(x,t) =& \sum_{k,l} a^*_k(t)\langle z_{kx}(t)|x\rangle\langle x|z_{lx}(t)\rangle \int \mathrm{d}y_1 \ldots \mathrm{d}y_f \langle z_{ky_1}(t)|y_1\rangle\langle y_1|z_{ly_1}(t)\rangle \ldots \\ & \langle z_{ky_f}(t)|y_f\rangle\langle y_f|z_{ly_f}(t)\rangle a_l(t). \end{aligned} \tag{H.3}$$

Now, for any $y = y_1, \ldots, y_f$ we have (here $\hbar$ is set to unity)

$$\begin{aligned} \int \mathrm{d}y \langle z_{ky}(t)|y\rangle\langle y|z_{ly}(t)\rangle =& \exp\left[-\frac{\gamma_y}{4}(q_{ly} - q_{ky})^2 - \frac{1}{4\gamma_y}(p_{ly} - p_{ky})^2 + \frac{\mathrm{i}}{2}(p_{ly}q_{ky} - q_{ly}p_{ky})\right] \\ =& \exp\left[-\frac{1}{2}(|z_{ky}|^2 + |z_{ly}|^2) + z^*_{ky}z_{ly}\right] \\ =& \langle z_{ky}(t)|z_{ly}(t)\rangle \end{aligned} \tag{H.4}$$

which is nothing but the overlap of two coherent states. Hence, the integral in (H.3) disappears and we get the simplified expression for $\rho_S(x,t)$ as

$$\rho_S(x,t) = \sum_{k,l} a^*_k(t)\langle z_{kx}(t)|x\rangle\langle x|z_{lx}(t)\rangle\langle z_{ky_1}(t)|z_{ly_1}(t)\rangle \ldots \langle z_{ky_f}(t)|z_{ly_f}(t)\rangle a_l(t) \tag{H.5}$$

We note that there should be an elementwise multiplication between the overlaps of each individual degrees of freedom. Now, we are left with obtaining an expression for $\langle z_{kx}(t)|x\rangle\langle x|z_{lx}(t)\rangle$. As we know

$$\langle x|z_{lx}(t)\rangle = \left(\frac{\gamma_x}{\pi}\right)^{\frac{1}{4}} \exp\left[-\frac{\gamma_x}{2}(x - q_{lx})^2 + \mathrm{i}p_{lx}\left(x - \frac{q_{lx}}{2}\right)\right], \tag{H.6}$$

also

$$\langle z_{kx}(t)|x\rangle = \left(\frac{\gamma_x}{\pi}\right)^{\frac{1}{4}} \exp\left[-\frac{\gamma_x}{2}\left(x-q_{kx}\right)^2 - \mathrm{i}p_{kx}\left(x-\frac{q_{kx}}{2}\right)\right], \tag{H.7}$$

we need to express (H.6) and (H.7) in terms of displacements z_{kx}, z_{lx}. For that, we use the definition of time-dependent complex displacements given in terms of position and momentum variables

$$z_{lx}(t) = \sqrt{\frac{\gamma_x}{2}}q_{lx}(t) + \frac{\mathrm{i}}{\sqrt{2\gamma_x}}p_{lx}(t) \tag{H.8}$$

Therefore,

$$\begin{aligned}
\langle z_{kx}(t)|x\rangle &= \left(\frac{\gamma_x}{\pi}\right)^{\frac{1}{4}} \exp\left[-\left(\sqrt{\frac{\gamma_x}{2}}x - \mathrm{Re}\left(z_{kx}\right)\right)^2 - \mathrm{iIm}\left(z_{kx}\right)\left(\sqrt{2\gamma_x} - \mathrm{Re}\left(z_{kx}\right)\right)\right] \\
&= \left(\frac{\gamma_x}{\pi}\right)^{\frac{1}{4}} \exp\Bigg(-\left\{\frac{\gamma_x}{2}x^2 - x\sqrt{2\gamma_x}\mathrm{Re}\left(z_{kx}\right) + \left(\mathrm{Re}\left(z_{kx}\right)\right)^2\right\} \\
&\quad - \mathrm{i}x\sqrt{2\gamma_x}\mathrm{Im}\left(z_{kx}\right) + \mathrm{iIm}\left(z_{kx}\right)\mathrm{Re}\left(z_{kx}\right)\Bigg) \\
&= \left(\frac{\gamma_x}{\pi}\right)^{\frac{1}{4}} \exp\Bigg(-\frac{\gamma_x}{2}x^2 + x\sqrt{2\gamma_x}\left\{\mathrm{Re}\left(z_{kx}\right) - \mathrm{iIm}\left(z_{kx}\right)\right\} \\
&\quad - \mathrm{Re}\left(z_{kx}\right)\left\{\mathrm{Re}\left(z_{kx}\right) - \mathrm{iIm}\left(z_{kx}\right)\right\}\Bigg) \\
&= \left(\frac{\gamma_x}{\pi}\right)^{\frac{1}{4}} \exp\left[-\frac{\gamma_x}{2}x^2 + x\sqrt{2\gamma_x}z_{kx}^* - \mathrm{Re}\left(z_{kx}\right)z_{kx}^*\right] \\
&= \left(\frac{\gamma_x}{\pi}\right)^{\frac{1}{4}} \exp\left[-\frac{\gamma_x}{2}x^2 + z_{kx}^*\left(x\sqrt{2\gamma_x} - \mathrm{Re}\left(z_{kx}\right)\right)\right]
\end{aligned} \tag{H.9}$$

and

$$\begin{aligned}
\langle x|z_{lx}(t)\rangle &= \left(\frac{\gamma_x}{\pi}\right)^{\frac{1}{4}} \exp\left[-\left(\sqrt{\frac{\gamma_x}{2}}x - \mathrm{Re}\left(z_{lx}\right)\right)^2 + \mathrm{iIm}\left(z_{lx}\right)\left(\sqrt{2\gamma_x}x - \mathrm{Re}\left(z_{lx}\right)\right)\right] \\
&= \left(\frac{\gamma_x}{\pi}\right)^{\frac{1}{4}} \exp\Bigg(-\left\{\frac{\gamma_x}{2}x^2 - x\sqrt{2\gamma_x}\mathrm{Re}\left(z_{lx}\right) + \left(\mathrm{Re}\left(z_{lx}\right)\right)^2\right\} \\
&\quad + \mathrm{i}x\sqrt{2\gamma_x}\mathrm{Im}\left(z_{lx}\right) - \mathrm{iIm}\left(z_{lx}\right)\mathrm{Re}\left(z_{lx}\right)\Bigg) \\
&= \left(\frac{\gamma_x}{\pi}\right)^{\frac{1}{4}} \exp\Bigg(-\frac{\gamma_x}{2}x^2 + x\sqrt{2\gamma_x}\left\{\mathrm{Re}\left(z_{lx}\right) + \mathrm{iIm}\left(z_{lx}\right)\right\} \\
&\quad - \mathrm{Re}\left(z_{lx}\right)\left\{\mathrm{Re}\left(z_{lx}\right) + \mathrm{iIm}\left(z_{lx}\right)\right\}\Bigg) \\
&= \left(\frac{\gamma_x}{\pi}\right)^{\frac{1}{4}} \exp\left[-\frac{\gamma_x}{2}x^2 + x\sqrt{2\gamma_x}z_{lx} - \mathrm{Re}\left(z_{lx}\right)z_{lx}\right] \\
&= \left(\frac{\gamma_x}{\pi}\right)^{\frac{1}{4}} \exp\left[-\frac{\gamma_x}{2}x^2 + z_{lx}\left(x\sqrt{2\gamma_x} - \mathrm{Re}\left(z_{lx}\right)\right)\right].
\end{aligned} \tag{H.10}$$

Hence, we get

$$\langle z_{kx}(t)|x\rangle\langle x|z_{lx}(t)\rangle = \left(\frac{\gamma_x}{\pi}\right)^{\frac{1}{2}} \exp\Bigg(-\gamma_x x^2 + x\sqrt{2\gamma_x}\,(z_{kx}^* + z_{lx}) \\ - z_{kx}^*\mathrm{Re}\,(z_{kx}) - z_{lx}\mathrm{Re}\,(z_{lx})\Bigg). \tag{H.11}$$

The correctness of the above relation can be proved by integrating $\langle z_{kx}(t)|x\rangle\langle x|z_{lx}(t)\rangle$ over x, if the integration yields the overlap $\langle z_{kx}(t)|z_{lx}(t)\rangle$, because

$$\int \mathrm{d}x|x\rangle\langle x| = 1. \tag{H.12}$$

Therefore,

$$\begin{aligned}
\int \mathrm{d}x\langle z_{kx}(t)|x\rangle\langle x|z_{lx}(t)\rangle &= \left(\frac{\gamma_x}{\pi}\right)^{\frac{1}{2}} \int \mathrm{d}x \exp\Bigg(-\gamma_x x^2 + x\sqrt{2\gamma_x}\,(z_{kx}^* + z_{lx}) \\
&\quad - z_{kx}^*\mathrm{Re}\,(z_{kx}) - z_{lx}\mathrm{Re}\,(z_{lx})\Bigg) \\
&= \left(\frac{\gamma_x}{\pi}\right)^{\frac{1}{2}} \sqrt{\frac{\pi}{\gamma_x}} \exp\left(\frac{1}{2}\,(z_{kx}^* + z_{lx})^2 - z_{kx}^*\mathrm{Re}\,(z_{kx}) - z_{lx}\mathrm{Re}\,(z_{lx})\right) \\
&\quad \left(\text{Since} \int \mathrm{d}x \exp\left\{-ax^2 + bx + c\right\} = \sqrt{\frac{\pi}{a}} \exp\left\{\frac{b^2}{4a} + c\right\}\right) \\
&= \exp\left(\frac{1}{2}\left\{(z_{kx}^*)^2 + (z_{lx})^2\right\} + z_{kx}^* z_{lx} - z_{kx}^*\mathrm{Re}\,(z_{kx}) - z_{lx}\mathrm{Re}\,(z_{lx})\right) \\
&= \exp\left(-\frac{1}{2} z_{kx}^*\,(2\mathrm{Re}\,(z_{kx}) - z_{kx}^*) - \frac{1}{2} z_{lx}\,(2\mathrm{Re}\,(z_{lx}) - z_{lx}) + z_{kx}^* z_{lx}\right) \\
&= \exp\left(-\frac{1}{2} z_{kx}^* z_{kx} - \frac{1}{2} z_{lx} z_{lx}^* + z_{kx}^* z_{lx}\right) \\
&= \exp\left[-\frac{1}{2}(|z_{kx}|^2 + |z_{lx}|^2) + z_{kx}^* z_{lx}\right] \\
&= \langle z_{kx}(t)|z_{lx}(t)\rangle.
\end{aligned} \tag{H.13}$$

I. Ground-state energy of a linear harmonic oscillator refers to the zero temperature

The canonical density operator $\hat{\rho}$ in statistical mechanics is defined as:

$$\hat{\rho} = \frac{\mathrm{e}^{-\beta \hat{H}}}{Q} \tag{I.1}$$

where

$$\beta = \frac{1}{kT} \tag{I.2}$$

is the inverse temperature and the partition function

$$Q = \mathrm{Tr}\, \mathrm{e}^{-\beta \hat{H}}. \tag{I.3}$$

The position matrix elements of the canonical density matrix $\hat{\rho}$ for a linear harmonic oscillator with the Hamiltonian

$$H = \frac{p^2}{2m} + \frac{1}{2} m\omega^2 x^2 \tag{I.4}$$

is given by

$$\begin{aligned} \rho(x, x'; \beta) =& \langle x|\hat{\rho}|x'\rangle \\ =& \frac{1}{Q}\sqrt{\frac{m\omega}{2\pi\hbar \sinh(\beta\hbar\omega)}} \\ & \times \exp\left\{\frac{-m\omega}{2\hbar\sinh(\beta\hbar\omega)}\left[\left(x^2 + x'^2\right)\cosh(\beta\hbar\omega) - 2xx'\right]\right\} \end{aligned} \tag{I.5}$$

with the canonical partition function of the harmonic oscillator

$$Q = \frac{1}{2\sinh(\frac{\beta\hbar\omega}{2})}. \tag{I.6}$$

The expression (I.5) can be derived using Feynman's path integral formulation, see [210].

Now, for temperature $T = 0$, we get $\beta \to \infty$. In this limit, $\sinh(\beta\hbar\omega) = \cosh(\beta\hbar\omega)$ and is much larger compared to the term $2xx'$ and hence we can completely neglect this last term in the bracket

of the exponent in (I.5). Therefore,

$$\begin{aligned}\lim_{\beta\to\infty}\rho(x,x';\beta) &= \lim_{\beta\to\infty}\sqrt{\frac{4m\omega\sinh^2(\frac{\beta\hbar\omega}{2})}{4\pi\hbar\sinh(\frac{\beta\hbar\omega}{2})\cosh(\frac{\beta\hbar\omega}{2})}}\times\exp\left\{\frac{-m\omega}{2\hbar}\left(x^2+x'^2\right)\right\}\\ &=\left(\frac{m\omega}{\pi\hbar}\right)^{\frac{1}{2}}\exp\left\{\frac{-m\omega}{2\hbar}\left(x^2+x'^2\right)\right\}\\ &=\langle x|\Psi(0)\rangle\langle\Psi(0)|x'\rangle \end{aligned} \tag{I.7}$$

where the ground-state wavefunction of the harmonic oscillator in position representation is

$$\Psi(x,0)=\langle x|\Psi(0)\rangle=\left(\frac{m\omega}{\pi\hbar}\right)^{\frac{1}{4}}\exp\left\{-\frac{m\omega}{2\hbar}x^2\right\}. \tag{I.8}$$

Hence, it is proved that the ground-state of a harmonic oscillator refers to zero temperature.

Bibliography

[1] S. Goldstein, J. L. Lebowitz, R. Tumulka, and N. Zanghì: *Canonical Typicality*, Phys. Rev. Lett. **96** (2006), 050403.

[2] J. Gemmer, M. Michel, and G. Mahler: *Quantum Thermodynamics: Emergence of Thermodynamic Behavior Within Composite Quantum Systems*, vol. 784 of *Lecture Notes in Physics*, (Springer Verlag, Berlin), (2009).

[3] P. Reimann: *Typicality for Generalized Microcanonical Ensembles*, Phys. Rev. Lett. **99** (2007), 160404.

[4] S. Popescu, A. J. Short, and A. Winter: *Entanglement and the foundations of statistical mechanics* **2** (2006), 754.

[5] R. Steinigeweg, J. Gemmer, and W. Brenig: *Spin-Current Autocorrelations from Single Pure-State Propagation*, Phys. Rev. Lett. **112** (2014), 120601.

[6] E. Fermi, J. Pasta, and S. Ulam: *Collected Papers of Enrico Fermi*, (University of Chicago Press, Chicago, IL), (1965).

[7] M. V. Berry and J. M. Robbins: *Chaotic classical and half-classical adiabatic reactions: geometric magnetism and deterministic friction*, Proc. R. Soc. Lond. A **442** (1993), 659–672.

[8] C. Jarzynski: *Thermalization of a Brownian Particle via Coupling to Low-Dimensional Chaos*, Phys. Rev. Lett. **74** (1995), 2937–2940.

[9] M. V. S. Bonanca and M. A. M. de Aguiar: *Classical dissipation and asymptotic equilibrium via interaction with chaotic systems*, Physica A **365** (2006), 333–350.

[10] J. Rosa and M. W. Beims: *Dissipation and transport dynamics in a ratchet coupled to a discrete bath*, Phys. Rev. E **78** (2008), 031126.

[11] S. Smith and R. Onofrio: *Thermalization in open classical systems with finite heat baths*, Eur. Phys. J. B **761** (2008), 271–275.

[12] M. A. Marchiori and M. A. M. de Aguiar: *Energy dissipation via coupling with a finite chaotic environment*, Phys. Rev. E **83** (2011), 061112.

[13] M. A. Marchiori, R. Fariello, and M. A. M. de Aguiar: *Energy transfer dynamics and thermalization of two oscillators interacting via chaos*, Phys. Rev. E **85** (2012), 041119.

[14] F. Jin, T. Neuhaus, K. Michielsen, S. Miyashita, M. A. Novotny, M. I. Katsnelson, and H. De Raedt: *Equilibration and Thermalization of Classical Systems*, New Journal of Physics **15** (2013), 033009.

[15] T. Dittrich and S. Pena Martínez: *Toppling Pencils—Macroscopic Randomness from Microscopic Fluctuations*, Entropy **22** (2020), 1046.

[16] F. Jin, T. Neuhaus, K. Michielsen, S. Miyashita, M. A. Novotny, M. I. Katsnelson, and H. De Raedt: *Equilibration and thermalization of classical systems*, New Journal of Physics **15** (2013), 033009.

[17] M. Buchholz, C.-M. Goletz, F. Grossmann, B. Schmidt, J. Heyda, and P. Jungwirth: *Semiclassical hybrid approach to condensed phase molecular dynamics: application to the I_2Kr_{17} cluster*, J. Phys. Chem. A **116** (2012), 11199–11210.

[18] J. G. Cosme and O. Fialko: *Thermalization in closed quantum systems: Semiclassical approach*, Phys. Rev. A **90** (2014), 053602.

[19] R. V. Jensen and R. Shankar: *Statistical Behavior in Deterministic Quantum Systems with Few Degrees of Freedom*, Phys. Rev. Lett. **54** (1985), 1879–1882.

[20] T. Klamroth and M. Nest: *Ultrafast electronic excitations of small sodium clusters and the onset of electron thermalization*, Phys. Chem. Chem. Phys. **11** (2009), 349.

[21] M. Galiceanu, M. W. Beims, and W. Strunz: *Quantum energy and coherence exchange with discrete baths*, Physica A **415** (2014), 294–306.

[22] C. Khripkov, D. Cohen, and A. Vardi: *Thermalization of Bipartite Bose-Hubbard Models*, J. Phys. Chem. A **120** (2016), 3136-3141.

[23] P. Reimann: *Typical fast thermalization processes in closed many-body systems*, Nature Communications **7** (2016), 10821.

[24] R. Borrelli and M. F. Gelin: *Quantum dynamics of vibrational energy flow in oscillator chains driven by anharmonic interactions*, New J. Phys. **22** (2020), 123002.

[25] K. Seki and S. Yunoki: *Emergence of a thermal equilibrium in a subsystem of a pure ground state by quantum entanglement*, Phys. Rev. Research **2** (2020), 043087.

[26] I. M. Khaymovich, M. Haque, and P. A. McClarty: *Eigenstate Thermalization, Random Matrix Theory, and Behemoths*, Phys. Rev. Lett. **122** (2019), 070601.

[27] S. Dogra, V. Madhok, and A. Lakshminarayan: *Quantum signatures of chaos, thermalization, and tunneling in the exactly solvable few-body kicked top*, Phys. Rev. E **99** (2019), 062217.

[28] J. M. Deutsch: *Eigenstate thermalization hypothesis*, Reports on Progress in Physics **81** (2018), 082001.

[29] L. D'Alessio, Y. Kafri, A. Polkovnikov, and M. Rigol: *From quantum chaos and eigenstate thermalization to statistical mechanics and thermodynamics*, Advances in Physics **65** (2016), 239–362.

[30] N. T. Maitra: *Perspective: Fundamental aspects of time-dependent density functional theory*, The Journal of Chemical Physics **144** (2016), 220901.

[31] H.-D. Meyer, U. Manthe, and L. Cederbaum: *The multi-configurational time-dependent Hartree approach*, Chemical Physics Letters **165** (1990), 73–78.

[32] M. Beck, A. Jäckle, G. Worth, and H.-D. Meyer: *The multiconfiguration time-dependent Hartree (MCTDH) method: a highly efficient algorithm for propagating wavepackets*, Physics Reports **324** (2000), 1–105.

[33] D. V. Shalashilin and M. S. Child: *Time dependent quantum propagation in phase space*, J. Chem. Phys. **113** (2000), 10028.

[34] M. Werther, S. L. Choudhury, and F. Grossmann: *Coherent state based solutions of the time-dependent Schrödinger equation: hierarchy of approximations to the variational principle*, Int. Rev. in Phys. Chem. **40** (2021), 81.

[35] R. P. Feynman: *Space-Time Approach to Non-Relativistic Quantum Mechanics*, Rev. Mod. Phys. **20** (1948), 367–387.

[36] F. Grossmann and A. L. Xavier: *From the coherent state path integral to a semiclassical initial value representation of the quantum mechanical propagator*, Physics Letters A **243** (1998), 243–248.

[37] M. F. Herman and E. Kluk: *A semiclassical justification for the use of non-spreading wavepackets in dynamics calculations*, Chemical Physics **91** (1984), 27.

[38] K. G. Kay: *Numerical study of semiclassical initial value methods for dynamics*, J. Chem. Phys. **100** (1994), 4432–4445.

[39] K. G. Kay: *Integral expressions for the semiclassical time-dependent propagator*, J. Chem. Phys. **100** (1994), 4377.

[40] E. J. Heller: *Quantum corrections to classical photodissociation models*, The Journal of Chemical Physics **68** (1978), 2066–2075.

[41] J. Shao, J.-L. Liao, and E. Pollak: *Quantum transition state theory: Perturbation expansion*, The Journal of Chemical Physics **108** (1998), 9711–9725.

[42] X. Sun, H. Wang, and W. H. Miller: *Semiclassical theory of electronically nonadiabatic dynamics: Results of a linearized approximation to the initial value representation*, J. Chem. Phys. **109** (1998), 7064.

[43] X. Sun and W. H. Miller: *Forward-backward initial value representation for semiclassical time correlation functions*, J. Chem. Phys. **110** (1999), 6635.

[44] X. Sun, H. Wang, and W. H. Miller: *On the semiclassical description of quantum coherence in thermal rate constants*, J. Chem. Phys. **109** (1998), 4190.

[45] H. Wang, X. Sun, and W. H. Miller: *Semiclassical approximations for the calculation of thermal rate constants for chemical reactions in complex molecular systems*, J. Chem. Phys. **108** (1998), 9726.

[46] H. Wang, M. Thoss, K. L. Sorge, R. Gelabert, X. Giménez, and W. H. Miller: *Semiclassical description of quantum coherence effects and their quenching: A forward-backward initial value representation study*, J. Chem. Phys. **114** (2001), 2562.

[47] S. V. Antipov, Z. Ye, and N. Ananth: *Dynamically consistent method for mixed quantum-classical simulations: A semiclassical approach*, J. Chem. Phys. **142** (2015), 184102.

[48] M. M. Ali, W. M. Huang, and W. M. Zhang: *Quantum Thermodynamics of single particle systems*, Sci. Rep. **10** (2020), 13500.

[49] F. Grossmann: *Theoretical Femtosecond Physics: Atoms and Molecules in Strong Laser Fields*, (Springer International Publishing AG, Cham), 3rd edn., (2018).

[50] M. D. Feit, J. A. Fleck, and A. Steiger: *Solution of the Schroedinger equation by a spectral method*, J. Comp. Phys. **47** (1982), 412.

[51] S. R. Billeter and W. F. V. Gunsteren: *A Comparison of Different Numerical Propagation Schemes for Solving the Time-Dependent Schrödinger Equation in the Position Representation in One Dimension for Mixed Quantum-and Molecular Dynamics Simulations*, Molecular Simulation **15** (1995), 301–322.

[52] W. Witschel: *Ordered operator expansions by comparison*, J. Phys. A **8** (1975), 143.

[53] L. S. Schulman: *Techniques and Applications of Path Integration*, (Dover, Mineola), (2005).

[54] J. A. Fleck, J. R. Morris, and M. D. Feit: *Time-dependent propagation of high energy laser beams through the atmosphere*, Appl. Phys. **10** (1976), 129.

[55] W. H. Press, S. A. Teukolsky, W. T. Vetterling, and B. P. Flannery: *Numerical recipes in FORTRAN*, (Cambridge University Press, Cambridge), 2nd edn., (1992).

[56] M. Frigo and S. Johnson: *The Design and Implementation of FFTW3*, Proceedings of the IEEE **93** (2005), 216–231.

[57] D. V. Shalashilin and I. Burghardt: *Gaussian-based techniques for quantum propagation from the time-dependent variational principle: Formulation in terms of trajectories of coupled classical and quantum variables*, J. Chem. Phys. **129** (2008), 084104.

[58] J. R. Klauder and B. S. Skagerstam: *Coherent States*, (World Scientific, Singapore), (1985).

[59] W. H. Louisell: *Quantum Statistical Properties of Radiation*, (Wiley, New York), (1990).

[60] W.-M. Zhang, D. H. Feng, and R. Gilmore: *Coherent states: Theory and some applications*, Rev. Mod. Phys. **62** (1990), 867–927.

[61] F. Grossmann, M. Werther, L. Chen, and Y. Zhao: *Generalization of the Davydov-Ansatz by squeezing*, Chem. Phys. **481** (2016), 99–107.

[62] V. Bargmann, P. Butera, L. Girardello, and J. R. Klauder: *On the completeness of the coherent states*, Rep. Math. Phys. **2** (1971), 221–228.

[63] D. J. Tannor: *Introduction to Quantum Mechanics: A Time-Dependent Perspective*, (University Science Books, Sausalito), (2007).

[64] A. M. Perelomov: *On the completeness of a system of coherent states*, Theoretical and Mathematical Physics **6** (1971), 156–164.

[65] J. von Neumann: *Mathematical Foundations of Quantum Mechanics*, (Princeton University Press, Princeton), (1955).

[66] M. Boon and J. Zak: *Discrete coherent states on the von Neumann lattice*, Phys. Rev. B **18** (1978), 6744–6751.

[67] F. Grossmann: *A semiclassical hybrid approach to many particle quantum dynamics*, J. Chem. Phys. **125** (2006), 014111.

[68] P. A. M. Dirac: *Note on exchange phenomena in the Thomas atom*, Mathematical Proceedings of the Cambridge Philosophical Society **26** (1930), 376–385.

[69] J. Frenkel: *Wave Mechanics: Advanced General Theory*, (Oxford University Press, Oxford), 1st edn., (1934).

[70] J. Broekhove, L. Lathouwers, E. Kesteloot, and P. Van Leuven: *On the equivalence of time-dependent variational principles*, Chem. Phys. Lett. **149** (1988), 547–550.

[71] C. Lubich: *From Quantum to Classical Molecular Dynamics: Reduced Models and Numerical Analysis*, Zurich Lectures in Advanced Mathematics, (European Mathematical Society, Zürich), (2008).

[72] E. J. Heller: *Frozen Gaussians: A very simple semiclassical approximation*, J. Chem. Phys. **75** (1981), 2923–2931.

[73] M. S. Child and D. V. Shalashilin: *Locally coupled coherent states and Herman-Kluk dynamics*, J. Chem. Phys. **118** (2003), 2061.

[74] S. Habershon: *Linear dependence and energy conservation in Gaussian wavepacket basis sets*, J. Chem. Phys. **136** (2012), 014109.

[75] D. V. Shalashilin and M. S. Child: *Basis set sampling in the method of coupled coherent states: Coherent state swarms, trains, and pancakes*, J. Chem. Phys. **128** (2008), 054102.

[76] B. Gu and S. Garashchuk: *Quantum Dynamics with Gaussian Bases Defined by the Quantum Trajectories*, J. Phys. Chem. A **120** (2016), 3023–3031.

[77] I. Daubechies, A. Grossmann, and Y. Meyer: *Painless nonorthogonal expansions*, J. Math. Phys. **27** (1986), 1271–1283.

[78] J. C. Burant and V. S. Batista: *Real time path integrals using the Herman–Kluk propagator*, J. Chem. Phys. **116** (2002), 2748–2756.

[79] D. V. Shalashilin and M. S. Child: *Electronic energy levels with the help of trajectory-guided random grid of coupled wave packets. I. Six-dimensional simulation of H_2*, J. Chem. Phys. **122** (2005), 224108.

[80] J. L. Sanz-Vicario, H. Bachau, and F. Martín: *Time-dependent theoretical description of molecular autoionization produced by femtosecond xuv laser pulses*, Phys. Rev. A **73** (2006), 033410.

[81] J. Zanghellini, M. Kitzler, T. Brabec, and A. Scrinzi: *Testing the multi-configuration time-dependent Hartree–Fock method*, Journal of Physics B: Atomic, Molecular and Optical Physics **37** (2004), 763–773.

[82] E. Runge and E. K. U. Gross: *Density-Functional Theory for Time-Dependent Systems*, Phys. Rev. Lett. **52** (1984), 997–1000.

[83] F. Grossmann: *Semiclassical Real-Time Tunneling by Multiple Spawning of Classical Trajectories*, Phys. Rev. Lett. **85** (2000), 903–907.

[84] S. C. Creagh and N. D. Whelan: *Complex Periodic Orbits and Tunneling in Chaotic Potentials*, Phys. Rev. Lett. **77** (1996), 4975–4979.

[85] J. H. Van Vleck: *The Correspondence Principle in the Statistical Interpretation of Quantum Mechanics*, Proceedings of the National Academy of Sciences **14** (1928), 178–188.

[86] M. C. Gutzwiller: *Chaos in classical and quantum mechanics*, (Springer-Verlag, New York), (1990).

[87] S. Levit and U. Smilansky: *A New Approach to Gaussian Path Integrals and the Evaluation of the Semiclassical Propagator*, Annals Phys. **103** (1977), 198.

[88] C.-M. Goletz: *Semiclassical hybrid dynamics for open quantum systems*, Ph.D. thesis, Technische Universität Dresden, (2011).

[89] F. Grossmann: *A Hierarchy of Semiclassical Approximations Based on Gaussian Wavepackets*, Comm. At. Mol. Phys. **34** (1999), 141.

[90] K. G. Kay: *The Herman-Kluk approximation: Derivation and semiclassical corrections*, Chem. Phys. **322** (2006), 3.

[91] M. F. Herman: *Time reversal and unitarity in the frozen Gaussian approximation for semiclassical scattering*, J. Chem. Phys. **85** (1986), 2069.

[92] K. G. Kay: *Semiclassical propagation for multidimensional systems by an initial value method*, J. Chem. Phys. **101** (1994), 2250–2260.

[93] E. J. Heller: *Wavepacket Dynamics and Quantum Chaology*, in: *Chaos and Quantum Physics* (Eds. M. J. Giannoni, A. Voros and J. Zinn-Justin), Les Houches Session LII, 547–663, (Elsevier, Amsterdam), (1991).

[94] E. J. Heller: *Time-dependent approach to semiclassical dynamics*, J. Chem. Phys. **62** (1975), 1544.

[95] W. H. Miller: *The Semiclassical Initial Value Representation: A Potentially Practical Way for Adding Quantum Effects to Classical Molecular Dynamics Simulations*, J. Phys. Chem. A **105** (2001), 2942.

[96] N. Makri: *Forward-backward semiclassical and quantum trajectory methods for time correlation functions*, Phys Chem Chem Phys. **13** (2011), 14442–14452.

[97] R. Heather and H. Metiu: *Some remarks concerning the propagation of a Gaussian wave packet in a Morse potential*, Chem. Phys. Lett. **118** (1985), 558–563.

[98] R. Heather and H. Metiu: *A numerical study of the multiple Gaussian representation of time dependent wave functions of a Morse oscillator*, J. Chem. Phys. **84** (1986), 3250–3259.

[99] Z.-X. Wang and E. J. Heller: *Semiclassical investigation of the revival phenomena in a one-dimensional system*, J. Phys. A **42** (2009), 285304.

[100] J. Brickmann and P. Russegger: *Quasidecay of harmonic oscillator coherent states in nonharmonic potentials*, J. Chem. Phys. **75** (1981), 5744–5758.

[101] E. Kluk, M. F. Herman, and H. L. Davis: *Comparison of the propagation of semiclassical frozen Gaussian wave functions with quantum propagation for a highly excited anharmonic oscillator*, J. Chem. Phys. **84** (1986), 326.

[102] M. Hénon and C. Heiles: *The applicability of the third integral of motion; some numerical experiments*, Astronom. J. **69** (1964), 73–79.

[103] A. Walton and D. E. Manolopoulos: *A new semiclassical initial value method for Franck-Condon spectra*, Mol. Phys. **87** (1996), 961–978.

[104] R. N. Porter and M. Karplus: *Potential Energy Surface for H_3*, J. Chem. Phys. **40** (1964), 1105–1115.

[105] F. Grossmann: *Time-dependent semiclassical calculation of resonance lifetimes*, Chem. Phys. Lett. **262** (1996), 470–476.

[106] S. Garashchuk, F. Grossmann, and D. J. Tannor: *Semiclassical Approach to the Hydrogen Exchange Reaction: Reactive and Transition State Dynamics*, J. Chem. Soc., Faraday Transactions **93** (1997), 781–789.

[107] D. Secrest and B. R. Johnson: *Exact Quantum-Mechanical Calculation of a Collinear Collision of a Particle with a Harmonic Oscillator*, J. Chem. Phys. **45** (1966), 4556–4570.

[108] D. V. Shalashilin and M. S. Child: , J. Chem. Phys. **114** (2001), 9296.

[109] G. A. Worth and I. Burghardt: *Full quantum mechanical molecular dynamics using Gaussian wavepackets*, Chem. Phys. Lett. **368** (2003), 502–508.

[110] V. A. Mandelshtam and M. Ovchinnikov: *Extraction of tunneling splittings from a real time semiclassical propagation*, J. Chem. Phys. **108** (1998), 9206–9209.

[111] A. Tanaka: *Determination of the border between "shallow" and "deep" tunneling regions for the Herman-Kluk method by the asymptotic approach*, Phys. Rev. A **73** (2006), 024101.

[112] J. M. Moix and E. Pollak: *Semiclassical initial-value-representation study of helium scattering from Cu(110)*, Phys. Rev. A **79** (2009), 062507.

[113] G. van de Sand and J.-M. Rost: *Semiclassical time-dependent propagation in three dimensions for a Coulomb potential*, Phys. Rev. A **59** (1999), R1723–R1726.

[114] S. Yoshida, F. Grossmann, E. Persson, and J. Burgdörfer: *Semiclassical analysis of quantum localization of the periodically kicked Rydberg atom*, Phys. Rev. A **69** (2004), 043410.

[115] G. van de Sand and J.-M. Rost: *Irregular Orbits Generate Higher Harmonics*, Phys. Rev. Lett. **83** (1999), 524–527.

[116] G. van de Sand and J.-M. Rost: *Semiclassical description of multiphoton processes*, Phys. Rev. A **62** (2000), 053403.

[117] C. Harabati and K. G. Kay: *Semiclassical initial value calculations of the collinear helium atom*, J. Chem. Phys. **127** (2007), 084104.

[118] F. Grossmann and T. Kramer: *Spectra of harmonium in a magnetic field using an initial value representation of the semiclassical propagator*, J. Phys. A: Math. Theor. **44** (2011), 445309.

[119] F. Grossmann, M. Buchholz, E. Pollak, and M. Nest: *Spin effects and the Pauli principle in semiclassical electron dynamics*, Phys. Rev. A **89** (2014), 032104.

[120] P. Elliott and N. T. Maitra: *Electron correlation via frozen Gaussian dynamics*, J. Chem. Phys. **135** (2011), 104110.

[121] D. V. Shalashilin, M. S. Child, and A. Kirrander: *Mechanisms of double ionization in strong laser field from simulation with Coupled Coherent States: Beyond reduced dimensionality models*, Chem. Phys. **347** (2008), 257–262.

[122] M. Eidi, M. Vafaee, A. R. Niknam, and N. Morshedian: *A new version of fermion coupled coherent states method: Theory and applications in simulation of two-electron systems*, Chem. Phys. Lett. **653** (2016), 60–66.

[123] S. Ray, P. Ostmann, L. Simon, F. Grossmann, and W. T. Strunz: *Dynamics of interacting bosons using the Herman-Kluk semiclassical initial value representation*, J. Phys. A **49** (2016), 165303.

[124] C.-M. Goletz, F. Grossmann, and S. Tomsovic: *Investigating quantum transport with an initial value representation of the semiclassical propagator*, Phys. Rev. E **80** (2009), 031101.

[125] C. Zagoya, L. Schulman, and F. Grossmann: *Interference nature of quantum breather oscillation*, J. Phys. A **47** (2014), 165102.

[126] J. L. Schoendorff, H. J. Korsch, and N. Moiseyev: *Semiclassical quantization of a system with mixed regular/chaotic dynamics*, Europhys. Lett. **44** (1998), 290–295.

[127] G. M. Lando and A. M. O. de Almeida: *Quantum-Chaotic Evolution Reproduced from Effective Integrable Trajectories*, Phys. Rev. Lett. **124** (2020), 010402.

[128] J. Cao and K. R. Wilson: *Detecting wave packet motion in pump-probe experiments: Theoretical analysis*, The Journal of Chemical Physics **106** (1997), 5062–5072.

[129] G. Stock and M. Thoss: *Semiclassical Description of Nonadiabatic Quantum Dynamics*, Phys. Rev. Lett. **78** (1997), 578–581.

[130] F. Grossmann: *Semiclassical Wavepacket Propagation on Potential Surfaces Coupled by Ultrashort Laser Pulses*, Phys. Rev. A **60** (1999), 1791–1796.

[131] M. Ben-Nun, J. Quenneville, and T. J. Martinez: *Ab Initio Multiple Spawning: Photochemistry from First Principles Quantum Molecular Dynamics*, J. Phys. Chem. A **104** (2000), 5161–5175.

[132] B. F. E. Curchod and T. J. Martinez: *Ab Initio Nonadiabatic Quantum Molecular Dynamics*, Chem. Rev. **118** (2018), 3305–3336.

[133] D. V. Shalashilin: *Nonadiabatic dynamics with the help of multiconfigurational Ehrenfest method: Improved theory and fully quantum 24D simulation of pyrazine*, J. Chem. Phys. **132** (2010), 244111.

[134] S.-I. Sawada and H. Metiu: *A multiple trajectory theory for curve crossing problems obtained by using a Gaussian wave packet representation of the nuclear motion*, J. Chem. Phys. **84** (1986), 227–238.

[135] T. Murakami and T. J. Frankcombe: *Non-adiabatic quantum molecular dynamics by the basis expansion leaping multi-configuration Gaussian (BEL MCG) method: Multi-set and single-set formalisms*, J. Chem. Phys. **150** (2019), 144112.

[136] N. V. Golubev, T. Begusic, and J. Vanicek: *On-the-fly ab initio semiclassical evaluation of electronic coherences in polyatomic molecules reveals a simple mechanism of decoherence*, Phys. Rev. Lett. **125** (2020), 083001.

[137] S. Tomsovic and E. J. Heller: *Semiclassical dynamics of chaotic motion: unexpected long-time accuracy*, Phys. Rev. Lett. **67** (1991), 664–667.

[138] S. Tomsovic and E. J. Heller: *Long-time semiclassical dynamics of chaos: The stadium billiard*, Phys. Rev. E **47** (1993), 282–299.

[139] M. Ronto and D. V. Shalashilin: *Numerical implementation and test of the modified variational multiconfigurational Gaussian method for high-dimensional quantum dynamics*, J. Phys. Chem. A **117** (2013), 6948–6959.

[140] G. W. Richings, I. Polyak, K. E. Spinlove, G. A. Worth, I. Burghardt, and B. Lasorne: *Quantum dynamics simulations using Gaussian wavepackets: the vMCG method*, Int. Rev. in Phys. Chem. **34** (2015), 269–308.

[141] M. Ovchinnikov and V. A. Apkarian: *Mixed-order semiclassical dynamics in coherent state representation: The connection between phonon sidebands and guest-host dynamics*, J. Chem. Phys. **108** (1998), 2277–2284.

[142] M. Buchholz, F. Grossmann, and M. Ceotto: *Application of the mixed time-averaging semiclassical initial value representation method to complex molecular spectra*, J. Chem. Phys. **147** (2017), 164110.

[143] M. Buchholz, F. Grossmann, and M. Ceotto: *Simplified approach to the mixed time-averaging semiclassical initial value representation for the calculation of dense vibrational spectra*, J. Chem. Phys. **148** (2018), 114107.

[144] R. Hartmann, M. Werther, F. Grossmann, and W. T. Strunz: *Exact open quantum system dynamics: optimal frequency vs. time representation of bath correlations*, J. Chem. Phys. **150** (2019), 234105.

[145] M. Werther and F. Grossmann: *Apoptosis of moving non-orthogonal basis functions in many-particle quantum dynamics*, Phys. Rev. B **101** (2020), 174315.

[146] C.-M. Goletz and F. Grossmann: *Decoherence and dissipation in a molecular system coupled to an environment: An application of semiclassical hybrid dynamics*, J. Chem. Phys. **130** (2009), 244107.

[147] R. W. Robinett: *Quantum Wavepacket Revivals*, Phys. Rep. **392** (2004), 1–119.

[148] G. E. P. Box and M. E. Muller: *A Note on the Generation of Random Normal Deviates*, Ann. Math. Statist. **29** (1958), 610–611.

[149] C. Lasser and D. Sattlegger: *Discretising the Herman–Kluk propagator*, Numer. Math. **137** (2017), 119–157.

[150] S. K. Gray, D. W. Noid, and B. G. Sumpter: *Symplectic integrators for large scale molecular dynamics simulations: A comparison of several explicit methods*, J. Chem. Phys. **101** (1994), 4062–4072.

[151] J. Tatchen, E. Pollak, G. Tao, and W. H. Miller: *Renormalization of the frozen Gaussian approximation to the quantum propagator*, J. Chem. Phys. **134** (2011), 134104.

[152] MATLAB: *version 9.5.0.1033004 (R2018b) Update 2*, (The MathWorks Inc., Natick, Massachusetts), (2019).

[153] M. Eidi, M. Vafaee, and A. Landsmann: *Static Coherent States Method: One- and Two-Electron Laser-Induced Systems with Classical Nuclear Dynamics*, Appl. Sci. **8** (2018), 1252.

[154] C. Moler and C. Van Loan: *Nineteen Dubious Ways to Compute the Exponential of a Matrix, Twenty-Five Years Later*, SIAM Review **45** (2003), 3–49.

[155] A. H. Al-Mohy and N. J. Higham: *Computing the action of the matrix exponential, with an application to exponential integrators*, SIAM J. Sci. Comput. **33** (2011), 488–511.

[156] H. Tal-Ezer and R. Kosloff: *An accurate and efficient scheme for propagating the time-dependent Schrödinger equation*, J. Chem. Phys. **81** (1984), 3967–3971.

[157] E. J. Heller: *Wigner phase space method: Analysis for semiclassical applications*, J. Chem. Phys. **65** (1976), 1289.

[158] W. H. Miller: *Quantum mechanical transition state theory and a new semiclassical model for reaction rate constants*, J. Chem. Phys. **61** (1974), 1823–1834.

[159] J. Cao and G. A. Voth: *Semiclassical approximations to quantum dynamical time correlation functions*, J. Chem. Phys. **104** (1996), 273.

[160] X. Sun and W. H. Miller: *Semiclassical initial value representation for electronically nonadiabatic molecular dynamics*, J. Chem. Phys. **106** (1997), 6346.

[161] W. H. Miller and S. J. Cotton: *Classical molecular dynamics simulation of electronically non-adiabatic processes*, Faraday Discuss. **195** (2016), 9–30.

[162] M. V. Berry: *Semiclassical theory of spectral rigidity*, Proc. R. Soc. Lond. A **400** (1985), 229.

[163] M. F. Herman and D. Coker: *Classical mechanics and the spreading of localized wave packets in condensed phase molecular systems*, J. Chem. Phys. **111** (1999), 1801.

[164] Y. Zhao and N. Makri: *Quasiclassical dynamics methods from semiclassical approximations*, Chemical Physics **280** (2002), 135 – 151.

[165] W. G. Noid, G. S. Ezra, and R. F. Loring: *Optical response functions with semiclassical dynamics*, J. Chem. Phys. **119** (2003), 1003.

[166] F. Grossmann: *A semiclassical hybrid approach to linear response functions for infrared spectroscopy*, Physica Scripta **91** (2016), 044004.

[167] K. Husimi: *Some Formal Properties of the Density Matrix*, Proc. Phys. Math. Soc. Jpn. **22** (1940), 264–314.

[168] C. W. Gardiner and P. Zoller: *Quantum Noise: A Handbook of Markovian and Non-Markovian Quantum Stochastic Methods with Applications to Quantum Optics*, (Springer-Verlag, Berlin), 3rd edn., (2004).

[169] A. Polkovnikov: *Phase space representation of quantum dynamics*, Annals of Physics **325** (2010), 1790.

[170] R. P. Feynman and A. R. Hibbs: *Quantum Mechanics and Path Integrals*, (Mc Graw-Hill, New York), (1965).

[171] F. Grossmann: *Quantum effects in intermediate-temperature dipole-dipole correlation-functions in the presence of an environment*, J. Chem. Phys. **141** (2014), 144305.

[172] M. F. Herman: *Time reversal and unitarity in the frozen Gaussian approximation for semiclassical scattering*, J. Chem. Phys. **85** (1986), 2069.

[173] J. Ford: *The Fermi-Pasta-Ulam problem: Paradox turns discovery**, Physics Reports **213** (1992), 271–310.

[174] D. Hetterich, M. Fuchs, and B. Trauzettel: *Equilibration in closed quantum systems: Application to spin qubits*, Phys. Rev. B **92** (2015), 155314.

[175] T. Dittrich, F. Grossmann, P. Hänggi, B. Oelschlägel, and R. Utermann: *Coherent and Incoherent Dynamics in a Periodically Driven Bistable System*, in: *Stochasticity and Quantum Chaos* (Eds. Z. Haba, W. Cegla and L. Jakóbczyk), 39–55, (Kluwer, Dordrecht), (1995).

[176] F. Grossmann, T. Dittrich, P. Jung, and P. Hänggi: *Coherent destruction of tunneling*, Phys. Rev. Lett. **67** (1991), 516–519.

[177] F. Hund: *Zur Deutung der Molekelspektren III*, Z. Phys. **43** (1927), 805–826.

[178] J. Kurkijärvi: *Intrinsic Fluctuations in a Superconducting Ring Closed with a Josephson Junction*, Phys. Rev. B **6** (1972), 832.

[179] E. Kierig, U. Schnorrberger, A. Schietinger, J. Tomkovic, and M. K. Oberthaler: *Single-Particle Tunneling in Strongly Driven Double-Well Potentials*, Phys. Rev. Lett. **100** (2008), 190405.

[180] L. E. Reichl: *The Transition to Chaos: Conservative Classical Systems and Quantum Manifestations*, (Springer, New York), 2nd edn., (2004).

[181] A. J. Bray and M. A. Moore: *Influence of dissipation on quantum coherence*, Phys. Rev. Lett. **49** (1982), 1545.

[182] A. J. Leggett, S. Chakravarty, A. T. Dorsey, M. P. A. Fisher, A. Garg, and W. Zwerger: *Dynamics of the dissipative two-state system*, Rev. Mod. Phys. **59** (1987), 1–85.

[183] F. Grossmann and P. Hänggi: *Localization in a Driven Two-Level Dynamics*, Europhys. Lett. **18** (1992), 571.

[184] M. Grifoni and P. Hänggi: *Driven Quantum Tunneling*, Phys. Rep. **304** (1998), 229.

[185] G.-L. Ingold: *Path Integrals and Their Application to Dissipative Quantum Systems*, in: *Lecture Notes in Physics* (Eds. A. Buchleitner and K. Hornberger), vol. 611, 1–53, (Springer, Berlin), (2002).

[186] A. O. Caldeira and A. J. Leggett: *Quantum tunnelling in a dissipative system*, Ann. Phys. (N.Y.) **149** (1983), 374.

[187] S. Choi, R. Onofrio, and B. Sundaram: *Ehrenfest approach to open double-well dynamics*, Phys. Rev. E **92** (2015), 042907.

[188] P. A. J. Sherratt, D. V. Shalashilin, and M. S. Child: *Description of multidimensional tunnelling with the help of coupled coherent states guided by classical Hamiltonians with quantum corrections*, Chem. Phys. **322** (2006), 127.

[189] C.-M. Goletz, W. Koch, and F. Grossmann: *Semiclassical dynamics of open quantum systems: comparing the finite with the infinite perspective*, Chem. Phys. **375** (2010), 227.

[190] H. Wang and M. Thoss: *From coherent motion to localization: dynamics of the spin-boson model at zero temperature*, New J. Phys. **10** (2008), 115005.

[191] M. Buchholz, E. Fallacara, F. Gottwald, M. Ceotto, F. Grossmann, and S. D. Ivanov: *Herman-Kluk propagator is free from zero-point energy leakage*, Chem. Phys. **515** (2018), 231.

[192] Y. Tanimura: *Numerically "exact" approach to open quantum dynamics: The hierarchical equations of motion (HEOM)*, J. Chem. Phys. **153** (2020), 020901.

[193] S. L. Choudhury and F. Grossmann: *Quantum approach to the thermalization of the toppling pencil interacting with a finite bath*, Phys. Rev. A **105** (2022), 022201.

[194] M. Werther: *The multi Davydov-Ansatz: Apoptosis of moving Gaussian basis functions with applications to open quantum system dynamics*, Ph.D. thesis, Technische Universität Dresden, (2020).

[195] M. Baranger, M. A. M. de Aguiar, F. Keck, H. J. Korsch, and B. Schellhaaß: *Semiclassical approximations in phase space with coherent states*, J. Phys. A **34** (2001), 7227–7286.

[196] F. Grossmann and M. F. Herman: *Comment on "Semiclassical approximations in phase space with coherent states"*, J. Phys. A: Math. Gen. **35** (2002), 9489–9492.

[197] C. Harabati, J.-M. Rost, and F. Grossmann: *Long-time and unitary properties of semiclassical initial value representations*, J. Chem. Phys. **120** (2004), 26–30.

[198] A. Grigolo, T. F. Viscondi, and M. A. M. de Aguiar: *Multiconfigurational quantum propagation with trajectory-guided generalized coherent states*, J. Chem. Phys. **144** (2016), 094106.

[199] J. A. Green and D. V. Shalashilin: *Simulation of the quantum dynamics of indistinguishable bosons with the method of coupled coherent states*, Phys. Rev. A **100** (2019), 013607.

[200] N. Zhou, Z. Huang, J. Zhu, V. Chernyak, and Y. Zhao: *Polaron dynamics with a multitude of Davydov D2 trial states*, J. Chem. Phys. **143** (2015), 014113.

[201] S. L. Choudhury and F. Grossmann: *On the Husimi version of the classical limit of quantum correlation functions*, Condens. Matt. **5** (2020), 3.

[202] T. Halverson and B. Poirier: *Accurate quantum dynamics calculations using symmetrized Gaussians on a doubly dense Von Neumann lattice*, J. Chem. Phys. **137** (2012), 224101.

[203] S. Rau, J. Main, and G. Wunner: *Variational methods with coupled Gaussian functions for Bose-Einstein condensates with long-range interactions. I. General concept*, Phys. Rev. A **82** (2010), 023610.

[204] H. Cartarius and E. Pollak: *Imaginary time Gaussian dynamics of the Ar3 cluster*, J. Chem. Phys. **134** (2011), 044107.

[205] R. A. Jalabert, I. García-Mata, and D. A. Wisniacki: *Semiclassical theory of out-of-time-order correlators for low-dimensional classically chaotic systems*, Phys. Rev. E **98** (2018), 062218.

[206] U. Weiss: *Quantum Dissipative Systems*, (World Scientific, Singapore), 3rd edn., (2008).

[207] L. Mauritz Andersson: *Quantum dynamics using a discretized coherent state representation: An adaptive phase space method*, J. Chem. Phys. **115** (2001), 1158–1165.

[208] J. A. C. Gallas: *Some matrix elements for Morse oscillators*, Phys. Rev. A **21** (1980), 1829–1834.

[209] H. Goldstein: *Classical Mechanics*, (Addison-Wesley, Reading, Mass.), (1981).

[210] R. Feynman: *Statistical Mechanics: A Set Of Lectures*, Advanced Books Classics, (Avalon Publishing), (1998).

List of publications

1. **S. L. Choudhury** and R. K. Paul: *A new approach to the generalization of Planck's law of black-body radiation*, Ann. Phys. (N.Y.) **395** (2018), 317-325.

2. **S. L. Choudhury** and F. Grossmann: *On the Husimi version of the classical limit of quantum correlation functions*, Condens. Matt. **5** (2020), 3.

3. M. Werther, **S. L. Choudhury** and F. Grossmann: *Coherent state based solutions of the time-dependent Schrödinger equation: hierarchy of approximations to the variational principle*, Int. Rev. in Phys. Chem. **40** (2021), 81.

4. **S. L. Choudhury** and F. Grossmann: *Quantum approach to the thermalization of the toppling pencil interacting with a finite bath*, Phys. Rev. A **105** (2022), 022201.

Versicherung

Diese Arbeit wurde am Institut für Theoretische Physik der Technischen Universität Dresden unter der wissenschaftlichen Betreuung von Prof. Dr. Frank Großmann durchgeführt.
Hiermit versichere ich, dass ich die vorliegende Arbeit ohne unzulässige Hilfe Dritter und ohne Benutzung anderer als der angegebenen Hilfsmittel angefertigt habe; die aus fremden Quellen direkt oder indirekt übernommenen Gedanken sind als solche kenntlich gemacht. Die Arbeit wurde bisher weder im Inland noch im Ausland in gleicher oder ähnlicher Form einer anderen Prüfungsbehörde vorgelegt. Darüber hinaus erkenne ich die Promotionsordnung der Fakultät Mathematik und Naturwissenschaften der Technischen Universität Dresden vom 23. Februar 2011 an.

Sreeja Loho Choudhury

Dresden, 10.02.2022